Volume 2 No. 2

SOVIET ATOMIC ENERGY

АТОМНАЯ ЭНЕРГИЯ
(ATOMNAYA ÉNERGIYA)

TRANSLATED FROM RUSSIAN

C/b CONSULTANTS BUREAU, NEW YORK

ALL-UNION CONFERENCE ON THE APPLICATION OF RADIOACTIVE AND STABLE ISOTOPES IN THE NATIONAL ECONOMY AND SCIENCE

On the 4-11th of April, 1957, in Moscow, will be held an All-Union Scientific-Technical Conference on the Application of Radioactive and Stable Isotopes and Radiation in the National Economy and Science organized by the Academy of Sciences of the USSR and the Central Committee on the Utilization of Atomic Energy of the Council of Ministries of the USSR.

Research personnel of industrial installations, construction offices, institutes of higher education, and scientific research institutes of the Academy of Sciences of the USSR, the Academies of Science of the Soviet Republics, and affiliated academies are invited to attend the conference.

The Conference will hear reports of scientific investigation and experimentation concerned with the application of isotopes and nuclear radiation in science, industry, medicine and agriculture, of the results of industrial application of isotopes and radiation, and also of work in the fields of production of radioactive isotopes and the dosimetry of nuclear radiation.

The Conference will be divided into the following sessions:

1. Session on Technical Sciences and Industrial Uses of Isotopes (application of isotopes and radiation in metallurgy, metallography, machine construction and instrumentation, mechanics and heat technology, in the control of industrial processes, in prospecting and exploiting of useful minerals, as well as radiometric and dosimetric methods and apparatus for nuclear radiation).

2. Session on Chemistry (application of isotopes in investigation of the kinetics and mechanism of chemical reactions, radiation chemistry, radiochemistry, and application of isotopes in analytical chemistry).

3. Session on Isotope Production and High-Intensity γ-Systems (production of radioactive and stable isotopes and chemical compounds with them, construction of high-energy installations, on the basis of radioactive isotopes).

4. Session on Biology, Medicine and Agriculture (radiobiology, medicinal radiology, applications of isotopes and radiation in biology, physiology, the fishing industry, animal husbandry, industry, agrochemistry, and soil science).

In addition, questions of hygiene and safety precautions for work with radioactive substances and methods of disposal of radioactive wastes will be discussed.

Tickets to the conference will be allotted through the ministries and departments.

For further information, telephone as follows:

Session on Technical Science and Industrial Uses of Isotopes — B 2-00-00, ext. 165.

Session on Chemistry — B-2-00-00, ext. 64.

Session on Isotopes and High-Intensity γ-Systems — B 3-90-18.

Session on Biology, Medicine, and Agribulture — B 2-00-00, ext. 1-71.

The summaries of papers read at the Conference cited above have been published in complete English translation by Consultants Bureau. For titles and prices see the following page — Publisher.

ALL-UNION CONFERENCE ON THE APPLICATION OF RADIOACTIVE AND STABLE ISOTOPES IN THE NATIONAL ECONOMY AND SCIENCE

SECTIONS:

I.	ABSTRACTS OF PAPERS GIVEN IN THE SESSION ON ISOTOPE PRODUCTION AND HIGH-INTENSITY γ-SYSTEMS (22 pages, 24 papers)	$ 7.50
II.	ABSTRACTS OF PAPERS GIVEN IN THE SESSION ON TECHNICAL SCIENCES AND INDUSTRIAL USES OF ISOTOPES (128 pages, 179 papers)	20.00
III.	ABSTRACTS OF PAPERS GIVEN IN THE SESSION ON BIOLOGY, MEDICINE, AND AGRICULTURE (184 pages, 202 papers)	15.00
IV.	ABSTRACTS OF PAPERS, FIRST ALL-UNION CONFERENCE ON RADIATION CHEMISTRY, March 25 - April 2, 1957 (42 pages, 55 papers)	10.00
	All 4 sections, as a unit	35.00

PUBLISHER MISNUMBERED
PAGES 125 AND 126.

CERTAIN PROBLEMS IN THE OPERATION OF ATOMIC POWER STATIONS

A. N. Grigoryants

The experience acquired in operating the atomic power station of the Central Committee on the Use of Atomic Energy for the Council of Ministries, USSR, is evaluated. It is assumed that the reader is acquainted with the main characteristics of the reactor and the technological layout of the power station. A method of fuel-channel reloading is described in which only parts of the core are reloaded; using this scheme it is possible to achieve a greater burnup of the nuclear fuel (up to 20%) as compared with that which can be achieved when total reloading is used (11%). The partial reloading scheme increases the useful life of the fuel channels and makes it possible to use them more economically. It is shown that using the partial reloading scheme, in an effective day (24 hours of operation at full power) 1.2 channels are consumed whereas 1.7 channels are consumed when complete reloading is used. Furthermore, the use of the partial reloading scheme results in a considerable improvement in the uniformity of the neutron field at varying distances from the center of the core. The various problems which arise in starting up the atomic power station from "zero" level to the nominal level are described. The change in reactivity due to the temperature rise is found to be $\Delta k = 0.027 \pm 0.003$. The feasibility of dispensing with cooling in the side reflector of the reactor, because of the low heat dissipation is discussed. Heat dissipation in the fuel channels following shutdown is also considered. It has been found that the fuel channels can be removed without cooling two hours after the reactor is shut down. The results of a chemical analysis of the coolant water of the primary circuit after various periods of operation are given and it is found that the insignificant amount of washed down contaminants means that operation can be carried on without the use of bidistillate and the condensate from the turbine condenser can be used. Finally, there is a discussion of questions bearing on biological safety and dosimetry. The operation of the station and its technological plant does not constitute a source of danger to the personnel of the station or the population of the surrounding region.

INTRODUCTION

The first atomic power station in the world has been in successful operation in the Soviet Union for more than two and one-half years. All the auxiliary installations and the primary equipment (the reactor, the main circulating pumps, the steam generators, the headers and feed-pumps of the primary circuit, etc.) have been found more than satisfactory.

The performance of the main components of the power reactor – the uranium heat-generating elements – has been extremely good. During the entire period of operation not one of these elements has been removed from service.

We note that each of the 128 fuel channels of the reactor contains 4 shell-and-tube heat-generating elements cooled by water at a pressure of 100 atmos which is at a temperature of 190°C on entering the reactor and ~ 270°C upon exit.

TABLE 1

Performance Indices for the Fuel Channels as of October 15, 1956

No. of fuel channels	Effective operating days*	U^{235} burnup in %	Thermal loading kcal/m²·hr
6**	250	31.2	$(1.0-1,5)\cdot 10^6$
22	232	24.4	$(1.0-1.5)\cdot 10^6$
22	149	19.6	$(1.0-1.5)\cdot 10^6$
11	198	19.0	$(1.0-1.2)\cdot 10^6$
33	150	15.0	$(0.8-1.0)\cdot 10^6$
133***	100-150	12-15	$(0.8-1.0)\cdot 10^6$

* Effective day taken to be an operating period in which the reactor is operated at full power for 24 hours.

** The channels were placed in the reactor for an extended test to determine the limits of "robustness" of the heat dissipation elements.

*** At the present time the channels are in a purification bath and in subsequent reloadings will be placed in the reactor for further burnup.

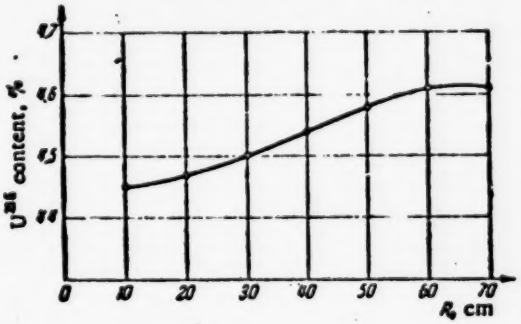

Fig. 1. U^{235} content by percentage along the reactor radius at the end of the first run.

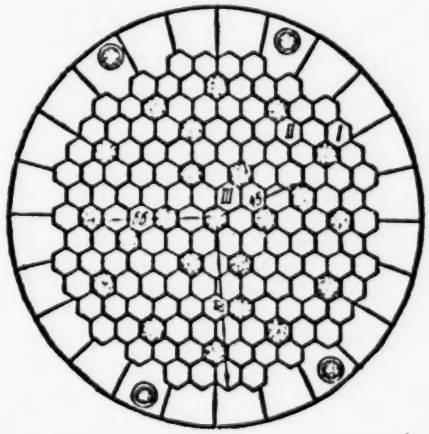

Fig. 2. Partial reloading zones of the reactor. The numbers indicate the zone radii in cm. The crosshatched channels are the control system and the protection system.

The reliable operation of the heat-generating elements has made it possible to extend the operating life of the fuel channels beyond the design values and to increase the U^{235} burnup.

Some data which characterize the operation of the fuel channels are shown in Table 1.

It is apparent from the table that a considerable number of the channels have been operated in the hottest zone of the reactor for more than 200 effective days; this period exceeds the design life of the channels by a factor of 2.

A considerable amount of operational experience has been obtained at the atomic power station. Within the scope of the present paper it is not possible to discuss all the problems which have been encountered so that we shall limit ourselves to those which are of the most importance.

Partial Reloading Scheme for the Reactor Fuel Channels

It is well known that U^{235} burnup is different in different fuel channels of the reactor as a function of distance from the center of the core, because of the variation in heat dissipation. It reaches a maximum value in the center channels and falls off at the periphery of the core. Consequently, the relatively large fraction of the reactor charge at the periphery of the core "burns" comparatively weakly (Fig. 1). Because of this situation a partial reloading scheme is used: in the first run, instead of a full charge of fresh fuel channels, only a part of the reactor core is charged. Fuel elements from the periphery of the core are subsequently moved to the center to increase burnup; that is, by charging the core with fresh elements at the periphery and moving these toward the center in gradual steps, a more complete burnup is achieved.

As an example, we shall consider this method as applied to the first three reloading operations. It is convenient to divide the core of the reactor into 3 zones as shown in Fig. 2:

Zone I – 42 fuel channels,
Zone II – 42 fuel channels,
Zone III – 44 fuel channels.

At the end of the first run, which was 75 effective days, the U^{235} burnup in the reactor averaged 11%. In this run, the reactor was operated with a charge of 128 fresh fuel channels with 5% content of U^{235}.

In the first reloading of the reactor, fresh fuel channels were used only to replace the channels in Zone I which had a burnup of 8%; the channels in the other two zones were allowed to remain for further "burning."

In the second reloading operation fresh channels were used only in Zone II where the fuel burnup was 11% and finally in the third reloading the substitution was carried out in Zone III, in which the fuel burnup had already reached 20%. In this third reloading the fresh channels were the low burnup channels from Zone I.

The subsequent reloading of the reactor was carried out according to this scheme, taking into account the duration of the run and the most judicious use of fresh channels. The fuel burnup in the channels in Zone III of the reactor amounted to approximately 20%, a considerable increase over the average fuel burnup when total recharging of the channels (11%) is used.

As is apparent from Table 1, the partial reloading scheme makes it possible to increase the useful life of the fuel channels in the reactor, thus offering the possibility of carrying out tests under conditions of prolonged operation and of realizing more economical utilization.

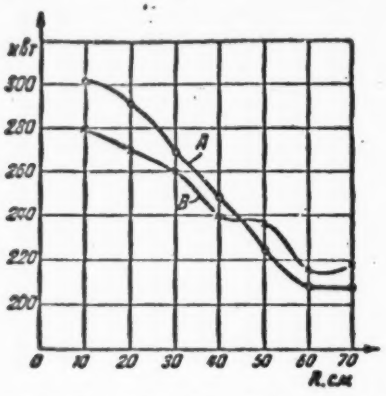

Fig. 3. Heat dissipation along the reactor radius at the end of the first run (A) and at the end of the fourth run (B). $K_A = 1.28$; $K_B = 1.19$.

To compute the advantage in the utilization of fresh channels (when this scheme is used) it is necessary to compute the time totals for 4 runs, using partial and total recharging: these are 175 and 300 effective days, respectively.

For the 4 runs in which partial recharging was applied the number of fresh fuel channels used were:

Run I – original charge	– 128 units
Run II – first recharging	– 42 units
Run III – second recharging	– 42 units
Run IV – third recharging	– 0 units
Total	212 units

In complete recharging 512 fuel channels would be required for the 4 runs.

The obvious advantage in the use of partial recharging may be shown by the following relations which determine the number of channels per effective day:

$$\text{for partial reloading } \frac{212}{175} = 1.2 \text{ channels/eff. day;}$$

$$\text{for complete reloading } \frac{512}{300} = 1.7 \text{ channels/eff. day.}$$

The additional "downtime" in partial recharging is not a serious drawback to normal operation of the reactor since reloading of separate zones of the reactor does not require more than 2.5-3 days while a full reloading requires up to 6-7 days.

In addition to the considerable economies in the utilization of fresh fuel channels and the more complete U^{235} burnup the partial recharging method produces a more uniform neutron field and makes the heat dissipation more uniform as a function of radius.

When the partial reloading scheme is used the fresh fuel channels, which contain 5% enriched fuel, are located in the outer zones of the reactor (II and III) where the neutron flux is low while the channels with higher burnup are located in the central part of the core where the neutron flux is at a maximum.

It is apparent from Fig. 3, that the radial nonuniformity factor of the neutron field was $K_A = 1.28$ at the end of the first run and had been reduced to $K_B = 1.19$ at the end of the fourth run. The reduction in nonuniform heat dissipation makes it possible to control the consumption of water in the fuel channels of the reactor and to obtain a minimum change in water temperature at exit from the channels as compared with the mean water temperature in the header (± 7-10°C).

Thus, the partial recharging method has a number of advantages and may be found extremely useful in the operation of similar power reactors.

Operation of the Power Reactor in the Transient Period

An atomic power station is a system in which mutally-interacting nuclear and thermal processes take place; a knowledge of these is necessary for the safe operation of the station.

The preparation of a power reactor for startup after a prolonged shutdown, for example, after the partial recharging of fuel channels, requires the following:

a) establishment of an operating pressure of 100 atmos for the water in the primary circuit and the adjustment of the flow rate to correspond with a given power level in the reactor;

b) adjustment of the water consumption in the fuel channels to correspond with heat dissipation in these following partial recharging of the channels;

c) filling the secondary circuit with water to the desired level in the evaporators by starting the supply pumps;

d) operation of the various devices for physically starting up the reactor, the process control instruments, and the system for automatic control and alarm signaling;

e) starting of the entire auxiliary system; the process condenser is adjusted to operate with nonconditioned steam in the startup period.

The elevation of the reactor operating level from zero to a level 0.01% of the nominal level (after which automatic control of the reactor starts) is carried out in accordance with standard operating procedures.

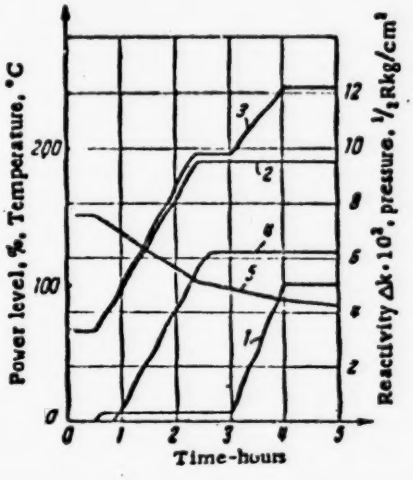

Fig. 4. Variation in the reactor parameters as a function of time in the power buildup period. 1) Power level; 2) water temperature at reactor exit; 3) water temperature on entry to the reactors; 4) steam pressure; 5) reactivity.

The further elevation of the reactor power level is carried out in conjunction with control of the thermal processes which occur in the reactor.

In Fig. 4 is shown the behavior of the important parameters when the power level is raised from zero to the normal level after a prolonged shutdown.

In the reactor used at the atomic power station, the time required to raise the power level to the point at which thermal equilibrium obtains is 4 hours. In case of need, this time may be reduced to 3-3.5 hours which corresponds approximately to the time required to start up a thermal power station.

Curve 1, the power buildup, (Fig. 4) has a section which corresponds with a relatively long period of reactor operation at 7% of the normal level which is required to avoid a sudden overheating of the elements of the heat removal system. The increase in the primary circuit water temperature upon entry to the reactor and exit are shown by Curves 2 and 3.

As the supply water starts to boil, the pressure in the evaporator increases gradually (Fig. 4) and the connection links to the main steam line are heated.

When the operating steam pressure is reached (12.5 atmos) in the evaporators, the temperature of the water at the input to the reactor becomes constant (190°C) and the further buildup of the power level in the reactor leads only to an increase in the temperature of the water at exit from the reactor and a simultaneous increase of the temperature and amount of steam in the steam generator.

The switching of the steam supply from the process condenser to the turbine is generally carried out after this since the output of the steam generator reaches 20 tons of steam per hour at a temperature 240-245°C, that is, this operation is independent of the power buildup in the reactor to the normal value (G = 42 tons) and the nominal steam parameters (t = 260°C).

Experience in the operation of the power station has shown that the thermal stability of the reactor is good provided there is a constant electric load on the turbo-generator of the system. A complete removal of the electric load on the generator (say in an emergency shutdown of the power system) does not disturb the operation of the reactor. There are valves which automatically reconnect the steam to the process condenser.

The increase in the water temperature which accompanies the power buildup in the reactor causes a reduction in the reactivity margin of the reactor.

The results of a number of measurements have established that the total temperature reactivity change of the reactor Δk is 0.027 ± 0.003, that is, the average change in the reactivity margin per 1°C is $\Delta k = 1.1 \cdot 10^{-4}$. Of this quantity, the change in reactivity per 1°C due to the water heating is approximately $0.65 \cdot 10^{-4}$.

It is apparent from Curve 5 (Fig. 4) that the actual drop in the reactivity in the power buildup in the reactor is greater than the magnitude of the negative temperature effect which in the present case is $\Delta k = 0.018$. This is explained by the fact that the increase in the power level of the reactor is accompanied by increased poisoning due to uranium fission products, mainly xenon and samarium.

Thus, the change in reactivity in the period during which the power level is increased is determined essentially by two factors: the temperature effect (up to the time in which the temperature is stabilized) and the poisoning due to uranium fission products.

When the reactor is operated for 72 hours after a stationary power level is reached, the poisoning effect reaches a constant maximum value for a given power level. The total magnitude of the poisoning effect Δk is 0.0869. Further operation of the reactor at a fixed power level leads to monotonic reduction in the reactivity as a consequence of U^{235} burnup and slag formation; the reduction of reactivity (in a poisoned reactor) per day of operation at full power is $\Delta k = 5.4 \cdot 10^{-4}$.

The temperature effect in the graphite of the side reflector of the reactor should be considered separately. Approximately 2.3% of the heat is dissipated in the side reflector which has an independent cooling system.

To determine experimentally the temperature effect in the reflector, two experiments were carried out at a reactor power level of 3,000 kw.

The first experiment consisted of shutting off the supply of cooling water only in the refrigerator of the reflector cooling system: in the second experiment the circulation of water in the reflector cooling system was cut off completely. As was expected, a positive temperature effect in the reactivity per 1°C, $\Delta k = 3.6 \cdot 10^{-5}$, was obtained; this value is in satisfactory agreement with the calculated value.

TABLE 2

Heat Dissipation in the Fuel Channels of the AES Reactor

Time following shutdown of the reactor, min.	After 20.6 effective days in %	After 34.8 effective days in %	After 56.8 effective days in %
1	–	3.93	5.80
10	–	3.52	5.13
20	–	2.48	4.03
30	–	1.93	3.32
40	–	1.45	2.77
50	0.80	1.17	2.34
60	0.65	0.83	2.13
70	0.49	0.71	1.81
80	0.46	0.77	1.62
90	0.45	0.66	1.48
100	0.43	0.64	1.32
110	0.42	0.49	1.13
120	–	0.42	1.08
130	0.40	–	1.06
140	0.37	–	0.96
150	0.31	–	0.90

The measured graphite temperature in the reflector is found to be somewhat smaller than the calculated value and hence does not exceed the temperature of the graphite in the center of the core when the reactor is operated at full power.

These experiments indicate that it is both possible and feasible to dispense with cooling of the side reflector; in the AES reactor this increases the length of a run by 4 effective days.

Heat Dissipation in the Fuel Channels of the Reactor After Shutdown

A knowledge of the magnitude and nature of the rate at which the heat generation falls off (as a function of time) in the fuel channels of the reactor is of practical interest inasmuch as it is necessary to establish the period of time required to cool the channels after shutdown.

The residual heat generation was determined experimentally in fuel channels which had been used

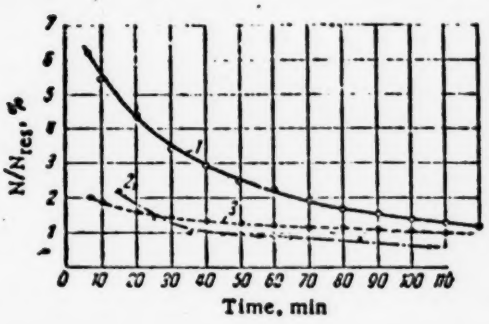

Fig. 5. Heat dissipation in a fuel channel after shutdown. 1) Experimental curve obtained taking into account the graphite heat; 2) experimental curve obtained without taking into account the graphite heat; 3) calculated curve.

in the reactor for 20.6, 34.8, and 56.8 effective days, respectively. The results of the experiments are shown in Table 2. The residual heat generation is given in percentage of the heat generation in a channel before shutdown.

In order to establish the residual heat generation in the fuel channel alone, a calculation was made of the heat removed in the graphite, which was cooled after the reactor was shut down.

In Fig. 5 are shown curves pertaining to heat generation in a fuel channel (operated for 56.8 effective days) obtained by computation and by experiment, with and without heat removal by cooling of the graphite. A comparison of the experimental curve, 2, with the calculated curve, 3, shows satisfactory agreement. The lower value of the calculated heat removal (as compared with the experimentally obtained value) during the first 25 min may be explained by the fact that the Way formula, which was used in this case, does not take into account fission fragments with a half-life $T_{1/2} \leq 3$ hours, which make a considerable contribution to the heat dissipation in the first minutes following shutdown of the reactor.

On the basis of the results of these experiments it is possible to draw the following conclusions which have practical value both for operation of the reactor of an atomic power station as well as similar reactors.

1. It is necessary to consider the contribution, in the residual heat dissipation of the fuel channels, of the heat in the graphite stack of the reactor.

2. The use of the Way formula in calculating heat dissipation in the fuel channels is justified.

3. It is possible to remove fuel channels as soon as 2 hours after reactor shutdown and to place them in storage without special cooling.

4. The magnitude of the residual heat dissipation in fuel channels means that it is not possible to dispense with an emergency system for reactor cooling in the event of failure in the electric supply.

Water Requirements in the Primary Circuit of the Power Reactor

The water used in the primary circuit must meet the following requirements:

1. The water must not produce boiler scale in the heat removal elements.

2. The water must not produce corrosion in the coils of the heat pump of the primary circuit which is fabricated from IX-18-N-9T steel.

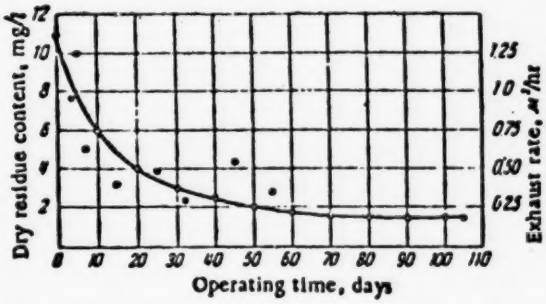

Fig. 6. Variation in the amount of dry residue in the water of the primary circuit.

3. The residual radioactivity of the water must be short-lived and the radiation intensity insignificant in order to make inspection and repair of the equipment possible.

It was decided to fill the primary circuit with bidistillate in which the dry residue content was approximately 0.3-0.5 mg/l.

After assembly all the equipment and turbine pipes in the primary circuit were washed for 32 hours with a 6% solution of NaOH at a temperature 60-70°C and then in a 12% solution of HNO_3 at 60-70°C for 12 hours. Following this, the circuit was rinsed for a day in the condensate at a temperature of 90°C and then in the bidistillate until the original value of the dry residue was obtained.

In the first operating period of the station a rapid increase of dry residue content of the water up to 11 mg/l was observed for a water replacement rate of approximately 1 m^3/hour which corresponded to 10% of the total circuit volume. Later a gradual reduction of the dry residue was observed which was a consequence of the extensive rinsing of the circuit. As is apparent from Fig. 6, a month after operation was initiated, the dry residue content was established at a level of 2.5-3 mg/l ; hence, the water replacement rate was reduced to 0.5-0.6 m^3/hr. At most, in operating the reactor at various power levels, the dry residue content is stabilized at a level of 1.5-2 mg/l at a water replacement rate of 0.2-0.25 m^3/hr.

TABLE 3

Content of Various Elements in the Water of the Primary Circuit (surface of turbine piping 450 m^2, water pressure 100 atmos, temperature 260-270°C, oxygen content $\leq$ $\leq 3 \cdot 10^{-3}$ ml/g)

Element	July 1954		November 1954		September 1956	
	Supply water	Primary circuit	Supply water	Primary circuit	Supply water	Primary circuit
Ca	50	200	50	150	20	70
Mg	30	100	10	30	5	20
Fe	10	100	10	30	10	50
Cr	5	70	5	20	1	10
Ni	10	50	4	4	4	4
Cu	5	20	5	20	3	10
Mn	5	20	5	10	0,1	1
Σ, mg/l	115	560	89	264	43,1	165

The relatively high temperature of the water in the primary circuit (270°C) and the pressure (100 atmos) tend to increase the contamination of the water by the products from the elements of the circuit materials (the turbine pipes, fittings, gland seals and gaskets).

The water contamination rate is an important factor in determining the water requirement of the primary circuit of the station. Furthermore, a determination of the contamination rate is of interest in connection with the operation of other power reactors in which water coolants are used.

To investigate the corrosion rate in the primary circuit due to dry residue, a test was made of the water used in the first operating period. It was submitted to spectral analysis; the results are shown in Table 3.

The results of the analysis indicate that the wash products may be divided into two groups, in terms of their origin:

1. Elements rinsed from stainless steel as a result of corrosion; barium, chromium, nickel, and manganese.
2. Elements washed from the gland seals and gaskets: calcium, magnesium, and copper.

Using the data which were obtained, a determination was made on the corrosion rate in the circuit which, in the first operation run of the station, was 11 mg/m^2 per day and in the steady-state mode (September, 1956) 0.5 mg/m^2 per day. Hence, the corrosion rate in the circuit decreased in time and there was a particularly sharp reduction in the initial operation stage. The latter is explained by the fact that, in spite of the alkali and acid washing of the circuit before startup, there was still a light oxide deposit on the surfaces of the turbine pipes and fittings which was gradually washed off, thereby reducing the purity of the water.

It should also be noted that the reduction of the corrosion rate favors the formation of a protective (inhibiting) film on the inner surfaces of turbine pipes of the primary circuit.

Because there is no boiling in the heat removal elements and because a relatively small corrosion rate is established for the materials in the turbine pipes, it is possible to dispense with the use of bidistillate and to use condensate from the turbine for supplying the primary circuit.

A test has shown that the amount of dry residue in the water of a primary circuit when condensate is used does not exceed 2 mg/l (for a water replacement rate in the circuit of 200-250 l/hour). The corrosion rate, however, remains at the previous level, 0.5 mg/m^2 per day.

Biological-Safety System and Dosimetry Control at the Power Station

The main sources of radioactive contamination at the power station are the water in the primary circuit and the nitrogen gas with which the reactor stack is filled to prevent overheating of the graphite moderator.

The radioactivity of the gas in the reactor is due to the following:

1) argon Ar^{40} (n, γ) Ar^{41} (γ-active), $T_{1/2}$ = 1.8 hours;

2) nitrogen N^{15} (n, γ) N^{*3} (γ- active), $T_{1/2}$ = 7.35 sec.;

3) oxygen O^{16} (n, p) N^{16} (γ-active), $T_{1/2}$ = 7.35 sec.

Inasmuch as the half-lives of the nitrogen and oxygen are small, the radioactivity of the gas dispersed in the atmosphere, neglecting dilution, is determined by the argon dose which is $1.1 \cdot 10^{-4}$ C/m³.

The water leaving the reactor has an activity of $\sim 5 \cdot 10^{-3}$ C/l which is due mostly to the short-lived oxygen radioactivity ($T_{1/2}$ = 7.35 sec.).

The long-term activity of the water of the primary circuit depends on the amount of dry residue and, in fact, amounts to 10^{-6} C/l, which is attributed to the presence of radioactive isotopes: sodium, manganese, calcium, nickel, iron, etc.

The process equipment of the station also are sources of radioactivity: the reactor, the steam generator, the circulation pumps, the piping in the primary circuit, the auxiliary reactor cooling system, the gas transfer system – located at a remote point are completely shielded against radiation.

As a safety measure for personnel of the station, the recharging of the radioactive fuel channels and removal to the storage chamber are performed by remote control. The concrete walls of the central chamber, 2 m in thickness, serve as complete shielding for the adjacent installations. Operational experience has shown the justification of the shield thickness choice which was made for process installations.

The plant of the electric power station has twenty-eight ventilating systems which make it impossible for radioactive air to propagate from one installation to another.

It was found especially important to have good ventilation in the space in front of the reactor to prevent the penetration of radioactive gas from the reactor into the central chamber of the power station.

The space between the reactor and the water shield is not ventilated since this would cause the undesirable removal by the tube of large amounts of radioactive air, having an activity of 10^{-3} C/l.

A dosimetry control system is used to control the level of γ-radiation in the installations of the power station. For this purpose use is made of ionization chambers set up in the process spaces with secondary indicating instruments which were located at a special remote dosimetry control board.

There is a special control system for the concentration of radioactive gases in the process spaces which is based on periodic sampling of the air in these spaces. If the activity in the installations becomes higher than the allowable limit, the alarm system is automatically activated.

The dosimetry group also has at its disposal portable dosimeters which are used to measure the radiation level at a given point. Personnel at the station are furnished with pocket film-badges (with high sensitivity x-ray film) and pocket dosimeters. The photographic monitors are inspected constantly and are taken into account in assigning the work for each operator.

In repairs or other operations which require the servicing of radioactive equipment, a special dosage allowance system is used which takes account of the working time and the protective equipment which is employed (gloves, pneumatic suits, spectacles, gas masks, etc.). A supplementary film-badge is used when work of this nature is carried out; thus it is possible to institute a system of continuous monitoring of the radiation to which the operators are subjected.

The system of adequate biological shielding in conjunction with the comprehensive dosimetry service and regular medical examinations for the operators ensure completely safe working conditions for the station personnel.

The decontamination of radioactive waste water from the plant is carried out in a special decontamination installation which has all the equipment required for extraction, removal and decontamination of the water, including an evaporation setup.

Inasmuch as the waste water of the primary circuit is not very radioactive and contains short-lived isotopes, it is purified and subsequently extracted. The decontamination time varies from 10-15 days. During this period,

the water activity falls from 10^{-8} C/l and following extraction is reduced to the allowable normal level 10^{-10} C/l (the normal level for supply water) after which the water is pumped into the sewage system.

The radioactive air from the space just above the reactor is diluted in the general ventilation system to 10^{-8} C/l and is exhausted to the atmosphere through a chimney 100 m in height.

The total activity of the air exhausted through the ventilating chimney amounts to 1.6 C/hour which is considerably below the design level. Hence, the nuclear power station presents no hazard for the population of the surrounding region.

CONCLUSION

Experience obtained in operating the atomic power station has made it possible to draw a number of important practical generalizations in regard to the operation of power reactors of this type.

The reactor at the nuclear power station is simple in operation and reliable and is capable of operation over long periods of time.

The use of easily removable fuel channels makes it possible to reload the reactor in a relatively short time. The operation of the power reactor and the process equipment of the station do not constitute any hazard to the health of the service personnel and the inhabitants of the surrounding region. The favorable experience in the operation of the power reactor seems to indicate the extensive use of reactors of this type in atomic power applications.

This investigation of the operating characteristics of the power station was carried on by a large number of engineering-scientific workers. The greatest part of the work in the study of the operation of the station was carried out by G. N. Ushakov, Yu. V. Arkhangelsky, V. A. Konovalov, N. A. Sever'yanov, B. A. Semenov, N. T. Belinsky, B. B. Baturov, I. L. Kornilenko, and others.

The authors wishes to express a debt of gratitude to D. I. Blokhintsev, A. K. Krasin, and N. A. Nikolaev, whose general scientific and technical guidance made the reliable operation of the station possible.

LITERATURE CITED

[1] D. I. Blokhintsev and N. A. Nikolaev, First Atomic Power Station in the USSR and the Path for the Development of Atomic Power: Report of the Soviet Delegation to the International Conference on the Peaceful Uses of Atomic Energy (Acad. Sci. USSR Press, 1955).

[2] D. I. Blokhintsev, N. A. Dollezhal, and A. K. Krasin, J. Atomic Energy (USSR) 1956, 1, 10 (T.p. 7).*

[3] D. I. Blokhintsev, M. E. Minashin, and Yu. A. Sergeev, J. Atomic Energy (USSR) 1956, 1, 24 (T.p. 21).*

[4] A. K. Krasin, B. G. Dubovsky, E. Ya. Dollnitsyn, L. A. Matalin, E. I. Inyutin, A. V. Kamaev, and M. N. Lantsov, J. Atomic Energy (USSR) 1956, 2, 3 (T.p. 139).*

[5] E. Way, Phys. Rev. 70, 115 (1946).

Received October 18, 1956

* T. p. = C. B. Translation pagination.

BLANK
PAGE

SPATIAL DISTRIBUTION OF γ-RAYS AND MODERATED NEUTRONS IN THE GRAPHITE COLUMN OF THE RFT REACTOR

V. S. Berezin, L. V. Groshev, V. S. Dikarev, M. B. Eglazarov, E. N. Korolev, V. G. Madeev, and Yu. G. Nikolaev

Measurements have been made of the spatial distributions of neutrons of various energies and the γ-rays in the graphite thermal column of the RFT reactor. The fluxes of thermal, resonance, and fast neutrons were measured using the activity induced in various indicators. The decay in the intensity of the γ-radiation was determined by small condenser type ionization chambers. At distances from 80 to 160 cm the fluxes of resonance and fast neutrons fall off approximately exponentially with a decay length of ~ 13 cm and 15.7 cm, respectively. At large distances the fluxes of fast and resonance neutrons are in equilibrium. The flux of slowed-down neutrons in this region falls off exponentially with a decay length of 18.2 cm as determined by the penetrating fast-neutron component with an energy of approximately 6.6 Mev. The intensity of the γ-radiation in the graphite column falls off in an almost exponential manner with an attenuation coefficient $\mu = 3.78 \cdot 10^{-2}$ cm^{-1}. The theoretical predictions are found to be in satisfactory agreement with the experimental data.

In the spring of 1953 a series of experimental measurements of the spatial distribution of neutrons of various energy and of γ-radiation in the graphite thermal column of the physics-engineering reactor (RFT) was carried out [1]. The need for measurements of this type in planning intelligent operation of the column is obvious. In addition to their practical value, these results are of interest scientifically inasmuch as they provide an experimental basis for verifying various theoretical predictions and calculations involving the spatial distribution of γ-radiation and slowed-down neutrons.

EXPERIMENTAL

The graphite thermal column of the physics-engineering reactor has a cross section of 100 x 100 cm^2 and is 200 cm in length. It is separated from the core of the reactor by a graphite reflector 80 cm thick and an air gap of 45 cm and is surrounded by side walls of cement. An experimental channel, which is filled with graphite rods, runs along the axis of the column. The graphite rods have spaces in which indicators can be irradiated.

The density of thermal neutrons in the graphite is measured by a dysprosium indicator. The indicators for resonance neutrons were indium (E_ϕ = 1.44 ev), gold (E_ϕ = 4.9 ev), and iodine ($E_\phi \approx$ 20-50 ev), enclosed in cadmium. The fast neutron flux was measured by the activity induced in phosphorus and aluminum [the (n, p)-reaction with effective thresholds of approximately 1.5 Mev and 2.5 Mev, respectively). In irradiating the fast-neutron detectors, in order to reduce the background produced by (n, γ)-reactions the detectors were enclosed in boron-cadmium shields.

To reduce the background arising from cosmic rays, a β-instrument with an anti-coincidence scheme was used to measure the activity of the detectors. The half-life, in all experiments, was determined from the decay curve.

The decay in the intensity of γ-radiation along the axis of the thermal column was measured with small condenser type γ-ionization chambers of graphite. The ionization chambers were enclosed in lithium shields in order to eliminate effects due to thermal neutrons arising as a result of a (n, p)-reaction in nitrogen in the air in the ionization space of the chamber. For the ratio of fluxes of γ-radiation and fast neutrons which was measured in the thermal column, one is justified in neglecting the contribution of fast neutrons.

The measurements were performed under steady-state conditions in the reactor in which the power level is maintained at a given value with an accuracy of 1%.

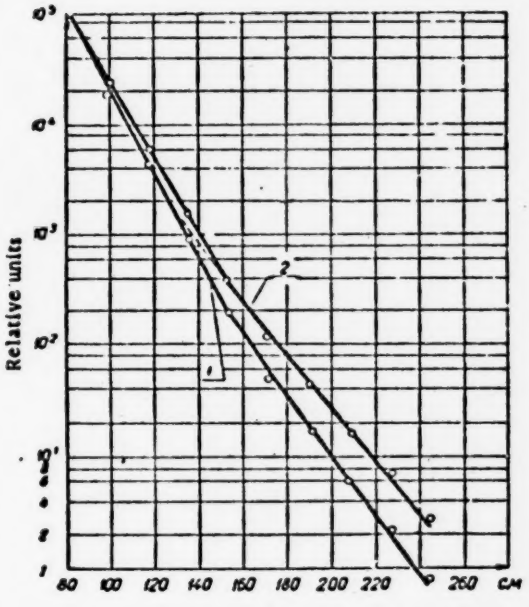

Fig. 1. Spatial distribution of the flux of resonance neutrons in the graphite column(indium, E_0 = 1.44 ev). 1) Results of the measurements; 2) results of the measurements multiplied by the square of the distance from the center of the core to the detector.

Results of the Measurements

The results of the measurements of the spatial distribution of the neutron flux in the graphite medium for various energies is plotted on a semi-logarithmic scale in Fig. 1. In Figs. 1, 2, and 3 the neutron fluxes are plotted along the ordinate axis in arbitrary units while the thickness of the graphite is plotted in centimeters along the abscissa axis (including the thickness of the graphite reflector, 80 cm). In these figures, the curves marked 1 are the raw measured neutron distributions along the axis of the graphite heat column. The curves marked 2 are obtained by multiplying the measured values of the neutron fluxes (curves 1) by the square of the distance from the measurement point to the center of the core. Thus, these curves, 2, correspond to a neutron distribution from a plane source, that is, the geometric attenuation factor due to the separation from the neutron source does not appear.

The mean square error of the measurements is less than 4%. Within the limits of the experimental errors the attenuation curves for the resonance-neutron fluxes measured with gold and iodine indicators are coincident so that they appear as one curve on the graph. A similar congruence was observed in the spatial distribution of fast neutrons measured with the phosphorus and aluminum indicators.

As is apparent from these curves, the decay of the neutron flux occurs at a faster rate in the nearer part of the thermal column than in the outer part. A fairly well-pronounced discontinuity in the slope of the neutron-flux attenuation curves occurs at approximately 160-180 cm. As an approximation it may be assumed that at a graphite thickness of 160 cm, the flux of resonance neutrons with energies 1.44 ev (indium) is higher than those with energies of 4.9 ev (gold, iodine) and that the fluxes of resonance and fast neutrons fall off exponentially with decay lengths of 13.0 ± 0.1, 13.6 ± 0.2, and 15.7 ± 0.2 cm, respectively. Further out, at a distance of 180 cm, the flux of resonance neutrons is attenuated with a decay length of approximately 19 cm and the flux of fast neutrons with a decay length of 18.2 ± 0.3 cm. The decay lengths for neutrons of various energies is found from the relations given by the curves marked 2.

The data pertaining to the measurements of the density of thermal neutrons are shown in Fig. 4. The curve is fairly accurately described by an exponent with a decay length L = 21.6 ± 0.1 cm. Because of various edge effects, the extreme points do not lie on the straight line.

In Fig. 5, in a semi-logarithmic plot is shown the curve of the decay of the γ-radiation level in the graphite column in relative units. The mean square error in the measurements is 3%. The decay curve for the intensity of γ-radiation can be approximated by 2 straight segments, characterized by attenuation coefficients $\mu = 5.8 \cdot 10^{-2}$ cm^{-1} (to a depth of approximately 120 cm) and $\mu = (4.6 \pm 0.04) \cdot 10^{-2}$ cm^{-1} (at depths exceeding 140 cm).

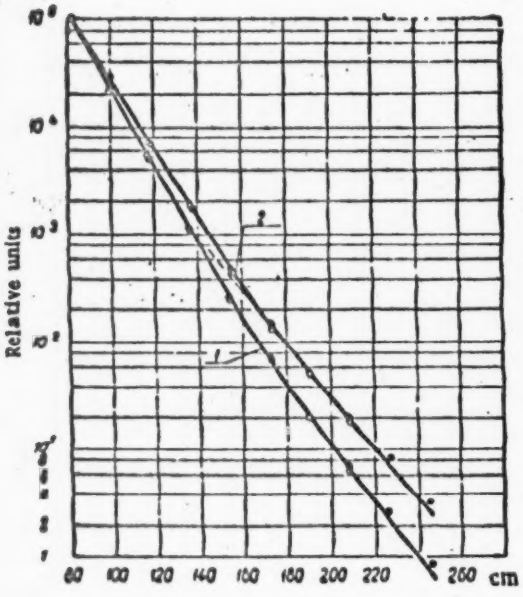

Fig. 2. Spatial distribution of the flux of resonance neutrons in the graphite column. ⊖) Gold, E_0 = = 4.9 ev; ⊛) Iodine, $E_0 \approx 20$-50 ev.

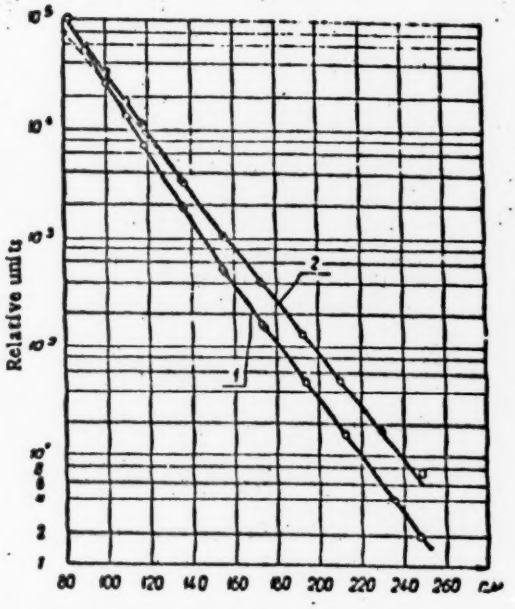

Fig. 3. Spatial distribution of the flux of fast neutrons in the graphite column. O) Aluminum, $E_{eff} \approx 2.5$ Mev; ⊛) phosphorus, $E_{eff} \approx 1.5$ Mev.

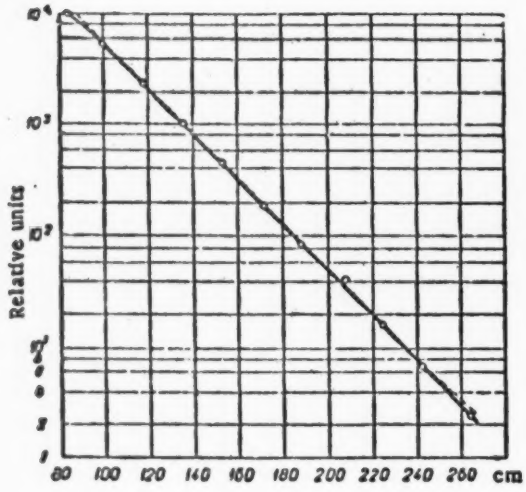

Fig. 4. Spatial distribution of the density of thermal neutrons in the graphite column of the RFT.

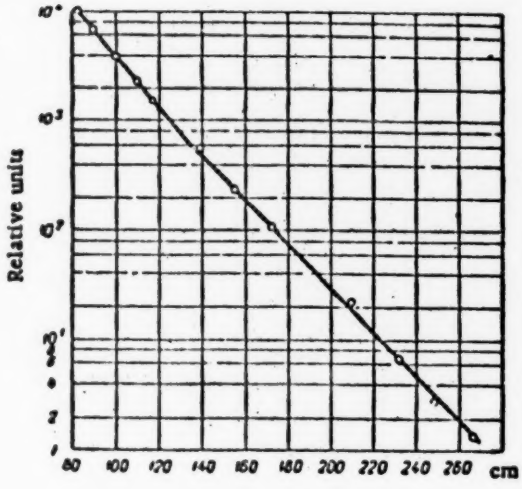

Fig. 5. Spatial distribution of the γ-ray dose in the graphite column of the RFT.

DISCUSSION OF RESULTS

S. I. Drozdov [3] has extended, in an approximate fashion, the calculations given by Wick [2] which make it possible to analyze the asymptotic distribution of the density of slowed-down neutrons from a nonmonochromatic source. In accordance with [3], the flux of slowed-down neutrons in the asymptotic region, in the case of a plain isotropic nonmonochromatic source, is determined by the expression

$$v \cdot n(z, E) \approx \frac{w(E) \cdot l(E)}{2} \cdot \frac{e^{-z/l(E)}}{z} + \\ + \frac{l(E)}{E} \sum_i g_i \cdot Q_i \left(\frac{E_i}{E}\right)^{\eta_i} \cdot \left(\frac{z}{l(E_i)}\right)^{1-p_i} \cdot e^{-z/l(E_i)}. \quad (1)$$

Here $w(E)$ is the spectrum characterizing the neutrons from the source and $g_i = \int_{E_{i-1}}^{E_i} w(E)dE$; Q_i, p_i and η_i are coefficients which depend on the scattering cross section of the moderating medium at the neutron energy in the source E_i. This expression has been obtained using certain simplifying assumptions. In particular, capture and inelastic neutron scattering in the moderating medium are not considered and the free-path length for neutrons $l(E)$ is assumed to fall off monotonically.

The first term in (1) represents the flux of nonscattered (primary) neutrons while the second term represents the flux of neutrons slowed down to a given energy E. The distance from the source may be neglected in the first term.

At very large values of z, because of the strong exponential dependence $e^{-z/l(E_i)}$ only one term will remain under the summation sign in Eq. (1); this corresponds to the maximum scattering length $l(E_i) = l_{max}$, that is, in the asymptotic region the spatial and energy dependences of the slowed-down neutrons are determined by the energy $E_i = E_k$, which corresponds to the maximum scattering length.

The nature of the decay of the experimental curves at large distances (> 180 cm) furnishes a basis for assuming that in this region the resonance neutrons are produced by the penetrating fast neutrons; the flux of resonance neutrons is found to be in equilibrium with the flux of fast neutrons and the spatial distribution of the latter determines the spatial distribution of the resonance neutrons.

The dashed curves in Figs. 1, 2, and 3 correspond to the theoretical distributions for fluxes of neutrons with energies of 1.44 ev, 4.9ev, and 2 Mev. The experimental and theoretical points meet at z = 190 cm. A calculation was performed using Eq. (1) for an infinite graphite medium with a plane neutron source, characterized by a neutron spectrum corresponding to the fission neutron spectrum. The parameters appearing in Eq. (1) were calculated from the computation formulas given in [3].

The true scattering cross section for neutrons in graphite may be approximated by the function

$$\sigma_s(E) = \frac{1}{Nl(E)},$$

where $N = 0.835 \cdot 10^{23}$ nuclei/cm^3 is the average nuclear density of graphite and the scattering length is taken to be a monotonic function. An essential feature of the dependence of the true scattering cross section on energy is the presence of a minimum at an energy of approximately 6.6 Mev where $\sigma_s(E) \approx 0.62 \cdot 10^{-24}$ cm^2 [4]. At this value of the energy the scattering length reaches its maximum value, 19.2 cm.

The value of the scattering cross section at energies greater than 6.6 Mev was not considered since, firstly, the source spectrum falls off sharply for E > 6.6 Mev and, secondly, the increase in the true scattering cross section for E > 6.6 Mev causes the density of neutrons at this energy to be small at distances far from the source.

At distances of 180-240 cm, the calculated decay lengths for resonance and fast neutrons is 18 cm which is in good agreement with the experimental value obtained for fast neutrons. However, the calculated values are somewhat smaller than the decay lengths of the main fast-neutron component determined by the minimum in the scattering cross section in carbon. This indicates that at these distances the factor in front of the exponential plays an important part in the spatial neutron distribution.

Thus, in general, the experimental results corroborate the theoretical predictions. Certain discrepancies between the experimental and theoretical data at distances from 80-160 cm appear as a result of approximations made in the theory, particularly in the computations.

It may be noted that the results of similar work by Hughes [5] are in agreement with the results of the present experiments.

The attenuation of the intensity of γ-radiation with a spectral distribution $w(E) \cdot dE$ is given by the integral

$$I(x) = \int w(E) \cdot f(x, E) \cdot e^{-\mu(E) \cdot x} \cdot dE,$$

where I(x) is the intensity of the γ-radiation at a depth x; $\mu(E)$ is the attenuation factor for γ-quanta with an energy E in the scattering medium, f (x, E) is a certain function of the distance x and the energy of the γ-quanta.

The dependence of the exponential term $e^{-\mu(E) \cdot x}$ on thickness x is much stronger than that of the term in front of the exponential f(x, E). Hence, at rather large depths, the most penetrating component of the γ-radiation is absorbed in the material and the decay of the intensity of radiation will be determined basically by an exponent with an attenuation factor $\mu(E) \approx \mu_{min}$ corresponding to the most penetrating γ-component of the spectrum.

These theoretical conclusions are supported by the experiment. The initial segment of the attenuation curve for the γ-radiation intensity (Fig. 5) corresponds to absorption of the soft part of the γ-radiation, coming from the core of the reactor. At large distances (exceeding 140 cm) an equilibrium sets in between the primary and scattered radiation and the decay of the intensity should be due to the most penetrating part of the γ-radiation. In this region the attenuation factor, taking into account the spherical experimental geometry, is $\mu = (3.78 \pm 0.04) \times 10^{-2}$ cm^{-1}.

As has been shown by measurements with a magnetic spectrometer [6], the most intense lines in the spectrum of γ-radiation produced by neutron capture in the construction materials of the RFT reactor and the graphite column are the iron lines at an energy of 7.63 Mev and the carbon line at an energy of 4.95 Mev. The calculated values of the absorption factors for these lines in graphite with a nuclear density $N = 0.835 \cdot 10^{23}$ nuclei/cm^3 are, respectively, $\mu = 3.62 \cdot 10^{-2}$ cm^{-1} and $\mu = 4.47 \cdot 10^{-2}$ cm^{-1} [7]. Both lines have attenuation coefficients in graphite close to those measured in the experiment.

LITERATURE CITED

[1] G. N. Kruzhilin, Reactor Design and Theory of Reactors: Report of the Soviet Delegation to the International Conference on the PeacefulUsesof Atomic Energy (Acad. Sci. USSR Press, 1955), p. 49.

[2] G. C. Wick, Phys. Rev. 75, 738 (1949).

[3] S. L Drozdov, Report Acad. Sci. USSR 1953.

[4] D. J. Hughes and J. A. Harvey, Neutron Cross Sections (Brookhaven National Laboratory, New York, 1955).

[5] D. J. Hughes, Nucleonics 2, 30-35 (1953).

[6] U. Fano, Nucleonics 8, 8-12 (1953); 9, 55-61 (1953).

[7] L. V. Groshev, B. P. Adyasevich,and A. M. Demidov, Physics Research: Report of the Soviet Delegation to the International Conference on the PeacefulUsesof Atomic Energy (Acad. Sci. USSR Press, 1955), p. 252.

Received May 17, 1956

BLANK
PAGE

AN INVESTIGATION OF THE DIFFERENTIAL CROSS SECTION FOR ELASTIC SCATTERING OF 19.4-MEV PROTONS BY NUCLEI OF T, He^3, He^4, N^{14}, AND O^{16}

R. A. Vanetsian and E. D. Fedchenko

The differential cross section has been measured for elastic scattering of 19.4-Mev protons by nuclei of T, He^3, He^4, N^{14}, and O^{16}. The proton source was a linear accelerator. The protons were scattered on a gas target at pressures from 520 to 620 mm Hg. The scattered protons were recorded by two CsI(Tl) crystal scintillation counters. The differential cross sections for T, He^3, and He^4 have about the same variation, but the minimum for He^4 is somewhat higher and is displaced in the direction of small angles. At small angles the cross section for T is considerably higher than for He^3 and He^4.

The differential cross sections for N^{14} and O^{16} are also of similar structure, but the depth of the minima and height of the maxima are greater for O^{16} than for N^{14}. Comparison of our data with that of other authors shows that as the atomic number increases for a given proton energy, the positions of the minima for all elements are displaced towards smaller angles. As the energy of the scattered protons increases, the minima in the differential cross section for T and He^3 is displaced towards larger angles, whereas for all heavier nuclei this displacement is towards smaller angles.

The investigation of differential cross sections for elastic scattering of nucleons with energies from one to several times ten megavolts by nuclei has recently attracted the attention of many experimentalists [1-19]. The shape of the differential cross section in this interval is very sensitive to energy changes.

By examining the dependence of the differential cross section on the energy of the scattered nucleons and on the atomic weight of the scattering nuclei, one may verify various models and define the limits of their applicability. This explains the intensive experimental and theoretical investigation of elastic scattering of nucleons on various nuclei in this energy region.

The present work is devoted to the investigation of the differential cross section for elastic scattering of 19.4-Mev protons by nuclei of T, He^3, He^4, N^{14}, and O^{16}.

Experimental Apparatus

The source of 20-Mev protons was a linear accelerator, whose complex construction and equipment was developed in 1950 at the Physico-Technical Institute of the Academy of Sciences USSR by P. M. Zeidlits, A. M. Nekrashevich, L. L. Bolotina, Ya. A. Shutskever, B. S. Akshanova, N.E. Kovpak, and K. A. Leontovich.

The protons are accelerated by electromagnetic standing waves excited in volume resonators. The accelerator operates on a 215 cm wave.

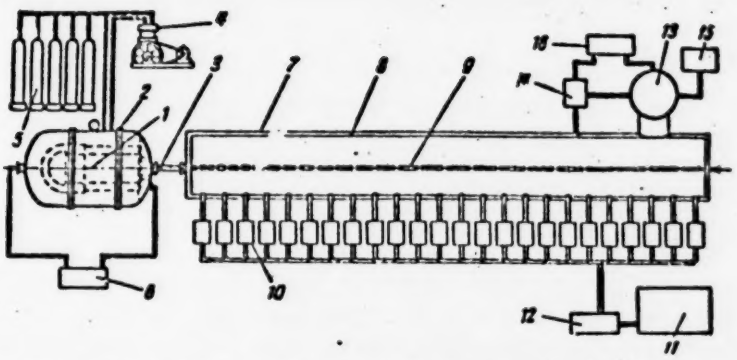

Fig. 1. Diagram of the linear accelerator. 1) Electrostatic generator; 2) container; 3) connecting tube; 4) compressor; 5) gas tanks; 6) control panel; 7) resonator casing; 8) resonator; 9) drift tubes; 10) high-frequency generators; 11) rectifier; 12) control panel; 13) diffusion pump; 14) pre-vacuum pump; 15) refrigerator; 16) control panel.

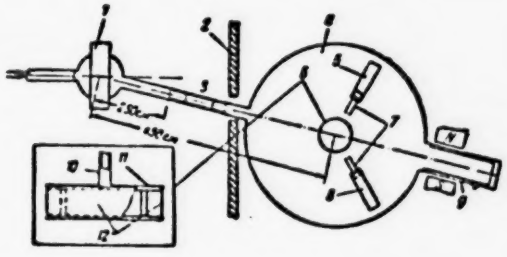

Fig. 2. Diagram of the experiment. 1) Magnet; 2) shielding; 3) collimator; 4) scattering chamber; 5) counter I; 6) target; 7) collimators; 8) counter II; 9) Faraday cylinder; 10) evacuation tube; 11) casing; 12) foil.

Figure 1 shows the fundamental principle of the accelerator. The vacuum chamber 7 is a 15 m steel tube with a diameter of 200 cm, separated along its length into two parts. Within the vacuum chamber is the volume resonator 8 of the accelerator, whose length is 14.5 m. Fifty drift tubes 9 are located along the axis of the resonator. The accelerator is supplied by twenty high-frequency generators with a pulsed power output of 1.2 megawatts. Within the accelerator the pressure is maintained at $1\text{-}2\cdot10^{-6}$ mm Hg. The evacuation is performed by an oil diffusion pump 13 of capacity 40,000 liters/sec. The proton injector is an electrostatic generator 1 under pressure, of the horizontal type, whose pulsed output consists of 500 μsec pulses of protons accelerated to an energy of 1.7 Mev. The mean proton current of the injector in a pulse is about 1 ma.

The accelerator gives two proton pulses per second, lasting for 250 μsec each. The intensity of each pulse is about 10^9 protons. The beam is collimated by a 10 mm slit, and is deflected through 12° by a magnet. At a distance of 2.5 m from the center of the magnet there is a second collimator whose length is 680 mm, consisting of four diaphragms. The diameters of the diaphragms, in the order in which the proton beam reaches them, are 5, 5.5, 5.3, and 8 mm. After the second collimator the beam enters the scattering chamber (Fig. 2) which is a hollow cylinder of diameter 1 m and height 0.5 m. The interior of the chamber may be observed through its upper plexiglas cover. The pressure within the chamber is maintained at 10^{-5} mm Hg. At the center of the scattering chamber is a gas target, and 25 cm from it are two CsI(Tl) crystal scintillation counters which can be placed at any angle to the proton beam. The gas target can be filled and evacuated and the counters can be moved without removing the cover of the chamber. The unscattered proton beam enters a Faraday cylinder behind the gas target.

The gas target is a hollow cylinder of diameter 130 mm and height 20 mm. The upper and lower planes are in the form of heavy discs 10 mm thick held together in four places by cross pieces, with the remaining openings sealed by a 22 μ copper foil. The measurements were taken at pressures from 520-620 mm Hg. In order to avoid counting protons scattered by the front and rear walls of the target, collimators are placed in front of the counters to exclude the points where the beam enters and leaves the target from the field of view of the crystals; these collimators also determine the effective thickness of the target. In measuring the background, the crystals were covered with aluminum foils 2.5 mm thick.

Recording Circuit

From the photomultipliers the signals were applied to amplifiers with amplification constant from 50-100. From one of the amplifiers the signals were applied to a single-channel discriminator capable of analyzing pulse heights from 1-100 v with a gate varying from 2-10 v. The pulses from the second amplifier were applied to an integrating discriminator with a cutoff which could be continuously varied from 1-80 v. The total resolving time is about 2.5 μsec.

The beam current was measured by a current integrator (developed by Zalyubovsky) connected to the Faraday cylinder. A test and calibration of the integrator showed that it is linear for currents from 10^{-9} - 10^{-11} amp.

In order to exclude errors due to secondary electrons in the current measurements, the Faraday cylinder was located in a lateral magnetic field of 1 kilogauss.

Measurement

Before measuring the differential cross sections, the initial energy of the proton beam was measured in the following two ways: 1) by absorption in aluminum; 2) by measuring the deflecting magnetic field. Both methods showed that the maximum intensity of the proton beam corresponds to an energy of 19.8 Mev and a half-width of 0.4 Mev.

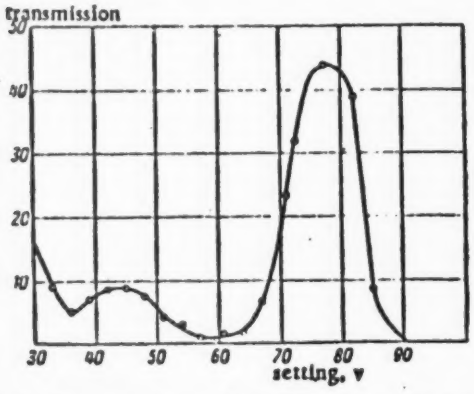

Fig. 3. Energy spectrum of protons scattered by T nuclei at an angle of 30°.

The stability of the magnetic field deflecting the beam was maintained to ± 0.3%. This stabilization, in conjunction with the above-described collimation, made it possible to obtain protons with energy 19.8 ± 0.3 Mev. In passing through the front wall of the target, the protons lose an energy of 0.370 Mev. The energy lost in the gas target, even for oxygen, was no greater than 0.06 Mev. Thus the mean energy of the scattered protons was taken as 19.4 ± 0.3 Mev.

After measuring the initial proton energy, the energy spectrum of scattered protons was measured at several angles for each gas.

The scattered protons, before entering the crystal scintillation counter, lose energy in the gas target, in the copper foil (target wall), and in the aluminum foil which shields the crystal from light. Therefore the energy at which the elastically scattered protons are incident on the crystal had to be calculated for each angle. The corresponding curves were drawn for each element.

The spectrum for several angles was measured for the following purposes: 1) in order to determine the width of the spectrum of elastically scattered protons, so that the inelastically scattered ones could be properly discriminated against; 2) to investigate the change of the spectrum of elastically scattered protons for different angles, in order to verify the linearity of the recording circuit for various energies.

The results of these measurements showed that the recording circuit causes some increases in the width of the spectrum. The half-width of the elastically scattered proton spectrum was about 8% for all gases, whereas that for the primary beam was only about 3%. The displacement of the elastically scattered spectrum with change of angle agreed with calculation, which indicated the linearity of the recording circuit. In measuring the energy spectrum of the protons scattered by T at an angle of 30°, in addition to the peak corresponding to elastic proton scattering, a peak due to recoil tritium nuclei was observed, which could be easily discriminated against (Fig. 3).

In the case of He^3 and He^4, the peaks due to recoil nuclei were very much smeared out and had very low energies. For O^{16} the inelastically and elastically scattered protons had clearly different energies and were easily separated, but for N^{14} the separation of elastic scattering required careful measurements of the spectra at large energies due to the presence of inelastic scattering corresponding to the excitation of the 2.3 Mev level.

After the spectra were measured, the single-channel discriminator was switched to the integral form of operation, the necessary cutoff was set for each angle, and the two counters and Faraday cylinder were used to observe the absolute differential cross section for elastic scattering in the interval of angles from 15° to 160° in 5° steps.

Experimental Errors

The angular resolution of each counter due to the dimensions of the target was 4°. The position of the counters was accurate to 0.2°. The angle of divergence of the direct beam was no greater than 0.5°.

A significant error in determining the absolute value of the cross section arises due to the inaccurate measurement (± 5%) of the experimental geometry. The pressure and temperature of the gases investigated was measured with accuracy sufficient to determine the number of nuclei with an uncertainty no greater than ± 0.5%. The beam current was measured to an accuracy of ± 1%. Therefore the absolute cross section can be considered accurate only to ± 6%. Errors in the relative shape of the cross section could be particularly large for small and large angles due to the background. The background at small angles was determined primarily by radiation from the target walls. Small displacements of the maximum intensity within the direct beam made this background very irregular, and since at small angles (15°) this background was from 40 to 70% of the total effect, the cross section at these angles could be measured only with an accuracy from ± 15 to ± 25%. For angles from 35 to 150° the background due to the target was practically absent.

For large angles the greatest background was observed in the case of T, He^3, and He^4, for which the energy of the scattered protons, starting at 120-130°, was of the same order as the energy of the γ-rays and neutrons from the linear accelerator.

Some error in the relative shape of the cross section for N^{14} could be due to inelastic scattering from the 2.3-and 3.9-Mev levels. Careful measurements of the spectra for these elements, however, showed that the maximum error for angles greater than 130° could be no greater than ± 5%.

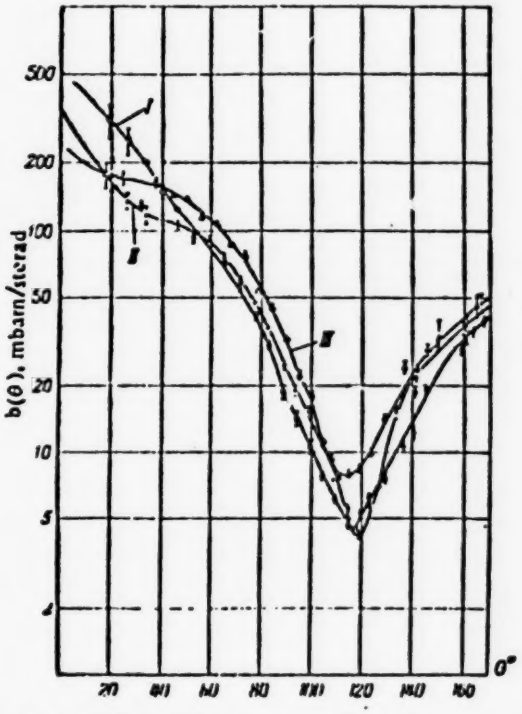

Fig. 4. Differential cross section for elastic scattering of protons with E_p = 19.4 Mev on T(I), He^3(II), and He^4(III) in the center-of-mass system.

The cross sections obtained in the region of sharp minima may be somewhat too high due to the insufficient angular resolution.

The experimental curves presented include the maximum experimental errors. At large and small angles the maximum errors are determined by the distribution of measurements, and at angles in the region of 90° they are determined by statistics. The statistical error at each point was no greater than ± 2.5%.

Results

The experimental results are shown in Figs. 4 and 5.

The differential cross sections for elastic scattering on T, He^3, and He^4 have similar shapes: as the scattering angle is increased the cross sections drop to a minimum in the region of 110-120°, and then increase again. The details of variation of these curves, however, are different for the three elements.

Comparison of the cross sections for T and He^3 shows that the positions and depths of their minima practically coincide. The magnitude of the cross sections at small angles, however, is greater for T than for He^3. Comparison of the cross sections for He^3 and He^4 shows that at small angles the cross sections vary differently, with that of He^4 being greater than that of He^3. The

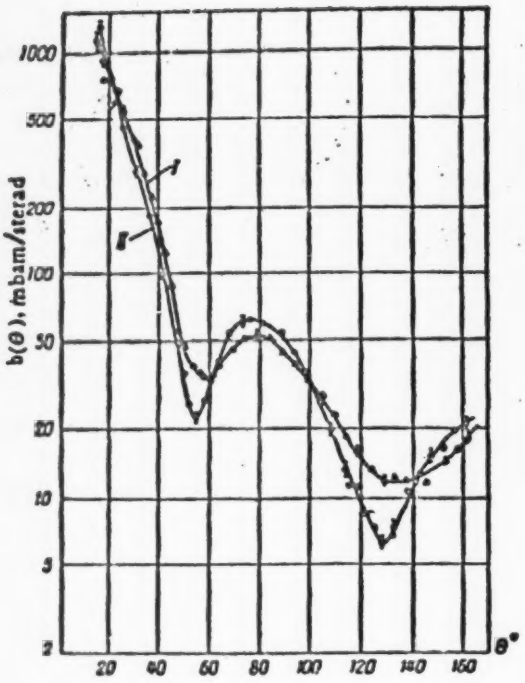

Fig. 5. Differential cross section for elastic scattering of protons with E_p = 19.4 Mev on N^{14}(I), O^{16} (II) in the center-of-mass system.

TABLE 3

E_p, Mev.	1.5	2.5	3.04	3.59	5.8	9.5	19.4
θ_{min}	75°	95°	115°	120°	117°	115°	110°

minimum for He^4 is located at a somewhat lower angle and is somewhat higher. For comparison, we note that the differential cross section for elastic scattering of 20.6-Mev protons on deuterium [3] is of the same character, except that the low-angle cross section for D is less than for T, He^3, or He^4, and that the minimum is at about 130° and is equal to $2.64 \cdot 10^{-27}$ cm^2/sterad. The differential cross sections for N^{14} and O^{16} have similar structures, but that for O^{16} at the minimum is less, and the maximum is greater, than for N^{14}. Comparison of the position of the minima shows that in O^{16} they are located at smaller angles. Comparison of the location of the minima (or maxima) for all available elements from D to U^{238} in the given energy region leads to the conclusion that they move towards smaller angles with increasing atomic numbers [3, 16].

TABLE 1

E_p, Mev	1.5	5.78	9.7	20.6
θ_{min}	90°	117°	120°	130°

TABLE 2

E_p, Mev	1	1.45	2.5	3.5	19.4
θ_{min}	80°	88°	100°	107°	118°

If we compare the energy dependence of the differential cross sections for elastic scattering of nucleons on nuclei, the lightest elements (such as T, He^3, D) do not obey the general rules. The energy dependence of the position of the minima in the differential cross sections for deuterium [1-3] and tritium [4-6] are shown in Tables 1 and 2.

For He^3 a similar dependence is observed: as the proton energy is varied from 1 to 19.4 Mev, the minimum moves from 80 to 119°. Thus as the energy is increased, the minimum for all these nuclei moves monotonically towards higher angles [7]. The cross section for He^4 [8, 9] behaves differently (Table 3).

In this case, as the proton energy is increased to 3.5 Mev, the minimum moves towards larger angles, and above 3.5 Mev it begins to move in the opposite direction.

If we compare the differential cross sections for elastic scattering on N^{14} and O^{16} for E_p = 9.5 Mev [14] with our data, it is seen that the minima and maxima move towards smaller angles as the energy is increased. This same behavior is observed for all heavier nuclei.

The difference in the energy dependence of the differential cross sections for the lightest nuclei (D, T, He^3) from that for all other nuclei, would seem to indicate different types of interaction between the nuclei, depending on whether saturation of nuclear forces has occurred.

The various magnitudes for the cross sections at the minima and maxima for various nuclei as shown on our experimental curves may be due both to the spin-dependence of nuclear forces (different magnitudes for the cross sections are obtained for similar elements with different spins: $S_T = 1/2$; $S_{He^3} = 1/2$; $S_{He^4} = 0$; $S_{N^{14}} = 1$; $S_{O^{16}} = 0$), and to different probabilities for elastic processes.

At the present time an attempt is being made to solve this problem of irregularity by suitable calculations.

In conclusion the authors express their gratitude to I. V. Kurchatov, K. D. Sinelnikov, E. K. Zavoisky, and A. P. Klyucharev for valuable advice and constant attention to the work, to P. V. Chikin who carried out the work on the electronic circuit, and to the maintenance personnel of the accelerator under the direction of A. M. Smirnov, and to A. I. Bazi for discussion of the results.

LITERATURE CITED

[1] J. C. Allred, A. H. Armstrong et al., Phys. Rev. 88, 433 (1952).

[2] J. C. Allred, A. H. Armstrong, and L. Rosen, Phys. Rev. 91, 90 (1953).

[3] D. O. Coldwell and J. R. Richardson, Phys. Rev. 98, 28 (1955).

[4] A. Hemmendinger and J. Taschek, Phys. Rev. 76, 1137 (1949).

[5] M. E. Ennis and A. Hemmendinger, Phys. Rev. 95, 772 (1954).

[6] Classen, Brown, Frier et al., Phys. Rev. 82, 589 (1951).

[7] Famularo, Brown et al., Phys. Rev. 93, 928 (1954).

[8] T. M. Putman, Phys. Rev. 87, 932 (1952).

[9] J. R. Smith, Phys. Rev. 95, 730 (1954).

[10] D. C. Dodder and J. L. Gammel, Phys. Rev. 88, 520 (1952).

[11] R. M. Frank and J. L. Gammel, Phys. Rev. 99, 1409 (1955).

[12] G. E. Fischer, Phys. Rev. 96, 704 (1954).

[13] W. E. Burcham, W. M. Gibson et al., Phys. Rev. 92, 1268 (1953).

[14] E. J. Burge, Y. Fujumotto, and A. Hoslen, Phil. Mag. 1, 19 (1956).

[15] J. E. Dayton, Phys. Rev. 95, 754 (1954).

[16] B. L. Cohen and R. V. Neidigh, Phys. Rev. 93, 282 (1954).

[17] R. D. Woods and D. J. Saxon, Phys. Rev. 95, 577 (1954).

[18] T. W. Bonner, F. Albo, and A. Fernader, Phys. Rev. 97, 987 (1955).

[19] W. D. Whitehead and S. C. Snowdon, Phys. Rev. 92, 114 (1953).

Received July 19, 1956

A MEASUREMENT OF THE U^{233}, U^{235}, Pu^{239} TOTAL CROSS SECTIONS, AS WELL AS THE FISSION CROSS SECTION OF U^{235} FOR RESONANCE NEUTRONS

V. V. Sokolovsky, V. V. Vladimirsky, I. A. Radkevich, and A. A. Panov

The measurement of the interaction cross sections between resonance neutrons and fissionable isotopes are of definite importance both for reactor calculations and for the construction of various nuclear models. In this work we present the results of measurements of the U^{233}, U^{235}, and Pu^{239} total cross sections, as well as the fission cross section of U^{235}. The measurements were performed on a mechanical neutron spectrometer (neutron chopper) with a resolution of 0.1-0.2 μsec/m in the neutron energy region from 3-5 to about 500 ev. The resonance parameters are calculated to energies of about 30-50 ev, for which the levels may still be considered resolved. For these resonances the neutron widths $g\Gamma_n$ are determined; the total widths Γ are determined for sufficiently excited levels when the uncertainty in this determination is no greater than about 50%. For U^{235} resonance in the energy region from 2.5 to 20 ev, in addition to the above parameters, the ratio of the fission width Γ_f to the total width Γ is found.

INTRODUCTION

Before the International Conference on the Peaceful Uses of Atomic Energy at Geneva, the literature contained only data on the U^{235} cross section in the thermal neutron energy region [1-3]. At the Geneva conference, experimental values for the total cross sections and fission cross sections of U^{233}, U^{235}, and Pu^{239} were presented primarily by scientists from the USSR [4-7], the U.S.A. [8, 9], and England [10, 11]; the most complete data both for the variation of the cross section and for the characteristic resonance levels were obtained for U^{235}. The experiments were performed primarily by time-of-flight methods, with various resolutions from about 0.1 to 0.4 μsec/m.

The observed variation of the cross section and the positions of the resonance levels up to energies of about 50-100 ev are in good agreement with each other. The resonance parameters for these elements are measured with sufficient accuracy for neutron energies from thermal to about 3-5 ev.

Literature on the characteristic resonance levels of U^{233}, U^{235}, and Pu^{239} at energies greater than 3-5 ev (with the possible exception of U^{235}) is still insufficiently accurate or complete, since many weak levels may remain unobserved by transmission measurement methods.

In the present work we present the results of total cross section measurements for U^{233}, U^{235}, and Pu^{239}. The measurements were performed on a neutron spectrometer with a resolution of about 0.1-0.2 μsec/m from 3-5 to 500 ev. The resonance parameters are calculated up to energies of the order of 30-50 ev, at which the levels may still be considered resolved. For these resonances we determine the neutron widths Γ_n; the total widths are determined for sufficiently excited levels if the error in this determination is no greater than 50%. On the whole about 100 resonances were investigated. An attempt is made to treat the obtained data statistically in order to compare it with theory.

Method of Treating the Results

The construction of the neutron spectrometer used for measuring the U^{232}, U^{235}, and Pu^{239} cross sections is described elsewhere [4, 12, 13]. The total cross-section measurements were performed by measuring the transmission by samples of various thicknesses. The resonance parameters of the nuclear levels, namely the total cross section at resonance σ_0, the total level width Γ, and the neutron width $g\Gamma_n$ [up to a factor $g = 1/2\,[1 \pm 1/(2I+1)]$, where I is the spin of the target nucleus] were determined by using the "area method" [14, 15] with corrections for the Doppler effect.

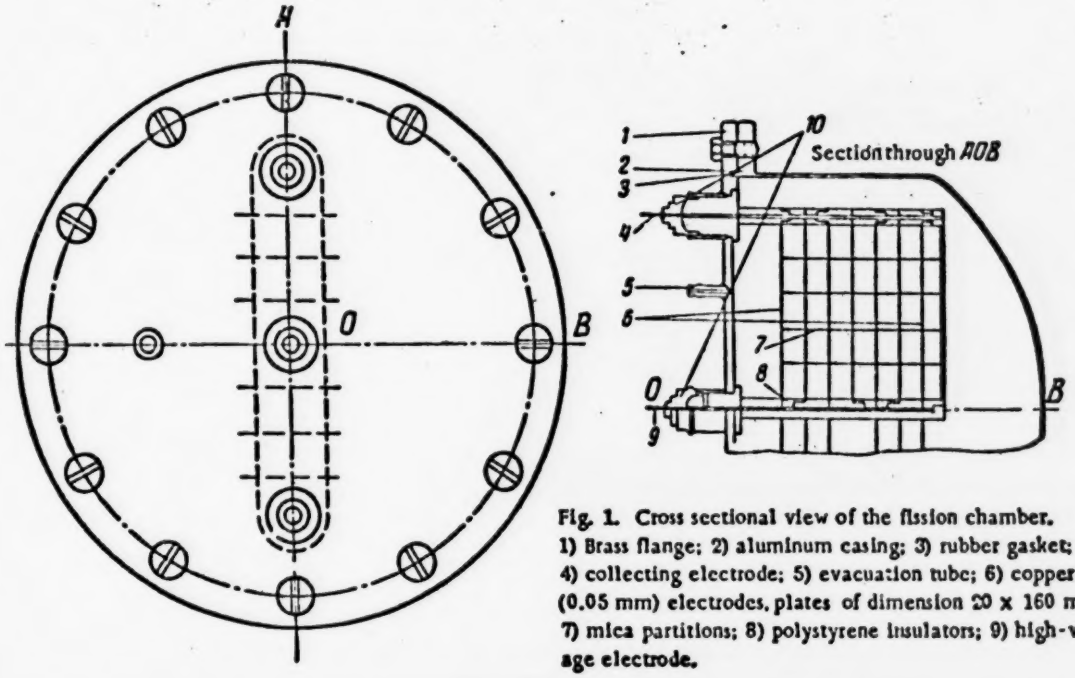

Fig. 1. Cross sectional view of the fission chamber. 1) Brass flange; 2) aluminum casing; 3) rubber gasket; 4) collecting electrode; 5) evacuation tube; 6) copper (0.05 mm) electrodes, plates of dimension 20 x 160 mm^2; 7) mica partitions; 8) polystyrene insulators; 9) high-voltage electrode.

The accuracy of this method is determined primarily by the proper choice of the sample thickness and the accuracy in the measurement of the area A_E of the dip in the transmission curve. The inaccuracy in the area A_E depends on the statistical error in the determination of the total and nonresonance transmission and on such difficult-to-calculate factors as the uncertainty in the wings of the resonance dip, the effects due to close-lying levels, etc. In our results we include only the statistical error.

The fission cross section of U^{235} was measured in a fission chamber containing about 280 mg of U^{235}. The chamber (Fig. 1) consisted of eight electrodes covered with layers of U^{235} oxide which was deposited electrolitically. The area of these layers is 20 x 160 mm^2. To avoid the α-particle background, the spaces between the electrodes were divided by mica partitions into separate cells whose dimensions were 10 x 20 mm^2. The chamber was filled with chemically pure argon to a pressure of 600 mm Hg. In order to increase the counting efficiency, the chamber was located at a distance of about 10 m from the neutron chopper; the spectrometer resolution was about 0.2 μsec/m.

The relative energy dependence of the fission cross section (corrected for the incident neutron spectrum) was normalized to the value of 580 barns at 0.0253 ev. The area of the resonance A_f is related to the resonance parameters by the relation

(1)

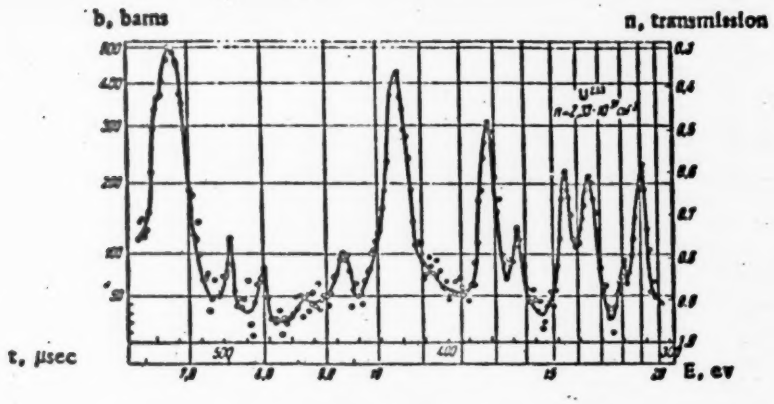

Fig. 2. Transmission by U^{233} in the neutron energy region from 6.5 to 20 ev for sample No. 2.

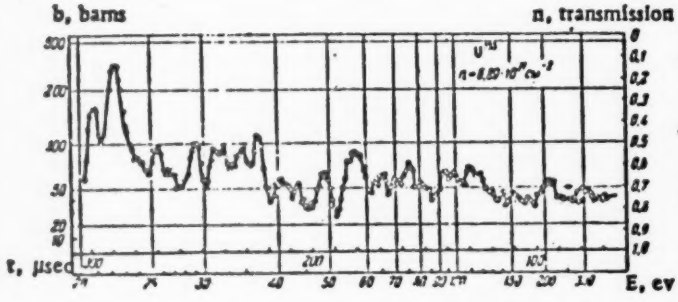

Fig. 3. Transmission by U^{233} in the neutron energy region from 20-350 ev for sample No. 1.

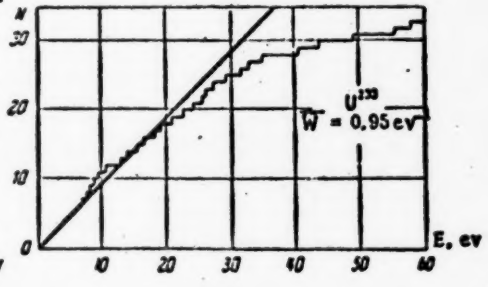

Fig. 4. The number of levels N observed in U^{233} as a function of energy.

where Γ_f is the fission width, and σ_{0f} is the fission cross section at resonance. This expression is valid for a thin sample, i. e., for the condition $n\sigma_{0f} \ll 1$, which was satisfied in our case.

If Γ and $g\Gamma_n$ are known from independent measurements, Eq. (1) can be used to calculate σ_{0f} and Γ_f. It is easy to see, however, that the accuracy in the determination of these quantities will be lower than in Γ and Γ_n due to additional sources of error such as the correction for the incident spectrum and the normalization. The results given for these quantities include only the statistical uncertainty.

Results

1. Total U^{233} cross section. Three samples of U^{233} oxide containing 86.76% uranium were investigated. Mass-spectrographic analysis of the samples gave the following results: U^{233} – 93.3%, U^{238} – 3.85%, U^{234} – 2.34%, U^{235} – 0.5%, and $Th^{232} < 0.2\%$. The surface density of U^{233} nuclei was $6.89 \cdot 10^{21}$ cm^{-2} (sample No. 1), $2.33 \cdot 10^{21}$ cm^{-2} (sample No. 2), and $0.917 \cdot 10^{21}$ cm^{-2} (sample No. 3). Samples Nos. 2 and 3 were investigated in the neutron energy region from 6-22 ev; Samples Nos. 1, 2, and 3 were investigated in the energy region from 18-450 ev. The observed transmission is shown in Figs. 2 and 3.

In order to determine the limiting energy at which weak resonance levels may remain unobserved, we investigated the dependence of the number levels observed on the energy (Fig. 4). This graph shows that at energies above 20 ev there arises a noticeable error in the number of energy levels observed. The slope of the straight line gives an average energy density $\overline{W} = 0.95 \pm 0.11$ ev^{-1} for the two possible spin states of the compound nucleus $I_1 = 2$ and $I_2 = 3$.

TABLE 1

Resonance Parameters of U^{239}

E_0 ev	σ_0 barns	Γ mv	$\sigma\Gamma_n$ mv	$\sigma\Gamma_n^0=\sigma\Gamma_n\left(\frac{1ev}{E_0 ev}\right)^{1/2}$ mv	Remarks
6.80±0.03	1360±680	120±40	0.424±0.064	0.163±0.025	Sample No. 2. 3
7.5±0.1			0.015	0.006	" No. 2: $\sigma_0\Gamma=5$
8.0±0.1			0.03	0.01	" No. 2: $\sigma_0\Gamma=10$
8.6±0.1			0.02	0.007	" No. 2: $\sigma_0\Gamma=7$
9.3±0.1			0.04	0.013	" No. 2: $\sigma_0\Gamma=12$
10.44±0.05	500±200	300±100	0.593±0.048	0.187±0.015	" No. 2. 3
12.82±0.05	400±150	370±160	0.571±0.061	0.160±0.017	" No. 2. 3
13.74±0.07			0.160±0.03	0.043±0.008	" No. 2. 3
15.54±0.09			0.441±0.085	0.112±0.022	" No. 2. 3
16.45±0.10		90±60	0.705±0.132	0.174±0.033	" No. 2. 3
18.0±0.2			0.050	0.012	" No. 2: $\sigma_0\Gamma=7$
19.05±0.12	830±230	120±25	0.714±0.060	0.164±0.014	" No. 1. 2, 3
20.85±0.15 *)	1200±350	60±20	0.560±0.041	0.123±0.009	" No. 1. 2, 3
22.35±0.15	660±160	450±80	2.57±0.14	0.545±0.030	" No. 1. 2, 3
25.4±0.2			0.12	0.024	" No. 1. 2; $\sigma_0\Gamma=12$
25.9±0.2			0.08	0.016	" No. 1. 2; $\sigma_0\Gamma=8$
29.2±0.2	280±180	300±150	0.965±0.14	0.178±0.026	" No. 1. 2
31.3±0.3			0.588±0.119	0.105±0.021	" No. 1. 2
32.3±0.3			0.655±0.106	0.115±0.019	" No. 1. 2
34.7±0.3			1.11±0.174	0.188±0.030	" No. 1. 2
37.0±0.3		55±25	2.18±0.39	0.358±0.064	" No. 1. 2
40.4±0.4			0.63±0.18	0.10±0.03	" No. 1. 2
43.5±0.4			0.22±0.040	0.034±0.006	" No. 1. 2
49.0±0.5			1.35±0.39	0.193±0.056	" No. 1. 2
55.5±0.6			1.41±0.35	0.189±0.047	" No. 1. 2
58.0±0.7			3.2±0.7	0.42±0.09	" No. 1. 2

* The U^{238} level at 21 ev is not eliminated.

Table 1 shows the resonance parameters as calculated by the above method.

The positions of the resonance levels as obtained in our investigation are in good agreement with the results of several other authors [5, 6, 10]. Previous values [5] for $\sigma_0\Gamma^2$ at energies of 6.8, 10.44, and 12.82 ev are in agreement with ours within the limits of experimental error.

The resonance levels at the energies 62.5, 65.5, 70, 75.5, 84, 93, 100 and 110 ev cannot be considered resolved, and therefore we have not calculated their parameters.

2. The total U^{235} cross section. Three samples of U^{235} oxide were investigated with nuclear surface densities of $7.92\cdot10^{21}$ cm^{-2} (sample No. 1), $2.87\cdot10^{21}$ cm^{-2} (sample No. 2), and $0.89\cdot10^{21}$ cm^{-2} (sample No. 3). These samples had the following isotope content: U^{235} – 90.0%, U^{238} – 8.8%, U^{234} – 1.2%. Samples Nos. 1 and 2 were used for measurements in the neutron energy region from 3.3 to 7 ev (using a neutron chopper with curved slits), and all three samples were used in the energy region from 6 to 500 ev. The experimental results from sample No. 2 are shown in Figs. 5, 6, and 7. The resonance level at 5.2 ev, which according to other authors [18] does not exist in U^{235}, was assigned to U^{234}. On this assumption this level has the following resonance parameters: $E_0 = 5.18 \pm 0.02$ ev, $\sigma_0\Gamma = 1730 \pm 170$ barns·ev, $\sigma_0 = (75 \pm 20)\cdot10^3$ barns, $\Gamma = 24 \pm 6$ mv, $\Gamma_n = 3.4 \pm 0.3$ mv. The levels at 6.7 and 21 ev belong to U^{238}, since both the positions and resonance parameters of these levels calculated for this isotope are in agreement with known data on the U^{238} levels. A graph of the dependence of the number of levels observed on the energy (Fig. 8) shows that energy levels begin to be lost for energies greater than 20 ev. The mean level density as determined from the slope of the line is $\overline{W} = 1.65 \pm 0.05$ ev^{-1} for both spin states of the compound nucleus $I_1 = 4$ and $I_2 = 3$.

Table 2 gives the resonance parameters of U^{235} calculated from the measurements of the three samples. Similar data by others [8] is in good agreement with our values for the neutron widths Γ_n. It should be noted,

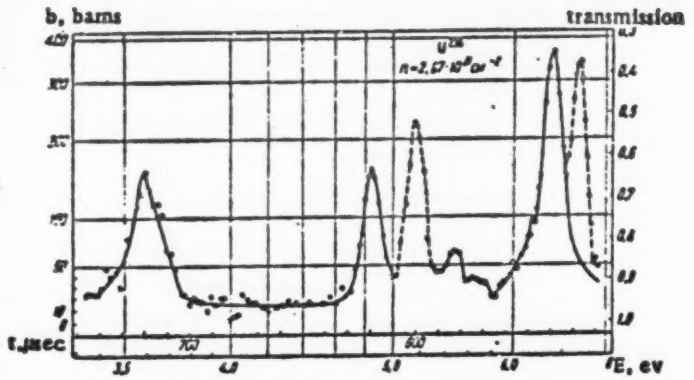

Fig. 5. Transmission by U^{235} in the neutron energy region from 3.4 to 7.0 ev for sample No. 2.

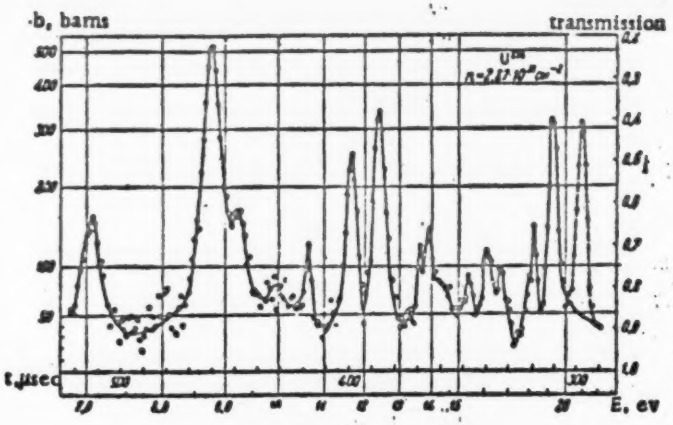

Fig. 6. Transmission by U^{235} in the neutron energy region from 7 to 20 ev. for sample No. 2.

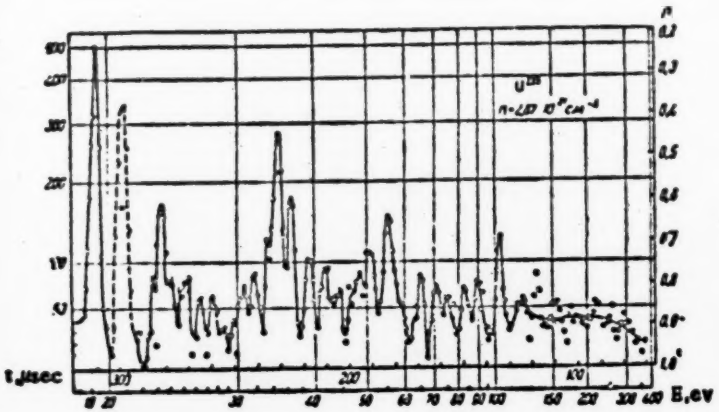

Fig. 7. Transmission by U^{235} in the neutron energy region from 19 to 400 ev for sample No. 2.

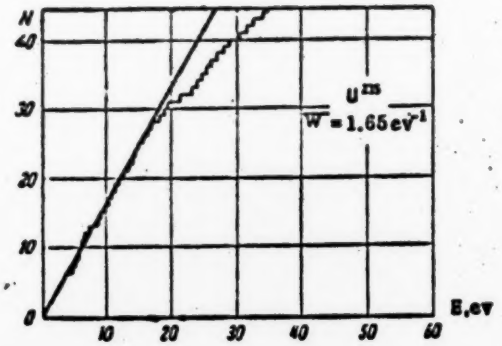

Fig. 8. The number of levels N observed for U^{235} as a function of energy.

TABLE 2

Resonance Parameters of U^{238}

E_0 ev	σ_0 barns	Γ mv	$g\Gamma_n$ mv	$g\Gamma_n^0$ mv
3.609±0,005	200±120	80±40	0.021±0.002	0.0107±0.0011
4.85±0,01	330±190	45±22	0.0278±0.0028	0.0126±0.0013
5.47±0,02		50±20	0.0103±0.006	0.0044±0.003
5.85±0,02			0.0098±0.0015	0.0041±0.0008
6.15±0,05 *)			0.010±0.003	0.004±0.001
6.42±0,02	800±160	65±10	0.131±0.008	0.052±0.003
7.08±0,02	350±90	55±15	0.050±0.005	0.019±0.002
8.79±0,03	1150±130	130±10	0.515±0.023	0.174±0.008
9.30±0,03	280±140	90±40	0.087±0.009	0.029±0.003
9.82±0,05			0.034±0.003	0.011±0.001
10.2±0,1 *)			0.042±0.003	0.013±0.001
10.6±0,1			0.024±0.003	0.0075±0.0008
11.11±0,04 *)			0.027±0.004	0.0082±0.001
11.76±0,04	740±170	80±15	0.271±0.018	0.079±0.005
12.40±0,05	1400±250	80±10	0.545±0.033	0.155±0.010
13.1±0,1 *)			0,02	0,006
13.4±0,1 *)			0.032±0.011	0.009±0.003
13.80±0,05			0.104±0.008	0.028±0.003
14.15±0,07			0.138±0.012	0.036±0.004
14.62±0,07			0.088±0.009	0.023±0.003
15.42±0,08	220±100	90±35	0.117±0.011	0.030±0.003
16.16±0,08			0.21±0.02	0.052±0.005
16.8±0,91			0.106±0.011	0.026±0.003
17.1±0,1 *)			0.06	0,015
18.1±0,1			0.21±0.07	0.049±0.017
18.6±0,1			0.10±0.01	0.023±0.002
19.30±0,08	2700±500	80±10	1.57±0.11	0.357±0.025
22.2±0,2			0.15±0.03	0.032±0.006
23.0±0,2			0.30±0.09	0.063±0.019
23.7±0,1			0.89±0.09	0.183±0.019
24.5±0,1			0.31±0.04	0.062±0.008
25.2±0,2			0.29±0.04	0.057±0.007
25.8±0,2			0.24±0.05	0.047±0.009
28.7±0,2			0.35±0.17	0.068±0.033
28.0±0,2			0.44±0.20	0.083±0.038
30.1±0,3			0.34±0.10	0.062±0.020
31.2±0,3			0.58±0.10	0.105±0.020
32.3±0,3			0.85±0.12	0.145±0.020
33.9±0,3			0.77±0.10	0.130±0.020
34.6±0,4			0.64±0.08	0.109±0.015
35.4±0,3	2150±1400	155±70	4.47±0.87	0.75±0.15

* The parameters of these levels are determined only from measurements with the thick sample (No. 1).

however, that the average value for the neutron widths in our results is somewhat lower than that in the cited work [8], which may be explained by systematic errors in one or the other sets of data. The total widths Γ are determined with large experimental uncertainties, although within these uncertainties good agreement is obtained with the previous data [8]. Levels for energies greater than 35 ev were not analyzed, since the resolution was known to be insufficient.

3. The U^{238} fission cross section. The fission cross section of U^{238} is measured at five energy intervals from 0.0263 to 100 ev. In the energy region from 0.2 to 30 ev the same resonance levels (within experimental uncertainty) are observed as in the measurements of the total cross section.

Table 3 gives the values for $\sigma_{0f}\Gamma = 4\pi\lambda_0^2 \frac{g\Gamma_n\Gamma_f}{\Gamma}$ determined, as was mentioned above, from the measured area A_f of the resonance level. In order to obtain the ratio of the fission width Γ_f to the total width Γ, we used values for the neutron widths $g\Gamma_n$ measured in the present work and by others [18]. The column labeled Γ_f gives

TABLE 3

E_0, ev	$g\Gamma_n^0/\Gamma$ barns·ev	$g\Gamma_n^0$ barns·ev	$\frac{\Gamma_f}{\Gamma}$	Γ mv	Γ_f mv	Γ_γ mv	Γ_f [18] mv
0.29	10.5±0,6	13.9±0,5	0.75	138±5	103±14	35±5	98±7
1.14	11.0±0,4	17.6±0,5	0.62	142±7	88±10	54±7	107±10
2.04	1.2±0,1	5.0±0,2	0.24	43±5	10±2	33±9	12±3
2.9	1.4±0,1	1.8±0,3	0.78	90±40	70±55	20±16	—
3.14	7.7±0,4	13.0±1,3	0.62	150±40	93±38	57±23	115±44
3.61	6.3±0,6	15.6±1,5	0.4	80±40	32±22	48±34	45±24
4.82	3.2±0,5	15.0±1,5	0.15	45±22	6.7±4,5	38±28	4±2,5
5.8	2.2±0,2	4.4±0,6	0.5	90±40	45±31	45±31	—
6.44	8.3±0,7	53±3	0.155	65±10	10±2	55±13	18±14
7.1	5.2±0,5	18.5±1	0.28	55±15	15±6	40±16	21±19
8.8	62±5	155±10]	0.4	130±10	52±10	78±15	59±19
9.3	13±2	25±3	0.52	90±40	47±33	43±30	—
11.7	10±0,8	60±4	0.16	80±15	13±4	67±21	6±19
15.7	13±2	19.8±2	0.25	90±35	22±14	68±43	—
19 3	68±5	220±15	0.31	80±10	25±6	55±14	82±24

Note. The total widths Γ of the levels with energies 0.29, 1.14, 2.04, 2.9, and 3.14 ev are taken from [18].

the values determined from the ratio $\frac{\Gamma_f}{\Gamma}$ with the Γ values from the following column. The column labeled Γ_γ gives the values of the radiative widths $\Gamma_\gamma = \Gamma - \Gamma_f$. The last column gives the fission widths according to Pilcher, Harvey and Hughes [18], obtained on the assumption of a constant radiative width $\overline{\Gamma}_\gamma = 35 \pm 7$ mv. It can be seen that the values of Γ_f determined by both methods vary considerably. To come to any final conclusions, however, on the values of Γ_γ and on the character of the fission width Γ_f distribution is not yet possible due to the large statistical errors and small number of levels measured.

4. Total Pu^{239} cross section. This total cross section was measured with samples of metallic plutonium covered with nickel layers of about 0.017 gm/cm² to preserve them from corrosion. The samples had the following isotope content: Pu^{239} – 97.1%, Pu^{240} – 2.55%, and Pu^{241} – 0.3%. Three samples of various thicknesses were in-

TABLE 4

Resonance Parameters of Pu^{239}

E_0 ev	Γ mv	σ_0 barns	$\sigma_0\Gamma$ barns·ev	$g\Gamma_n$ mv	$g\Gamma_n^0$ mv	Remarks
7.85±0.02	37±12	5200±3000	190±50	0.58±0.16	0.21±0,06	Sample № 1—4
10.95±0.03	150±20	1850±520	280±30	1.17±0.08	0.353±0,024	" № 1—4
11.86±0.04	85±15	1600±450	135±15	0.59±0.06	0.171±0,017	" № 1—4
14.30±0.05	135±40	450±200	60±10	0.32±0.05	0.085±0,013	" № 1—4
14.68±0.05	110±30	2300±900	250±40	1.44±0.21	0.376±0,055	" № 1—4
15.40±0.08			35	0,2	0,06	" № 1—4
17.68±0.06	80±10	2100±500	170±17	1.04±0.10	0.243±0,023	" № 1—4
18.6±0.1			3	0,02	0,005	" № 1
22.31±0.07	55±6	4600±900	250±20	2.22±0.16	0.472±0,034	" № 1, 2, 3, 4
23.7±0.2			3	0,03	0,006	" № 1
26.4±0.1	140±30	1000±300	140±10	0.84±0.06	0.164±0,012	" № 1, 2, 3
27.5±0.2			5	0.05	0.01	" № 1, 2
30.0±0.2			9	0.1	0.02	" № 1, 2
32.5±0.2			22	0.3	0.05	" № 1, 2
35.5±0.2			11	0.2	0.03	" № 1, 2
38.5±0.2			10	0.3	0.05	" № 1, 2
41.7±0.1	140±30	1700±500	240±30	3.82±0.46	0.592±0,071	" № 1, 2, 3
44.8±0.2	170±70	900±450	150±20	2.70±0.37	0.404±0,055	" № 1, 2, 3
48.1±0.1			60±10	1.08±0.15	0.155±0,022	" № 1, 2, 3
50.3±0.2	70±20	2500±1000	170±20	3.24±0.42	0.46±0,06	" № 1, 2, 3
53.0±0.2	90±25	2700±1100	240±35	5.0±0.8	0.69±0,11	" № 1, 2, 3
58.7±0.3			730±100	16.4±2.3	2.14±0,3	" № 1, 2
59.2±0.3				0.4	0,05	" № 1, 2
66.4±0.2	400±80	1400±400	580±70	14.6±1.7	1.8±0,2	" № 1, 2, 3
75.2±0.3	410±50	1300±300	550±60	15.7±1.6	1.8±0,2	" № 1, 2, 3
85.9±0.3				18	2	" № 1, 2

vestigated: $8.29 \cdot 10^{21}$ cm^{-2} (sample No. 1), $5.80 \cdot 10^{21}$ cm^{-2} (sample No. 2), $2.03 \cdot 10^{21}$ cm^{-2} (sample No. 3), and $1.18 \cdot 10^{21}$ cm^{-2} (sample No. 4); in the energy interval from 6 to 30 ev all four samples were used, and in the energy interval from 18-450 ev, samples Nos. 1, 2, and 3 were used. The results for sample No. 2 are shown in Figs. 9 and 10.

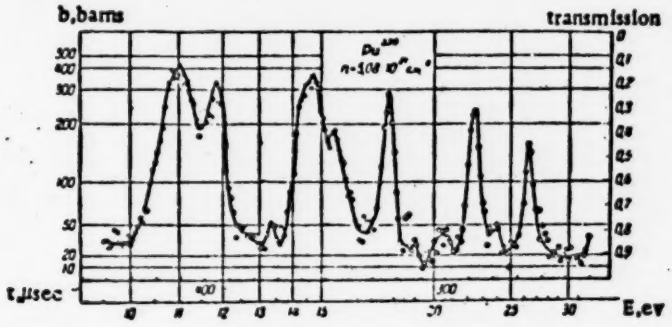

Fig. 9. Transmission by Pu^{239} in the neutron energy region from 9.5 to 30 ev for sample No. 2.

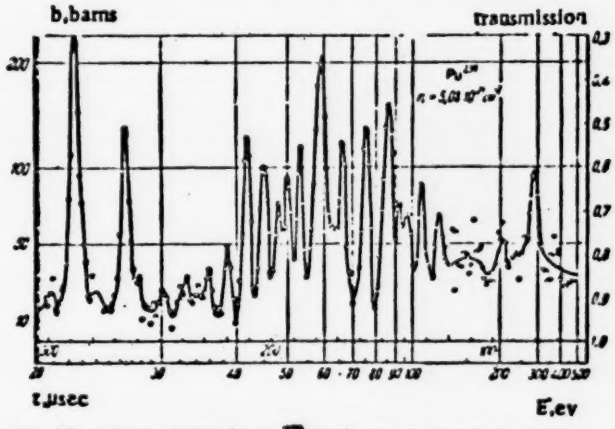

Fig. 10. Transmission by Pu^{239} in the neutron energy region from 20 to 500 ev for sample No. 2.

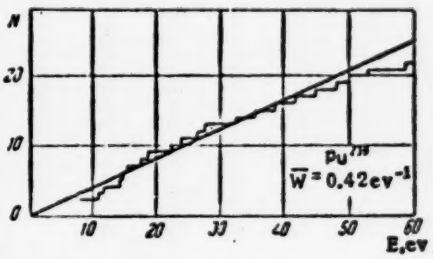

Fig. 11. The number of levels N observed in Pu^{239} as a function of energy.

The energy dependence of the number of levels observed (Fig. 11) shows a noticeable deviation from a straight line at energies greater than 50 ev. The mean level density in the interval from 0 to 30 ev for both spin states of the compound nucleus $I_1 = 0$ and $I_2 = 1$ is $\overline{W} = 0.42 \pm 0.05$ ev^{-1}.

Table 4 shows the results of calculation for the resonance parameters of Pu^{239} for those levels which could be considered resolved. The group of three almost-coincident levels at about 15 ev is not resolved and therefore the actual errors in the resonance parameters for the 14.3, 14.7, and 15.4 ev levels may be significantly greater than those given in the table.

CONCLUSIONS

The reduced neutron widths $g\Gamma_n^0$ for a given nucleus undergo significant fluctuations (of approximately two orders of magnitude). Previous authors [16, 17] arrived at the same conclusion. Figures 12, 13, and 14 show the distributions of the reduced neutron widths $g\Gamma_n^0$ for U^{233}, U^{235}, and Pu^{239}, respectively. On these graphs the abscissa gives the reduced width, and the ordinate gives the number of levels for which $g\Gamma_n^0$ is no less than the corresponding abscissa. Noticeable deviations from exponential variation of the distribution (straight line) are observed on all three graphs. These deviations are difficult to explain even by significant failure to observe weak levels. We may thus conclude that the distribution of neutron widths cannot be described by a simple exponential formula. This conclusion is in agreement with the results of Hughes and co-workers [16].

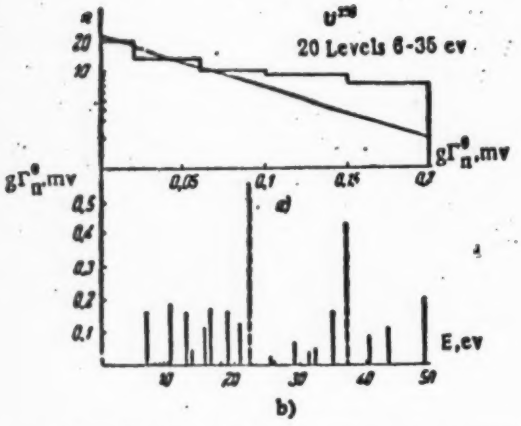

Fig. 12. Distribution of reduced neutron widths (a) and level spectrum (b) in U^{233}.

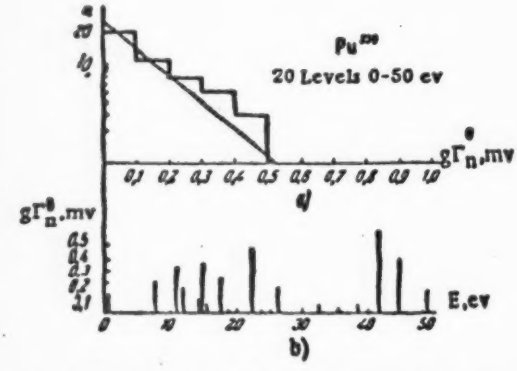

Fig. 14. Distribution of reduced neutron widths (a) and level spectrum (b) for Pu^{239}.

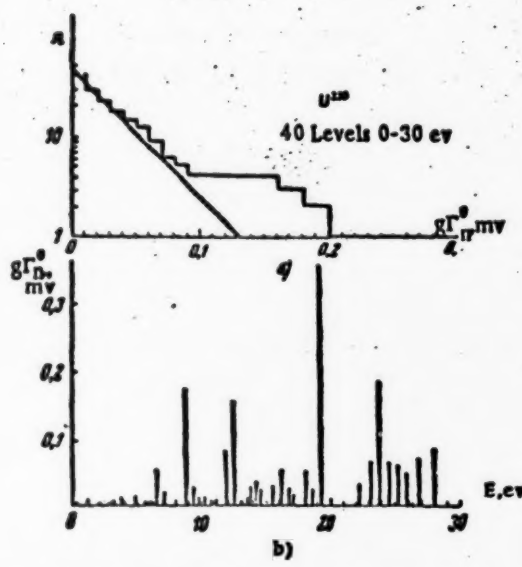

Fig. 13. Distribution of reduced neutron widths (a) and level spectrum (b) in U^{235}.

The same figures give the level spectra of the elements we investigated, where the ordinate gives the reduced width for the given level. The Monte Carlo method was used to calculate the probability for clustering of levels. This was done by dividing the energy interval in which the levels were examined into n parts, and calculating, for each of these parts, the mean square deviation of the sum of the widths from the arithmetic mean, i. e., the quantity φ given by

$$\varphi = \left[\sum_{i=1}^{n} \left(\sum_{k_i=1}^{l_i} (g\Gamma^0_n)_{k_i} - \frac{\sum_{i=1}^{n} \sum_{k_i=1}^{l_i} (g\Gamma^0_n)_{k_i}}{n} \right)^2 \right]^{1/2}$$

where i is the number of the interval, k_i is the number of the level in the ith interval, and l_i is the number of levels in the ith interval.

Figure 14 gives the integrated dependence of φ for chance distribution of nuclear levels as calculated on an electronic computer for all three elements. The points give the observed values.

It can be seen that the distribution of levels can in all cases be explained by chance, with the possible exception of Pu^{239}, for which the probability of clustering of levels is 90% for n = 4.

The authors express their gratitude to U Chzhi-Khua and Sian Chzhi-Linyu for aid in the mathematical treatment of the results, as well as to G. V. Rukolaina for aid in performing the measurements.

The authors are grateful to A.S. Kronroda who developed the statistical methods for treating the spectra, and to G. M. Kukavadze who performed the mass-spectrographic analysis.

Doctor D. J. Hughes and Doctor P. A. Egelstaff kindly made it possible for us to compare our results with unpublished data from the Brookhaven National Laboratory and the Harwell Laboratory. We take this opportunity to express our gratitude to them.

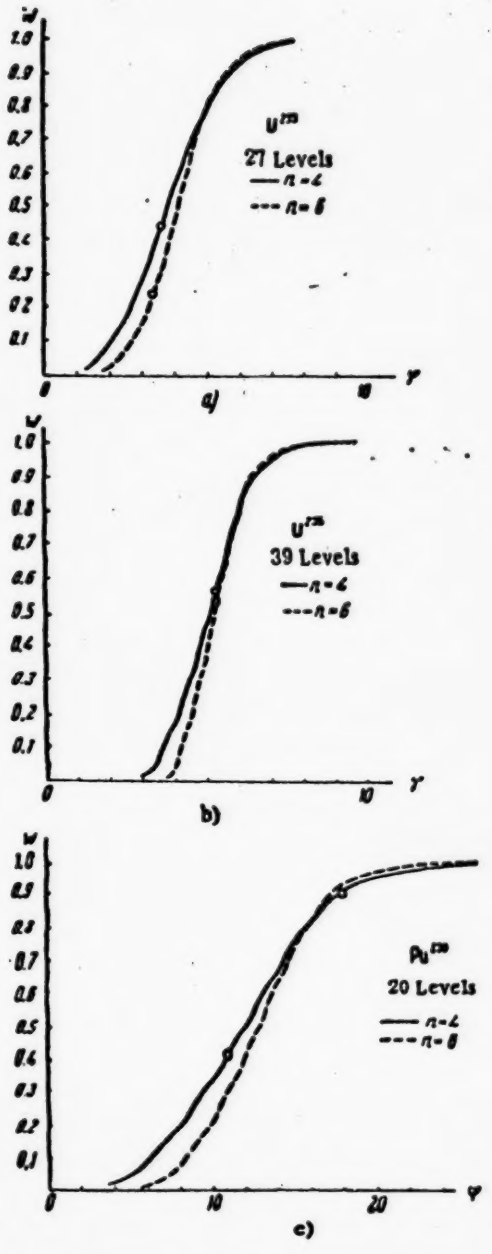

Fig. 15. The probability for clustering of levels, as calculated by the Monte Carlo method, for a) U^{233}, b) U^{235}, c) Pu^{239}. The points give the experimental values of φ.

LITERATURE CITED

[1] Can. J. Phys. 29, 203 (1951).

[2] H. Palevsky, R. Carter, R. Elsberg, and D. Hughes, Phys. Rev. 94, 1088 (1954).

[3] P. Egelstaff, J. Nucl. Energy 1, 92 (1954).

[4] V. V. Vladimirsky, L A. Radkevich, and V. V. Sokolovsky, Physical Investigations, Reports of the Soviet Delegation to the International Conference on the Peaceful Uses of Atomic Energy (Acad. Sci. USSR Press, 1955), p. 26.

[5] S. Ya. Nikitin, S. L Sukhoruchkin, K. G. Ignatyev, and N. D. Galanina, Session of the Acad. Sci. USSR on the Peaceful Uses of Atomic Energy, Meeting of the Division of Phys.-Math. Sciences (Acad. Sci. USSR Press, 1955), p. 87.

[6] S. Ya. Nikitin, N. D. Galanina, K. G. Ignatyev, V. V. Okorokov, and S. L Sukhoruchkin, Physical Investigations, Reports of the Soviet Delegation to the International Conference on the Peaceful Uses of Atomic Energy (Acad. Sci. USSR Press, 1955), p. 106.

[7] Yu. V. Adamchuk, V. F. Gerasimov, V. V. Efimov, B. S. Zenkevich, V. L Mostovoi, M. L Pevzner, and A. P. Tsitovich, Physical Investigations, Reports of the Soviet Delegation to the International Conference on the Peaceful Uses of Atomic Energy (Acad. Sci. USSR Press, 1955), p. 86.

[8] V. L. Sailor et al., The Low-Energy Cross Sections of U^{235}, Report No. 586. Presented by the USA at the International Conference on the Peaceful Uses of Atomic Energy, Geneva, 1955.

[9] B. R. Leonard, The Total and Fission Cross Sections of Plutonium, Report No. 589, Presented by the USA at the International Conference on the Peaceful Uses of Atomic Energy, Geneva, 1955.

[10] J. E. Linn and N. Pattenden, Slow-Neutron Cross Sections of the Uranium Isotopes, Report No. 423, Presented by England at the International Conference on the Peaceful Uses of Atomic Energy, Geneva, 1955.

[11] J. F. Raffle and B. T. Price, Cross Sections of the Plutonium Isotopes, Report No. 422, Presented by England at the International Conference on the Peaceful Uses of Atomic Energy, Geneva, 1955.

[12] V. V. Sokolovsky, V. V. Vladimirsky, and L A. Radkevich, Instructions for Technical Exploitation (in press).

[13] L A. Radkevich, V. V. Vladimirsky, and V. V. Sokolovsky, Instructions for Technical Exploitation (in press).

[14] E. Melkonian, Analysis of Low-Energy Neutron Resonances, Report No. 583, Presented by the USA at the International Conference on the Peaceful Uses of Atomic Energy, Geneva, 1955.

[15] D. J. Hughes, J. Nucl. Energy 1, 237 (1955).

[16] J. Harvey, D. Hughes, R. Carter, and V. Pilcher, Phys.Rev. 99, 10 (1955).

[17] D. Hughes and J. Harvey, Phys. Rev. 99, 1032 (1955).

[18] V. R. Pilcher, J. Harvey, and D. Hughes, Phys. Rev. 103, 1342 (1956).

Received May 4, 1956

BLANK
PAGE

STABILIZATION OF ELECTRON ENERGIES IN A 30-MEV SYNCHROTRON

M. V. Karpov, E. P. Ovchinnikov, and B. S. Ratner

We describe an apparatus for stabilizing the maximum bremsstrahlung energy from a 30-Mev synchrotron. This apparatus was tested by measuring the yield for photonuclear reactions, and it was shown that the maximum energy remains constant within ± 30 kev.

In many experiments using synchrotrons it is necessary to maintain the maximum bremsstrahlung energy $E_{\gamma m}$ constant with good accuracy. The stability of $E_{\gamma m}$ is particularly important, for instance, in examining the excitation curves of the various photonuclear reactions. Fluctuations in $E_{\gamma m}$ lead to significant spreads in the experimental points at the lower ends of the excitation curves, where the yield depends strongly on $E_{\gamma m}$.

Recently, energy-stabilization systems have been developed on several betatrons [1-4]. The present article describes the energy-stabilization system developed for the 30-Mev synchrotron of the P. N. Lebedev Physical Institute of the Academy of Sciences USSR. Fluctuations in $E_{\gamma m}$ are caused directly by oscillations in the magnetic field strength at the synchrotron orbit at the instant the high-frequency field is turned off. These oscillations, in turn, are caused by the instability of the amplitude and frequency of the magnetic field, as well as by the instability of the time at which the high-frequency field is turned off. The uncertainty in $E_{\gamma m}$ due to the above reasons is usually about 2-3%. The authors were presented with the problem of developing an apparatus which would maintain the energy constant to an accuracy of no less than 0.5%.

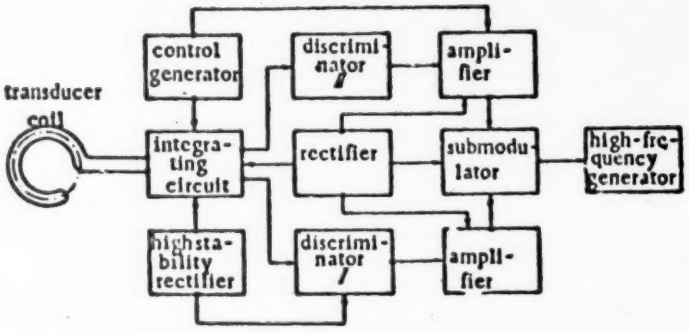

Fig. 1. Block diagram of the synchrotron electron-energy stabilizer.

As is well known, the energy $E_{\gamma m}$ in a synchrotron is determined by the following equation:

$$E_{\gamma m} = \sqrt{(300HR)^2 + (m_e c^2)^2} - m_e c^2, \qquad (1)$$

where $E_{\gamma m}$ is given in electron volts; H is the magnetic field strength at the synchrotron orbit when the high-frequency field is turned off, in oersteds; R is the radius of the synchrotron orbit, in centimeters; and $m_e c^2$ is the rest energy of the electron (about 0.51 Mev).

If a coil is inserted into the gap of the synchrotron magnet then the emf e_1 induced in it is related to $E_{\gamma m}$ by the equation

$$E_{\gamma m} = \sqrt{\left(\frac{H}{A}\int_0^t e_1 dt\right)^2 + (m_0c^2)^2} - m_0c^2, \qquad (2)$$

where t is the time at which the high-frequency generator is turned off, with $t = 0$ when the magnetic field strength is zero, and A is a constant which depends on the geometry of the coil. It follows from Eq. (2) that the integral of the emf induced in the coil is proportional to $E_{\gamma m}$ to a high order of approximation for $E_{\gamma m} \gg m_0c^2$. By applying the induced emf to a threshold circuit (pulse-height discriminator), a voltage pulse can be obtained when the energy $E_{\gamma m}$ is greater than any given value. If this pulse is used to turn off the high-frequency generator, stabilization of $E_{\gamma m}$ will have been achieved.

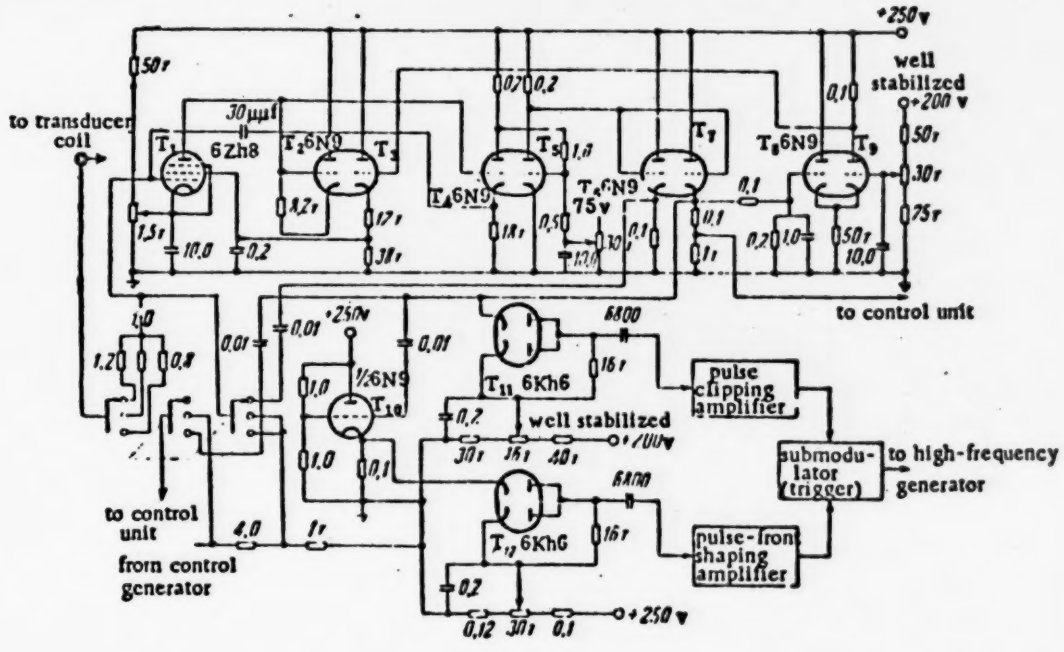

Fig. 2. Fundamental stabilizer circuit. *

The energy stabilizing system described is an electronic monitoring system consisting of a transducer winding, an integrating circuit, a pulse-height discriminator, pulse shaping amplifiers, a submodulator, power sources, and a control unit. A block diagram of the apparatus is shown in Fig. 1. The transducer consists of eight windings (PESh0-0.23 conductor). The coil, insulated by lacquering, is attached to the lower pole piece. The coil is made in such a shape that the integral of the emf induced in it is proportional to the mean value of the magnetic field strength at the equilibrium orbit of the synchrotron. Circuit diagrams of the integrating circuit and discriminators are shown in Fig. 2.

The integration is performed by an electronic integrator. The dc coupled amplifier at the input of the integration circuit has an amplification factor $k_0 = 4000$. The highly reactive feedback ($\beta \approx 1$) provides extremely accurate integration with an equivalent time-constant $\tau = RC(k_0 + 1)$. Calculation using the equivalent circuit of the integrator shows that the maximum error is no greater than 0.01%. The stability of the integrator operation is determined by the constancy of its transmission coefficient (k_β) and the accuracy of integration, which depends on the equivalent time constant τ. Any instability of the transmission coefficient when $\frac{k_0}{k_\beta} \approx 4000$ is determined

* [In Fig. 2, "T" = "kohm" – editor's note.]

almost entirely by variations in the RC of the feedback circuit. Small variations in the amplification factor (k_0) of the integrator are of practically no importance for the transmission coefficient and accuracy of integration; therefore no special measures have to be taken to achieve a sufficient control for k_0.

Measures are taken in the dc amplifier circuit to increase its stability. Among these are the fact that the dc filament supply is led through a barretter and automatic dc regulation at the integrator output. This circuit consists of a low-frequency filter, a difference amplifier (T-8, T-9), and a governing cathode follower (T-3). The operation of the integrating circuit is controlled by monitoring its amplification factor (k_0) and the constancy of the output potential of the integrator with a compensation voltmeter and a standard cell. Overloading of the dc amplifier under various operating conditions of the accelerator is avoided by stepwise regulation of the input signal. The signal from the integrator passes through cathode followers (T-7, T-10) to two pulse-height discriminators, one of which determines the time at which the high-frequency generator is turned on, and the other, the time at which it is turned off. The first discriminator (T-12) and the amplifier following it serve only for partial stabilization of the γ-ray beam.

We have chosen vacuum tube diodes for the stabilizing apparatus, since they are most stable in operation. The fact that the plate characteristic of these diodes have a tendency to "creep" in time, is to some extent overcome by the use of a stabilized filament supply. The instability of the discriminators due to aging of the tubes and variation of the contact potentials is compensated by the additional diode. This compensation increases the discriminator stability by a factor of ten.

Primary attention was paid to the stability of the apparatus which determines the time at which the high-frequency generator is turned off. A very important factor in the discriminator is the accuracy of reproduction of the initial potentiometer setting, which is instrumental in establishing the cutoff potential of the diodes (reference voltage) which determines the energy $E_{\gamma m}$. This problem was solved by constructing a special wire potentiometer of extreme accuracy. The reference potential on the discriminator potentiometer is maintained with an accuracy of $\pm$ 0.005% with the aid of a high-stability rectifier and a standard cell [5]. This same rectifier determines the reference potential of the difference amplifier (T-9). The voltage is applied to all the rectifiers of the apparatus from a ferroresonant stabilizer. The signals emitted by the discriminating diodes are applied to two wide-band amplifiers with clipping and differentiating elements, where they are shaped into sharp negative pulses with rise times less than one microsecond. Each amplifier has an amplification factor of 10,000, which makes it possible to attain energy stabilization for energies corresponding to extremely small rates of increase of the magnetic field. Regulation of the amplification factor for the shaping amplifiers is attained, as for the amplifiers in the integrating circuit, with the aid of a sinusoidal voltage generator and a cathode voltmeter.

The 15 v signals from the output of the shaping amplifiers start up a trigger circuit with two stable states. The trigger cascade produces a square pulse with an amplitude of 100 v and the rise, and the decay times of this pulse, are in strict agreement with the given instantaneous value of the magnetic field at the synchrotron orbit. This pulse is applied to the modulator of the high-frequency generator.

The desired accuracy of operation of the whole stabilizing circuit necessitates the use of well-stabilized power sources and control elements.

Basic instabilities, as has already been noted, occur in the pulse-height discriminators due to drift of the diode characteristics and variation of the reference cutoff potential. If the signal amplitude into the integrating circuit is increased, the relative error is decreased. Therefore under all operating conditions of the accelerator, the whole linear characteristic of the integrator is used, which makes it possible to obtain 60 v-high pulses at its output. Time lags in the wide-band shaping amplifiers are no greater than 1 μsec for an amplification factor $k = 10{,}000$; the same refers to the subsequent part of the circuit.

The operation of the stabilizing system was tested similarly as in [2] by the yield from the reaction $Cu^{63}(\gamma, n)Cu^{62}$ on the steep part of the activation curve. Copper samples in the shape of rings whose height and diameter was 28 mm and whose thickness was 0.2 mm were placed in a beam of γ-rays with maximum energy 13.1 Mev. The radiation dose was determined by an integration chamber (monitor) with an outer lead cover which protected the chamber from electrons and from low-energy scattered radiation. The copper sample was placed on this cover (Fig. 3). The activity induced in the sample by the reaction $Cu^{63}(\gamma, n)Cu^{62}$ ($T = 10$ min) was recorded by an AS-2 counter surrounded by γ-counters. The latter were connected in anti-coincidence. The sample was irradiated for 10 min, it took 2 min to carry it to the measuring apparatus, and the measurement took

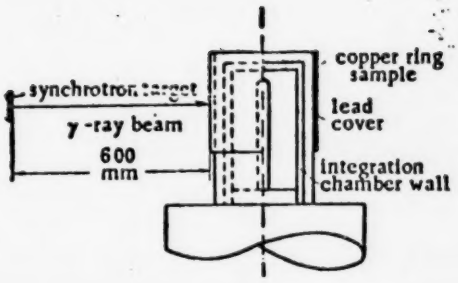

Fig. 3. Location of the sample and monitor in testing the operation of the stabilizing system.

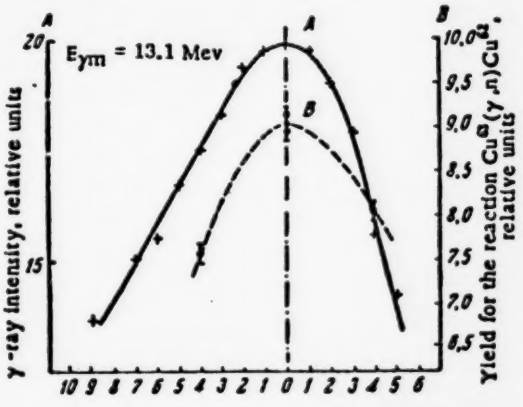

Fig. 4. The yield for the reaction $Cu^{63}(\gamma, n)Cu^{62}$ for $E_{\gamma m}$ = 13.1 Mev as a function of the position of the sample relative to the γ-ray beam. A) Angular distribution of the beam intensity; B) yield from the reaction (γ, n) as measured on the beam axis, and 4 cm from it.

Fig. 5. The dependence of $E_{\gamma m}$ on the amplitude of the synchrotron magnetic field for a constant potentiometer setting on the energy scale.

took 5 min. The sensitivities of the monitor and apparatus for measuring the induced activity were periodically checked with a sample of the γ-emitter Co^{60}, and were found to remain constant within the limits of ± 3%. This accuracy was sufficient, since on the part of the (γ, n) reaction curve for copper which we had chosen, a change in $E_{\gamma m}$ of only 100 kev leads to a change in the yield (that is, the activity, relative to the dose recorded by the monitor) of 10%. Thus the desired energy stability of ± 50 kev could be checked using the accuracy available in the recording apparatus. For two months the yield was measured several times a day for one potentiometer setting corresponding to an energy $E_{\gamma m}$ = 13.1 Mev. During this time the spread in the yield was about ± 140 kev. During any given day the spread in the yield was much lower. It should be noted that energy instability for measurements that take a long was observed also by other authors [2, 3]. We have assumed that the observed distribution in the yield from day to day is caused by inaccuracy in locating the sample and monitor relative to the beam axis. Special measurements of the angular distribution showed that for a given value of $E_{\gamma m}$ there is a clearly-expressed dependence of the (γ, n) yield on the distance between the sample and the beam axis (Fig. 4).

The angular distribution of the γ-ray beam intensity is not symmetric relative to its axis, due obviously to scattered radiation from the poles and yoke of the synchrotron magnet. Correspondingly asymmetric is the yield from the (γ, n) reaction. We must assume that the scattered radiation whose energy is below the threshold for the (γ, n) reaction in copper changes only the dose registered in the monitor and leads to errors not related to the stabilizing system. A four-day test of the energy stability, undertaken with this situation taken into account, showed that the energy $E_{\gamma m}$ remains constant within the limits of ± 30 kev.

To check the sensitivity of the stabilizing system to variations in the magnetic field strength, we undertook the measurements of the yield from the reaction $Cu^{63}(\gamma, n)Cu^{62}$ for a given energy value. The results of these measurements are shown in Fig. 5.

The energy scale of the stabilizing system was calibrated by measuring the already-known thresholds for the reactions $C^{12}(\gamma, n)C^{11}$ and $O^{16}(\gamma, n)O^{15}$, as well as that for the reaction $Cu^{63}(\gamma, n)Cu^{62}$, which has been given in several works [6]. Previous to this the null method was used to verify the linearity of the potentiometer which determines the energy $E_{\gamma m}$. In all the threshold measurements, the samples were placed in a fixed position close to the synchrotron chamber.

The irradiation dose was maintained constant within 5%. The carbon samples were prepared of graphite in the shape of cylindrical rings (height and diameter 28 mm, wall thickness 2 mm). The samples were irradiated for 30 min. Measurements of the induced activity indicated the presence of an insignificant amount of some impurity in the graphite, which had an activity with a half-life of about 5 min. Therefore in determining the

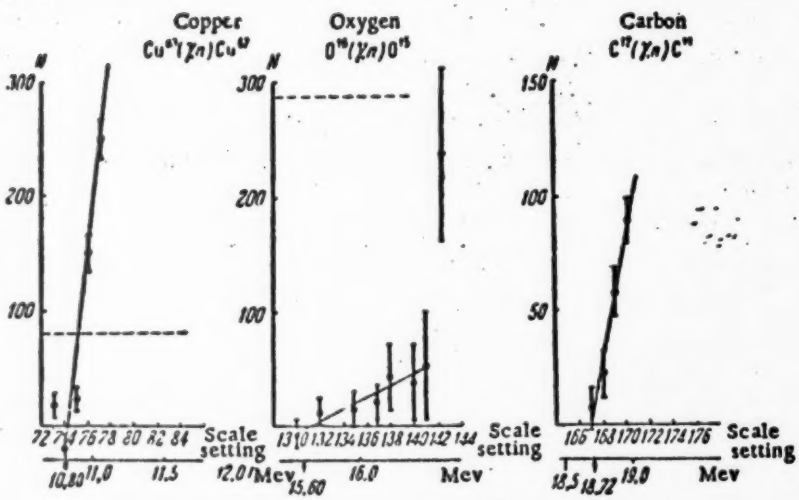

Fig. 6. Calibration of the energy scale of the stabilization system. The abscissa gives the scale setting and the corresponding value of $E_{\gamma m}$ in Mev. The ordinate gives the activity in the samples after the counter background, as given by the dotted horizontal lines, is subtracted. (In the case of the reaction $C^{12}(\gamma, n)C^{11}$, the background was 323 pulses in 20 minutes.) The arrows indicate the reaction threshold.

threshold ($E_{\gamma m}$ = 18.72 Mev) the activity was measured during a time interval from 11 to 31 min after the end of irradiation (the β half-life of C^{11} is 20.5 min).

The threshold for the reaction $O^{16}(\gamma, n)O^{15}$ ($E_{\gamma m}$ = 15.6 Mev) was determined with plexiglas cylinders of the same dimensions as the graphite ones. They were irradiated for 4 min. The activity was measured from 2 to 5 min after the end of irradiation. The photoneutron threshold for copper (Cu^{63}) was measured on copper rings of the dimensions given above. They were irradiated for 5 min. In order to avoid the activity due to the reaction $Cu^{65}(\gamma, n)Cu^{64}$ (T = 12 hr) we took the difference in activity as obtained in the intervals 2-7 min and 30-35 min.

The results of these measurements are shown in Fig. 6. In view of the fact that an accurate determination of the threshold for oxygen was made difficult in our experiment due to the slow increase of the activation curve at the threshold, the calibration points were taken from the threshold for copper and carbon. The threshold for the reaction $Cu^{63}(\gamma, n)Cu^{62}$ is taken as 10.80 Mev which is the average of four results [6].

With this calibration the threshold for the reaction $O^{16}(\gamma, n)O^{15}$ as obtained by us is not in contradiction with the calculated value of 15.60 Mev.

LITERATURE CITED

[1] C. V. von Tersch and R. L. Dody, Proc. Natl. Electron. Conf. (August, 1952).

[2] L. Katz, R. N. H. Haslam, R. S. Horsley, A. G. W. Cameron, and R. Montalbetti, Phys. Rev. 95, 464 (1954).

[3] Spicer and Penfold, Rev. Sci. Instr. 26, 952 (1955).

[4] R. Basile and C. Schuhe, J. Phys. Rad. 16, 372 (1955).

[5] Details and Elements of Radio-Location Stations (Soviet Radio Press, 1952) Vol. 2, p. 315.

[6] G. C. Baldwin and H.W. Koch, Phys. Rev. 67, 1 (1945); McElhinney, Hansen, Becker, Dufileld, and Diven, Phys. Rev. 75, 542 (1949); Sher, Halpern, and Mann, Phys. Rev. 84, 387 (1951); M. Birnbaum, Phys. Rev. 93, 146 (1954).

Received May 4, 1956

BLANK
PAGE

SOME PROPERTIES OF ALLOYS OF ZIRCONIUM WITH NIOBIUM

Yu. F. Bychkov, A. N. Rozanov, and D. M. Skorov

A diagram of state is given for the system zirconium—niobium, as constructed from experimental data obtained by the writers. Results of tension tests conducted at room temperature on the alloys of zirconium with niobium are described, and an estimate of their high-temperature strength is given on the basis of hardness measurements at temperatures up to 750°C, and also an estimate of the change of hardness of the alloys resulting from low-temperature anneals (aging). The data obtained are interpreted on the basis of the diagram of state. The high-temperature durability is determined for alloys oxidized in air at 570 and 650°C.

Data in the Literature

Only a very small amount of information on the properties of alloys of zirconium with niobium exists in the literature. Andersen and others [1] carried out tension tests at room temperature and at a temperature of 650°C on three alloys with 0.6, 5.1, and 12.9% niobium by weight. The alloys with zirconium reduced by a magnesium-thermal process were poured into a graphite mold and were forged and annealed. The limiting tensile strength of these alloys at 650°C ranged from 12.5 to 20 kg/cm^2. The maximum strength, of 105 kg/mm^2 at room temperature and fractional elongation 1%, was found for the alloy with 12.9% niobium.

Litton [1] studied several alloys of iodide-process zirconium with up to 27.5% by weight added niobium, fused in an arc furnace, after annealing at 725°C. He found that the maximum tensile strength was that of 75 kg/mm^2 for the alloy with 7.5% niobium by weight; all the alloys with greater niobium content had elongations of 1-2%.

Andersen and others indicate that at 750°C the alloys of zirconium with niobium are more strongly oxidized than pure niobium.

The present writers set themselves the problem of making a more systematic study of the properties of alloys of zironium with niobium; for this purpose we have investigated the system zirconium—niobium and have determined the mechanical properties of these alloys at room temperature, the high-temperature strength from hardness measurements, and the high-temperature durability.

Preparation of the Alloys and Method of Investigation

The alloys intended for the study of the system Zr—Nb and for the mechanical tests were prepared of rods of iodide-process zirconium with ~ 1.5% hafnium and niobium foil of thickness 0.2-.5 mm containing about 1% tantalum, melted in an arc furnace MIFI 9-3 with copper base and tungsten electrode. To obtain a compact charge, the zirconium was wrapped in the foil.

The melts were carried out in an atmosphere of argon, which had been purified by passage through a tube containing magnesium turnings heated to 600°C. The final purification of the argon in the furnace was accomplished by the fusing of a getter – a rod of iodide-process zirconium of weight 30-50 g. The use of an oscillator made it possible to ignite the arc without touching the melt with the electrode. Contamination by gases was negligible; control specimens of pure zirconium had hardness about 100 H_B after several meltings. According

to the data of a chemical analysis, after repeated meltings the melts were not contaminated with tungsten to as much as 0.1% by weight.

Castings of weight 20-30 g, containing up to 20% by weight of niobium, were forged in the hot state (at temperature 800-500°C) into plates of thickness about 4 mm. The smaller the niobium content of the alloy, the more easily it could be hot-forged. Alloys containing more than 20% niobium by weight were hot-forged with great difficulty; they had to be cold-worked on a rupture-test machine. The skin formed on the castings during the forging was removed with an emery wheel. After the cold or hot working the specimens were annealed for 4 hours in a TVV-2 vacuum furnace at 700°C.

The metallographic and x-ray examinations were carried out by the usual methods.

The determination of the solid and liquid lines was carried out in a TVV-2 vacuum furnace with a tungsten heater, using the incipient and complete fusion of the specimens. Pyramidal specimens (5 or more) of various compositions and of weight 3-5 g, with several machined edges on each, were placed on a plate of zirconium oxide hung from a tantalum suspension inside the furnace. After heating to a given temperature, which was maintained for 15-20 minutes, the furnace was cooled and the specimens were removed, after which the edges of the specimens not in contact with the ceramic were examined under a binocular microscope. It was assumed that specimens on whose edges no changes were detectible had been heated to a temperature below the solid line, and that those with rounded edges or ribs had been at a temperature below the liquid line but above the solid line. The more signs of fusion appeared on the specimen, the closer it had been to the liquid line. A specimen that had formed a drop had been heated above the liquid line. Up to 1600°c the temperatures were measured with a platinum–platinum-rhodium thermocouple, and above 1600°C with an optical pyrometer.

In order to avoid errors in the measurements with the optical pyrometer, the temperature determined was not that of the specimen, but that of the ceramic on which the specimens rested. With this method the interaction of the specimens with the ceramic, occurring only at the place of their contact, did not disturb the measurements.

From the annealed plates microspecimens were made with computed length 5.5 mm and diameter 1.2 mm. The tensile strengths of the alloys were determined on a Friedmann and Reutmann micro-testing machine. The fractional elongations were determined with a measuring microscope.

The hardness at elevated temperatures was measured with a special apparatus in which the indenter used was a "pobedite" (90% WC, 10% Co) cone of angle 90°, which retains its hardness up to 750°C. The specimen was heated in an atmosphere of chemically pure argon. The temperature in the furnace was maintained constant by means of a galvanometer relay. The specimen inside the furnace could be turned around an axis displaced relative to the center of the apparatus, and thus 3-5 indentations could be taken. Before the test the surface of the specimen was polished and then washed in acetone. The specimen was kept at the test temperature for about a half hour, and then the 3-5 indentations were made. The loading time was 1 min.

The optimal value of the load depends on the temperature at which the test is made and on the composition of the alloy. The hardness measurements on the alloys were carried out with a load of 50 kg. This gave indentation diameters of 0.5-2 mm, measured with a binocular microscope at room temperature. The hardness H_k was calculated from the specific load on the surface of the indentation.

Diagram of the State of the System Zirconium–Niobium

From the data of this investigation there was constructed the diagram of state for zirconium–niobium shown in Fig. 1. Metallographic and x-ray studies of the alloys tempered after homogenization at 1250°C, and also of the alloys in the cast state, showed that in this system at high temperatures there is formed a continuous series of solid solutions having the body-centered cubic lattice.

The positions of the lines for the beginning and completion of the $\alpha \rightarrow \beta$ transformation, and the solubility of niobium in α-zirconium at 650°C, equal to ~ 5%, were established by differential thermal analysis of 20 g specimens of alloys rich in zirconium. The transition temperatures shown in Fig. 1 were determined by thermal, expansion, and thermoelastic methods [5].

X-ray structure studies of the alloys heated for 100-500 hours at temperatures 675, 800, and 900°C showed that the alloys rich in niobium separate during the annealing process; all the lines in the x-ray patterns are

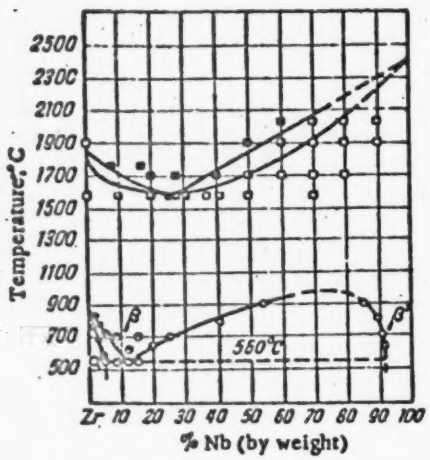

Fig. 1. Diagram of state of zirconium–niobium. ●) points obtained by thermal method; ⊖) points obtained with dilatometer; ○) points found by x-ray method; □) no traces of melting on specimen; ▣) traces of melting visible on specimen; ■) specimen melted.

doubled. The compositions of the stable solutions were determined by comparing the lattice parameters for annealed and tempered alloys.

The temperature of the eutectoid transition was established by expansion tests using a vacuum dilatometer with an indicator giving a value of 0.001 mm per division, and made on alloys with 5-15% niobium annealed at 700°C and then slowly cooled in the furnace. In the alloys with large niobium content the transition was not observed because of its small speed.

The solid and liquid curves of the system, determined from incipient and complete fusion, have a minimum at 25-28% niobium and 1600°C.

The diagram of state of zirconium–niobium recently published by Rogers and Atkins [2] is like that shown in Fig. 1, but on it the eutectoid transition lies at 615°C and 17.5% niobium instead of 560°C and 12% niobium. The minimum of the solid curve according to the data of [2] lies at 1740°C instead of the 1600°C of our data.

The difference in the results obtained is probably to be explained partly by the difference in the methods of investigation and also by the difference in the chemical composition of the original components used, since in the work of [2] zirconium of low hafnium content was used.

Mechanical Properties of the Alloys

Figure 2 shows the dependence of the limiting tensile strength and the fractional elongation on niobium content for alloys annealed at 700°C.

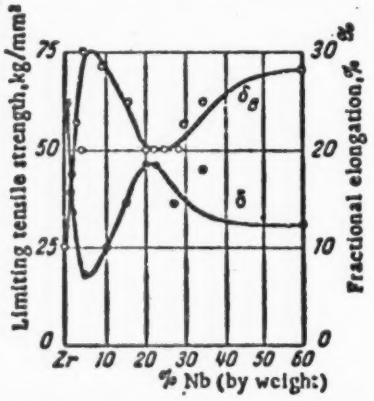

Fig. 2. Dependence on niobium conetnt of tensile strength and fractional elongation of alloys of zirconium with niobium, annealed at 700°C.

The maximum tensile strength 75 kg/mm² and the smallest fractional elongation 6% are those of an alloy with 7.5% niobium by weight; all the other alloys have relatively large fractional elongation, i. e., are rather plastic. The alloys with 5-10% niobium are rather brittle in the cast state and after quenching from high temperatures, they crack when cold-worked.

Figure 3 shows the results of hardness measurements on cast and heat-treated alloys.

The variation of the hardness as function of composition is like that of the tensile strength, i. e., a linear relationship exists between them. On the average the tensile strength of an alloy in kg/mm² is equal to 0.24 times its Brinnell hardness. As is shown by Shvope [3], such a relation also holds for other alloys based on zirconium.

The dependence on composition of the hardness of tempered and cast alloys can be regarded as a curve with a flat maximum in the region of 50-80% niobium, which is characteristic for a continuous series of solid solutions, on which there is superposed a peak caused by the diffusionless transformation of the cubic β-phase into the acicular α-phase.

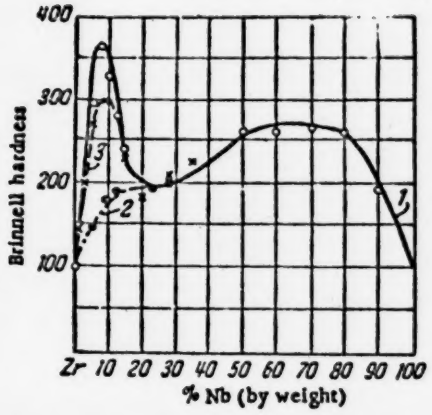

Fig. 3. Dependence of hardness of alloys of zirconium with niobium on niobium content. 1) Cast alloys, 2) alloys cooled in furnace from 650°C, 3) alloys quenched from 750°C.

Hardness (Brinnell) of Alloys Annealed at 300 and 500°C

Serial No.	% Nb (by weight)	After quenching	After annealing at 300°C (8 hours)	After quenching	After annealing at 500°C (44 hours)
1	2.1	185	205	—	—
2	6	320	375	321	290
3	9.4	295	340	285	270
4	11.3	295	350	300	330
5	19	168	223	180	202
6	40	—	—	190	200
7	60	—	—	212	245

The peak on the hardness curve of quenched alloys near 7.5% niobium disappears after slow cooling of the alloys from 650°C, since owing to the transformation of the β-solution into the α-phase there is a disintegration of the acicular structure. In the x-ray patterns of the alloy with 5% niobium the lines of the residual β-phase are observed after quenching from 750°C, but after cooling from 650°C they disappear. In an alloy with 20% niobium quenched from 650°C the β-phase is fixed, and after cooling in the furnace from this same temperature a large amount of the α-phase appears in an alloy with 22% niobium.

Some quenched alloys can be strengthened by low-temperature annealing, which indicates an effect of aging. Results of hardness determinations on alloys of zirconium with niobium that had been subjected to annealing are given below. The hardness was determined on a Rockwell apparatus and recomputed to the Brinnell scale.

The measurements showed that after 30 minutes anneal at 300°C the hardness is almost unchanged. The effect of aging at 300°C is rather large – the hardness of an alloy with 11.3% niobium is increased from 295 to 350 H_B.

Annealing of alloys containing up to 9.5% niobium at 500°C decreases their hardness, but for alloys with higher niobium content an increase of hardness is observed.

This is explained by the fact that a temperature of 500°C is high enough for the rapid occurrence of diffusion processes which lead to loss of strength in alloys with small amounts of added niobium, and for the alloys richer in niobium this temperature is low enough so that in these alloys there occur only aging processes – dispersion hardening, causing the hardness values to increase.

An x-ray pattern of a quenched alloy with 60% niobium that had been annealed at 525°C for 80 hours showed no new lines; there was only a change of the distances between the lines owing to a small decrease of the lattice parameter. After such an anneal the state of the alloy was still far from equilibrium.

High-Temperature Strength of the Alloys

An estimate of the high-temperature strength was made from the hardness at high temperatures.

Figure 4 shows the results of determinations of the hardness H_K of alloys of zirconium with niobium at temperature 750°C. In Fig. 5 is shown the change of hardness of several of the alloys with change of temperature. At 750°C the hardness of the alloys rich in zirconium is small, and it increases slowly with alloying with niobium. In the alloys with 30-50% niobium a considerable increase of the hardness is found. With increase of the niobium content from 50 to 90% the value of the hardness increases slowly, and at about 90% niobium it reaches a maximum. From Fig. 4 it can be seen that the high-temperature strength of the alloys rich in zirconium is considerably lower than that of the alloys based on niobium. On heating to 750°C alloys rich in niobium have their hardness reduced by several percent, but the hardness of the alloys rich in zirconium changes (cf. Fig. 5) from 250 units at room temperature to 5-10 units at 750°C.

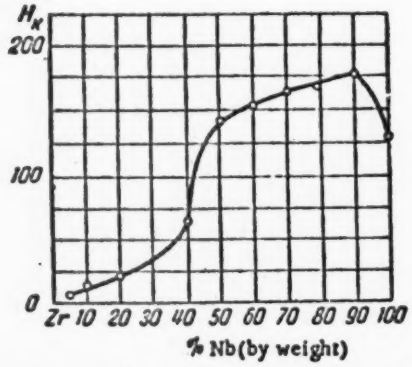

Fig. 4. Hardness of alloys of zirconium with niobium at 750°C as function of composition.

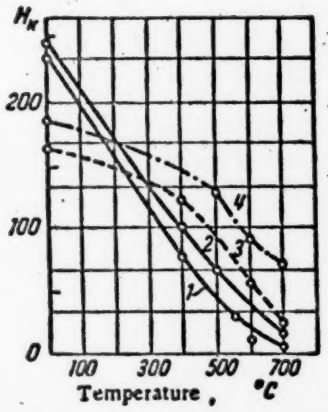

Fig. 5. Variation of hardness of alloys of zirconium with niobium as function of temperature. 1) Alloy with 5% niobium, 2) alloy with 10% niobium, 3) alloy with 20% niobium, 4) alloy with 40% niobium.

From a comparison of the curve of hardness at 750°C against composition with the curve tensile strength against composition it can be seen that the alloys that are strongest at room temperature, containing about 7% niobium, quickly lose their strength on heating and at 750°C have a hardness close to that of zirconium. The maximum of the hardness at 7.5% niobium, arising from structure hardening, disappears at 750°C.

At 750°C the alloys with 5 and 10% niobium are displacement β-solutions. The formation of solid solutions by displacement of zirconium with niobium does not lead to any considerable increase of the retention of strength on heating for alloys containing up to 20% niobium. This is in agreement with the general view that alloying with formation of solid solutions does not give alloys that retain their strength to temperatures appreciably above that at which recrystallization occurs for the main metal of the alloy [4].

High-Temperature Durability of the Alloys

Specimens in the shape of rectangular plates were prepared from the castings by machining and polishing. They were placed in refractory crucibles, which were put into a muffle furnace heated to the stated temperature; here oxidation took place. The temperature was maintained constant with galvanometer relays.

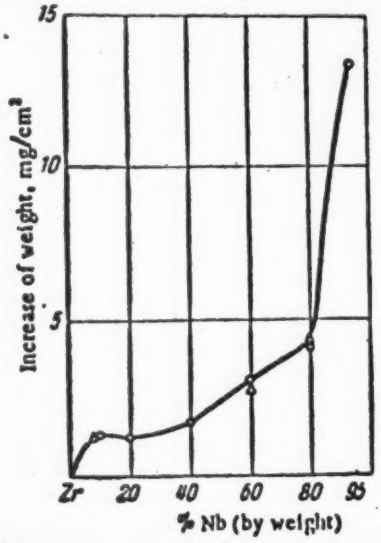

Fig. 6. High-temperature durability of cast alloys of zirconium with niobium at 650°C, as related to composition (time of test 1 hour 45 min).

The results of tests of several cast alloys at temperature 650°C for 1 hour 45 minutes (Fig. 6) show that the more niobium the alloy contains the poorer is its stability against oxidation. In these tests pure zirconium became covered with a thin black film, and pure niobium foil was burned up. Alloys rich in niobium are not stable against oxidation.

Analogous results are obtained after testing for 20 hours at the same temperature, but the increase of weight is several times as large (for example, the alloy with 80% niobium has increase of weight 50 mg/cm²).

The preliminary treatment of the specimens has a large effect on the speed of oxidation. Worked specimens are oxidized more rapidly than cast specimens.. For example, the cast alloy with 60% niobium gave an increase of weight of 30 mg/cm² after 20 hours at 650°C, but the worked alloy gave 100 mg/cm².

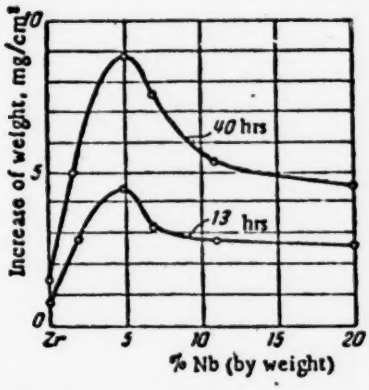

Fig. 7. High-temperature durability of forged alloys of zirconium with niobium at 570°C as function of composition, for different durations of test.

The nature of the products of corrosion also depends on the working. Specimens of cast alloys with 60 and 80% niobium corrode with the formation of powdered oxide, but on the surface of forged alloys with 34 and 60% niobium there is formed a many-layer film produced by the successive deposition of oxide films of almost white color formed at the surface.

Figure 7 shows the results of tests at 570°C of alloys with up to 20% added niobium, annealed after hot forging. The worst corrosion properties here are those of the alloy with 5% niobium, and the other alloys are also poorer than zirconium as regards high-temperature durability. Alloying of zirconium with niobium impairs its stability against oxidation.

LITERATURE CITED

[1] G. L. Miller, Zirconium (Foreign Lit. Press, 1955) p. 164.

[2] Rogers and Atkins, J. Metals 7, 9, 1034 (1955).

[3] A Shvope, Collection "Zirconium", Part II (Foreign Lit. Press, 1955).

[4] A. A. Bochvar, The Science of Metals (Metallurgy Press, 1956) p. 289.

[5] Yu. F. Bychkov, A. N. Rozanov, and D. M. Skorov, J. Atomic Energy (USSR) 2, 2, 152 (1957) (T.p. 171).

Received May 17, 1956

* T. p. = C. B. Translation pagination.

THE NORMAL ELASTIC MODULUS OF ALLOYS OF ZIRCONIUM WITH NIOBIUM

Yu. F. Bychkov, A. N. Rozanov, and D. M. Skorov

Results are described of measurements of the normal elastic modulus of alloys of zirconium with niobium in vacuum at temperatures up to 950°C, and also at room temperature after various heat treatments.

In the Soviet and Foreign literature there are no data on the elastic properties of alloys of zirconium with niobium.

The normal elastic modulus (Young's modulus) of zirconium was determined by Koster [1] by a dynamical method with heating up to 900°C; at room temperature, with a specimen cut from a freshly deposited rod of iodide-process zirconium, he obtained a value of 6950 kg/mm^2 for Young's modulus. In the opinion of Adenstedt [2] this value is decidely too low because of cracks or anisotropy in the specimen studied by Koster. According to Adenstedt's data [2], obtained by a dynamical method, the elastic modulus of iodide-process zirconium of high purity at room temperature is 10,270 kg/mm^2. Static methods give values of the modulus from 7900 to 9700 kg/mm^2.

Apparatus for Measuring the Normal Elastic Modulus

The determination of the normal elastic modulus of zirconium alloys at temperatures up to 1000°C was carried out with the apparatus shown in Fig. 1. The general plan of the measurements is like that developed for the measurement of the normal elastic modulus in vacuum at elevated temperatures [3].

The value of the elastic modulus was calculated from the results of determinations of the proper frequencies of bending vibrations of cylindrical specimens of length about 80 mm and diameter 4-6 mm. The transducer used for the vibrations was an ordinary telephone receiver 10, to the diaphragm of which there was welded a thin copper wire suspension. The receiver was connected directly to the output of a ZG-10 sound generator (Fig. 1, 14). The specimen 7, placed horizontally inside the furnace, was suspended by thin copper wires, at one end from the telephone receiver and at the other from the piezoelectric adapter 9, which served as detector for the vibrations. When the applied frequency agreed with a proper frequency of bending vibration of the specimen a resonance was observed on the screen of the oscilloscope 2, connected directly to the output of the piezoelectric crystal receiver. The resonance frequency was read off from the scale of the generator. The transducer and detector for the vibrations were supported on vacuum rubber suspensions 11 in the metal vacuum chamber 4, of diameter about 60 cm. During the heating a vacuum of 10^{-4} mm Hg was maintained in the chamber.

The apparatus described made it possible to determine the elastic modulus of the alloys with an accuracy of ± 3%.

Preparation of the Specimens

The specimens were prepared in an arc furnace MIFI-9-3 [5] with special equipment for casting rods in an atmosphere of argon. To obtain homogeneous refractory alloys with high niobium content 4 or 5 castings of weight 10-15 g and of the same composition were prepared, and then melted together. After this the material was remelted in the horizontal cavity of a copper furnace base into a rod of diameter about 15 mm and length

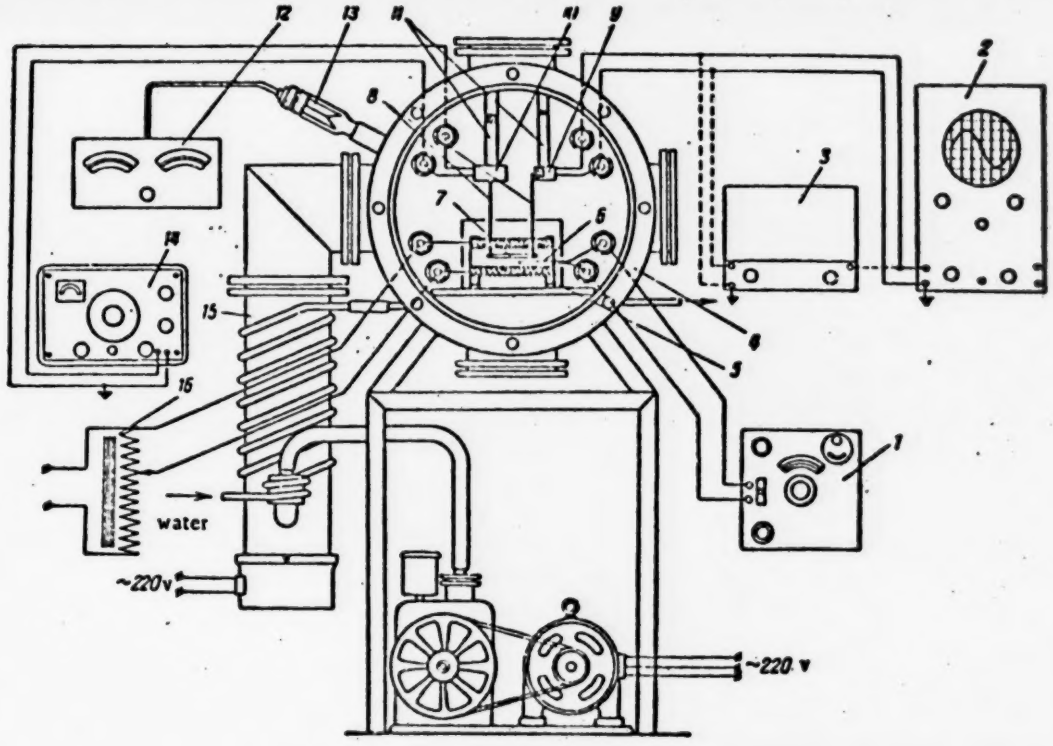

Fig. 1. Diagram of apparatus for measurement of normal elastic modulus. 1) Potentiometer PP; 2) oscilloscope EO-4; 3) amplifier; 4) vacuum chamber; 5) furnace; 6) thermocouple; 7) specimen; 8) suspensions; 9) piezoelectric adapter; 10) telephone receiver; 11) supports of vacuum rubber; 12) vacuum meter UTV-49; 13) thermocouple gauge tube LT-2; 14) sound generator ZG-10; 15) diffusion pump N-5; 16) LATR-1.

70 or 9 mm. During the carrying out of these operations the furnace was not opened. The cast rods, containing up to 20% niobium, were forged at 800-500°C to increase their length to ~ 100 mm. The heating of the castings in a muffle furnace before the forging was of short duration and facilitated the forging without leading to saturation of the metal with gases. After removal of the surface skin the rods were turned down into cylinders of diameter 4-6 mm and length 75-85 mm.

Specimens of higher niobium content were prepared from cast rods of length 90 mm, since forging them is difficult in both the hot and the cold states.

To investigate the effect of heat treatment on the elastic modulus the specimens were annealed in evacuated quartz bulbs in electric furnaces with the temperature kept constant by thermostats to accuracy ± 10°C.

Results of Measurements of Normal Elastic Modulus of the Alloys

Figure 2 shows the results of the measurements of the elastic modulus for quenched and annealed alloys, and also the electric resistance of the quenched alloys. From a comparison of the curve of Young's modulus against composition with the curve of electric resistance against composition for the alloys quenched in water from 1100°C, it is obvious that one of them is the mirror image of the other. The alloy with 15% niobium, having minimum normal elastic modulus, which is smaller than the moduli of the components by almost a factor two, has maximum electric resistance, of 100 μ ohm·cm, which is several times the specific electric resistance of the components. Between pure niobium and the composition giving the extreme values, these properties vary almost linearly.

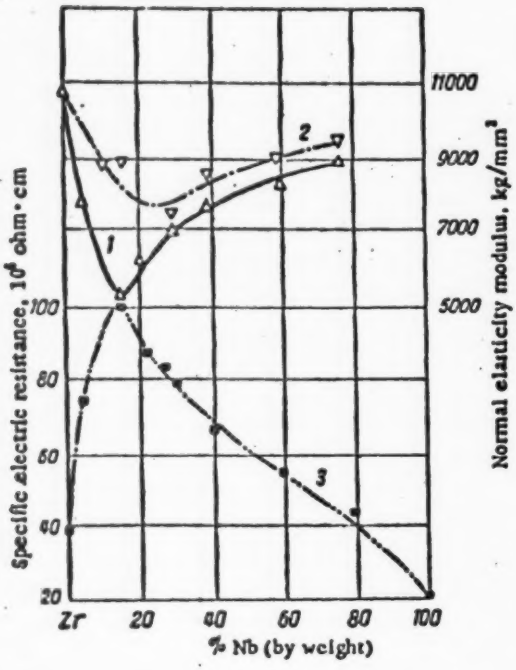

Fig. 2. Normal elastic modulus of alloys of zirconium with niobium. 1) Alloys quenched from 1100°C; 2) alloys annealed for 80 hours at 525°C; 3) electric resistance of alloys of zirconium with niobium quenched from 1100°C.

From a comparison of the curves it can be concluded that the cause of the variation of the modulus and of the electric resistance of the alloys in question is the same – distortion of the crystal lattice. The more zirconium there is dissolved in niobium, the more strongly the crystal lattice of the niobium is distorted. The extreme values of the properties in question occur for a quenched alloy of the composition (15% niobium) at which the maximum amount of zirconium is dissolved in the niobium. In the quenching of alloys with larger zirconium content the β-phase partially disintegrates; the quenched specimens have a martensite-like macrostructure, and the x-ray patterns show along with the lines of the cubic β-phase the lines of the hexagonal α-phase.

With distortion of the crystal lattice the electric resistance increases, so that curves of electric resistance against concentration for continuous solid solutions always show maxima, while the change of the elastic modulus as function of composition is frequently additive, and sometimes has small positive or negative departures from additivity. The value of the elastic modulus is determined by the size of the interatomic binding forces. Distortions of the lattice lead to a decrease of the interatomic binding forces in alloys, but other factors can compensate the influence of lattice distortions on the binding forces.

Since the elastic modulus of zirconium is lowered when it is alloyed with niobium, the influence of other factors that also help to determine the interatomic binding forces in these alloys is evidently very slight.

Quenched alloys of zirconium with niobium are in a metastable state, in which the binding forces are considerably smaller than in the stable state of those annealed at temperatures below the eutectoid (560°C).

Figure 2 shows the results of measurements of the elastic modulus after annealing for 80 hours at 525°C. The elastic modulus is increased, especially for concentrations near that for the minimum value of the modulus for the quenched specimens. In the annealed alloys with high niobium content the modulus is not so markedly changed.

The Normal Elastic Modulus of the Alloys at High Temperatures

Measurements of the dependence of the elastic modulus of the alloys on the temperature makes it possible to estimate the rate of fall of the binding forces in the alloys with change of temperature.

Figure 3 shows the results of measurements of the normal elastic modulus of pure iodide zirconium and of alloys of zirconium with niobium, annealed at 700°C and then slowly cooled in the furnace. Each specimen was tested several times during slow heating and during slow cooling of the furnace, at a rate of 3-4° per minute.

The table shows how the elastic modulus of alloys with various niobium contents decreases as the result of heating from room temperature to 900°C.

In the alloys with large niobium content, for example with 75%, the decrease of the modulus amounts to only 6-7%, i. e., almost ten times smaller than the decrease of the elastic modulus of pure zirconium. The minimum of the curve of the normal elastic modulus as function of composition at room temperature is also retained at high temperatures, but in a less sharply marked form. In our opion this is in agreement with the

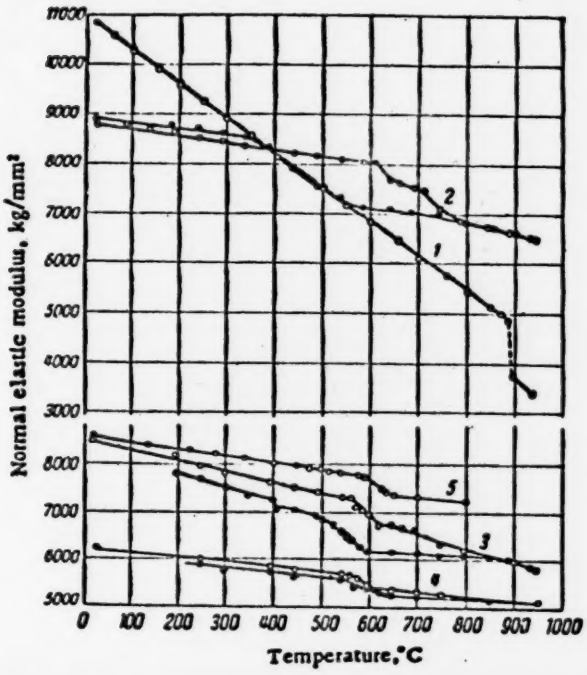

Fig. 3. Temperature dependence of the normal elastic modulus of alloys of zirconium with niobium. ○)Heating; ●) cooling: 1) pure zirconium; 2) alloy of zirconium with 5% niobium; 3)alloy of zirconium with 10% niobium; 4) alloy of zirconium with 20% niobium; 5) alloy of zirconium with 40% niobium.

Serial No.	% Nb (by weight)	Elastic modulus at 20°C	Elastic modulus at 900°C	Change of elastic modulus on heating to 900°C,%
1	0	10 800	3420	59
2	5	8 750	6600	28
3	10	8 380	5880	30
4	20	6 170	5020	18.6
5	40	8 400	7225	14
6	75	8 840	8250	6.6

fact that in the diagram of state for zirconium-niobium there is also a minimum of the solid and liquid curves, and there occurs disintegration of β-solutions (and not formation of compounds), indicating a smaller stability of alloys of intermediate composition in comparison with the slightly-alloyed members of this system.

It is interesting to compare the results of the measurements of the modulus with the results of the hardness measurements at high temperatures that have been carried out for the alloys of this system.

The greater the decrease of the value of the elastic modulus on heating to a high temperature, the smaller the high-temperature strength of the alloy.

Investigation of Transformations in Alloys of Zirconium with Niobium by a Thermoelastic Method

On the curves of the temperature dependence of the normal elastic modulus of alloys with 5, 10, 20, and 40% niobium (Fig. 3) the transitions occurring in the alloys can be well made out. During heating of the alloy with 10% niobium the eutectoid transformation at 560°C is well marked; in the alloy with 5% niobium the transformation begins at a higher temperature. The range covered by the transformation is wider in the alloy with 5% niobium than in that with 10%, which is closer to the eutectoid. These data were obtained in repeated tests of specimens after slow cooling in the furnace. In an alloy with 40% niobium tested after 80-hour annealing at 525°C, the eutectoid transformation had begun to a noticeable degree.

The formation of a new cubic β-phase on heating of an alloy above the eutectoid temperature leads to a rather sharp decrease of the elastic modulus. The inverse transformation – disintegration of the β-phase to the hexagonal α-phase and a β-phase of different composition – leads to an increase of the normal elastic modulus.

The points obtained by the thermoelastic method are close to the results of a dilatometer study of the system. From this it follows that the thermoelastic method is extremely sensitive even in the study of such low-temperature slowly-occurring transformations as the eutectoid disintegration at 560°C in alloys of the refractory elements zirconium-niobium.

LITERATURE CITED

[1] W. Koster, Z. f. Metallkunde 39, 1-12 (1948).

[2] H. K. Adenstedt, Transactions of ASM 44, 949 (1952).

[3] N. N. Sirota and Yu. F. Bychkov, Collected Contributions of MITSMIZ (in press).

[4] Yu. F. Bychkov, A. N. Rosanov, and D. M. Skorov, J. Atomic Energy (USSR) 2, 2, 146 (195·) (T.p. 165).

Received September 19, 1956

* T. p. = C. B. Translation pagination.

BLANK
PAGE

QUANTITATIVE RADIOMETRIC MEASUREMENTS OF RADIOACTIVE ORES IN NATURAL DEPOSITS

PART II*

V. L. Shashkin

A description is given of a method of radiometric sampling of radioactive ores by γ-radiation and of a method of interpreting the results of γ-ray tests of bore-holes made for such ores.

Radiometric Sampling

The radioactivity of uranium and thorium ores makes possible the determination of their uranium and thorium content directly in the natural deposits, without the necessity of taking samples of the ore. Such a method, based on the measurement of the intensity of the γ-radiation, has received the provisional name of the method of radiometric sampling. The method was developed in 1947-1948 by V. L. Baranov, V. L. Shashkin, A. G. Grammakov, M. B. Shiryaeva and M. D. Britaev, and since then has had rather wide practical application.

It is well known that the following relation holds between the intensity of the γ-radiation measured at the surface of an infinite layer with a uniform distribution of radioactive elements and the concentration of the radioactive elements:

$$I = \frac{2\pi k q \cdot \rho}{\mu},$$

where q is the concentration of the radioactive elements, referred to unit weight; $\frac{\mu}{\rho}$ is the effective mass absorption coefficient of the γ-radiation; and k is a proportionality coefficient, which for the case of a concentration of radium expressed in g/g is the γ-activity constant of radium.

From this formula it follows that for a constant mass absorption coefficient the concentration of the radioactive elements is proportional to the intensity of the γ-radiation.

In radiometric sampling it is necessary to separate out of the total γ-radiation registered by the counter the radiation from the wall of the mine working that is to be sampled. This problem is solved by the use of filtering screens as proposed by A. G. Grammakov.

The intensity of the γ-radiation registered by the counter without screen is

$$I_0 = I_1 + I_{sur} + I_b,$$

where I_1 is the γ-radiation from the wall being sampled, I_{sur} is the γ-radiation from the surrounding ore, and I_b is the natural background of the instrument.

If we place a lead plate — a screen — between the counter and the ore being sampled, then the γ-radiation from the ore being sampled will be partially absorbed and the total γ-radiation registered by the apparatus is given by the formula

$$I_{sc} = (1-\alpha)I_1 + I_{sur} + I_b.$$

* Cf. J. Atomic Energy 2, 1, 51 (1957).

where α is a coefficient characteristic of the absorption of the γ-radiation in the lead screen. The difference between the readings of the apparatus without the screen and with the screen

$$I_0 - I_{sc} = \alpha I_1$$

is thus proportional to the intensity of the γ-radiation from the ore beyond the screen. Recalling the proportionality of the intensity of the γ-radiation to the concentration of the radioactive elements, we can write

$$q = B(I_0 - I_{sc}),$$

where B is a proportionality coefficient between the concentration of radioactive elements in the ore and the difference of the γ-ray intensities measured without the screen and with the screen (called for brevity the "screen coefficient"). Numerically it is equal to the content of radioactive elements in the ore for which the intensity of γ-radiation absorbed by the given screen is equal to 1 microroentgen/hour.

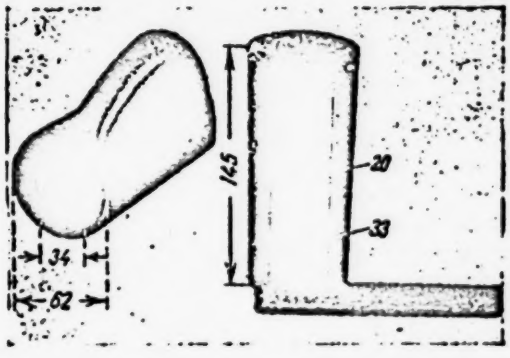

Fig. 1. Cylindrical perforated screen with insert, designed for radiometric sampling.

TABLE 1

Perforated Screen Coefficient(in $n \cdot 10^{-4}$ %U per μr /hr)

Casing	VS counter	MS counter	GS counter
Aluminum, thickness 1 mm	3.5	5.7	8.7
Iron-lead, 3 mm lead and 1 mm iron	11.8	13.4	14.5

Most widely used in practice is the so-called perforated screen with an insert that plays the role of the filtering screen (Fig. 1). Various designs are used for this type of screen.

It is most convenient to carry out the determination of the screen coefficient with a model of a stratum of ore, consisting of a box of dimensions 1 x 1 x 1 m, filled with pulverized and carefully mixed ore with a known content of uranium in equilibrium with its products. The ore must be nonemanating, or else the loss of radon must be taken into account in calculating the coefficient. The determination of the screen coefficient consists in carrying out at the surface of the box the measurements with the aperture in the screen open and closed.

The screen coefficient depends on the thickness of the counter casing and the material of the cathode, as follows from the analysis of the spectral composition of the γ-radiation of the radioactive ore. In Table 1 are shown coefficients determined for the perforated screen shown in Fig. 1.

As can be seen from Table 1, the screen coefficients for the different types of counter are decidedly different with the thin casing and are fairly closely the same with the thick casing.

If the distribution of the ore material is uniform one can, knowing the screen coefficient, determine the content of radioactive elements in a given seam from the difference of the intensities of γ-radiation measured with the aperture in the screen open and closed. In sampling uranium ores the screen coefficient is ordinarily expressed in percent uranium per microroentgen per hour difference in intensities, and accordingly the results of the sampling are expressed in percent uranium. This is correct only for the case of radioactive equilibrium and absence of elements of the thorium series. For uranium-thorium ores radiometric sampling is not applicable, and for uranium ores with disturbed equilibrium it gives the concentration not of uranium, but of radium, expressed in percent of uranium at equilibrium. The radiometric sampling of thorium ores that are practically free from uranium is carried out in a way analogous to that for uranium ores.

When the ore distribution is not uniform a single measurement with the screen does not provide a correct determination of the content of radioactive elements in the seam. In this case the measured difference of intensities of the γ-radiation will depend mainly on the distribution of the ore with respect to the surface at which the measurement is carried out. The uranium content calculated from the difference in intensity of γ-radiation measured with open and closed aperture in the screen can be either larger or smaller than the average content in the seam from which the γ-radiation is acting on the counter. When the results of radiometric sampling at a number of points are averaged, the unevenness of distribution of the ore will be smoothed out, and the average difference of the readings with the aperture in the screen open and closed will be the same as if the measurements were carried out at a seam with uniform ore distribution and a content equal to the average content for the section sampled.

Radiometric sampling is usually carried out along lines corresponding to the direction of the grooving adopted for furrow sampling of the given deposit. The points at which measurements are taken are spaced along the line at distances equal to the length of the cathode of the counter. This assures successive locations for registering γ-radiation under identical conditions from all points along the line. At each point two measurements are taken, with the aperture of the screen open and closed. In processing the results the average difference of measurements with open and closed aperture of the screen is calculated for the length of a conventional "sample," ordinarily equal to the length of the groove sample adopted for the given deposit. From the average difference multiplied by the screen coefficient one calculates the uranium content corresponding to the given "sample."

Radiometric sampling is conducted with various types of field radiometric instruments that posses sufficient stability of their readings. The constancy of the sensitivity of the instrument is checked during the course of the work by the use of standard sources of radiation.

In carrying out sampling in workings extending through the whole cross-section of the ore body, and also in sampling in workings with a large concentration of radon in the air, the γ-radiation from the surrounding ore or from the decay products of radon present in the air in the workings causes back-scattered radiation to come from the surface being tested, in the same direction as the γ-rays originating in the wall being sampled. As a result the differential effect in measurements with the screen is increased because of the effect of these rays, which leads to too high results from the radiometric sampling.

Owing to the small energy of the back-scattered γ-rays their influence can be eliminated by the use of counters that are not sensitive to soft γ-radiation, or by the shielding of the counters with a thick casing.

The registration of only hard, mainly primary, γ-radiation also makes it possible practically to eliminate the dependence of the intensity of the registered γ-radiation on the average atomic number of the rocks, and consequently makes possible the use of the same screen coefficients in radioactive sampling of different ores.

The results of radiometric sampling are as a rule checked by furrow sampling. Because of nonuniform ore distribution, the results of radiometric and furrow sampling differ for individual samples, these differences being the greater, the more nonuniform the distribution of ore. The correctness of the results of radiometric sampling is shown by the agreement of the average contents found from the data of radiometric and furrow samplings of a sufficiently large number of samples (25-30 samples of 1 meter length). An example of the comparison of results of radiometric and furrow samplings is given in Table 2.

Quantitative Interpretation of γ-Ray Bore-Hole Testing

Gamma ray bore-hole tesing, i. e., measurement of the intensity of γ-radiation along the axis of a bore hole, is widely used in searching and prospecting for radioactive ores. The quantitative interpretation of the results of γ-ray bore-hole testing provides a determination of the linear total of radioactive elements along the bore hole, i. e., the product of the thickness of the ore body by the concentration. When good cores cannot be obtained, γ-ray testing is the only method that enables one to find quantitatively the nature of the ore body penetrated by the drill.

The quantitative interpretation of γ-ray testing is based on the use of the area of the anomaly (Fig. 2). In 1947, A. P. Kazansky derived a formula relating the area of the anomaly with the thickness of the ore body and the intensity of γ-radiation,

$$S = h \cdot I_{\infty},$$

TABLE 2

Sample No.	Concentration of U in % by radiometric sampling	Concentration of U in % by furrow sampling	Sample No.	Concentration of U in % by radiometric sampling	Concentration of U in % by furrow sampling	Sample No.	Concentration of U in % by radiometric sampling	Concentration of U in % by furrow sampling
1	0.37	0.53	14	0.64	0.85	27	0.12	0.13
2	0.51	0.48	15	0.04	0.04	28	0.51	0.58
3	0.84	0.71	16	0.99	1.41	29	0.99	0.80
4	0.83	1.05	17	0.27	0.82	30	0.51	0.55
5	0.36	0.38	18	0.49	0.13	31	0.40	0.50
6	0.56	0.55	19	0.52	0.49	32	0.84	0.68
7	0.50	0.42	20	0.57	1.12	33	0.28	0.21
8	0.58	0.42	21	0.24	0.59	34	0.42	0.20
9	0.39	0.40	22	0.18	0.03	35	0.11	0.18
10	0.79	0.40	23	0.66	0.54	36	0.10	0.03
11	0.69	0.60	24	0.22	0.21	37	0.37	0.28
12	0.31	0.18	25	0 10	0.11	Cp.	0.46	0.46
13	0.08	0.09	26	0.57	1.37			

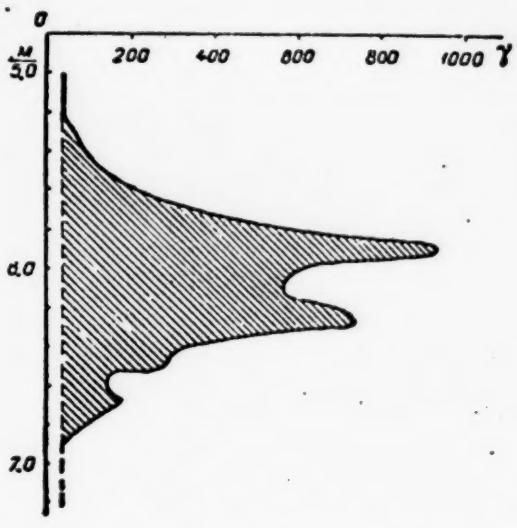

Fig. 2. Curve from γ-ray bore-hole test through an ore body. The area of the anomaly is shaded.

where S is the area of the anomaly, expressed in μr/hr·cm; h is the thickness of the ore body in centimeters; and I_∞ is the intensity of the γ-radiation of an infinite layer with concentration equal to that in the ore body. This formula was later derived in a more general form by Yu.P. Bulashevich [1]. If the drill traverses the ore body at an angle with its thickness, then the slant thickness occurs in the formula instead of the true thickness.

The intensity of the γ-radiation of an infinite layer is given by the formula

$$I_\infty = \frac{4\pi k \cdot q \cdot \rho}{\mu},$$

where q is the concentration of radioactive elements per unit weight; $\frac{\mu}{\rho}$ is the effective mass absorption coefficient for the γ-radiation; and k is a proportionality coefficient.

From this formula it can be seen that I_∞, and consequently also the area of the anomaly, does not depend on the density of the rock (for constant mass absorption coefficient), nor on the diameter of the hole. But for constant area of the anomaly the shape of the curve from the γ-ray testing depends strongly on the diameter of the hole.

Since the intensity of the γ-radiation of an infinite layer is proportional to the concentration of radioactive elements, the formula for the area of the anomaly can be written in the form

$$S = \eta \cdot h \cdot q,$$

from which it follows that the area of the anomaly is proportional to the linear total of radioactive elements along the hole (h·q).

For a succession of layers with different concentrations of radioactive elements but with the same density, proceeding from the principle of superposition of γ-ray fields one can easily show that the area of the anomaly

is proportional to the integrated linear total of the radioactive elements, independently of the distribution of concentration throughout the thickness.

The area of the anomaly, expressed in $\mu r/hr \cdot cm$, is also independent of the length of the cathode of the counter, but the shape of the γ-ray testing curve changes markedly with the length of the cathode.

Thus the area of the anomaly does not depend on the density of the rocks, the diameter of the hole, nor the length of the cathode of the counter, and therefore is the most convenient quantity characterizing the anomaly to use in the quantitative interpretation of γ-ray tests.

To calculate from the area of the anomaly the linear total of radioactive elements it is sufficient to know the conversion coefficient η. This coefficient can be determined from tests on models of infinite layers, constructed taking account of the emission of emanation by the ore. For uranium ores it is expressed in microroentgens per hour for 1% concentration of uranium, or, more frequently, for 0.01% concentration. Table 1 of [2] gives values of this coefficient for measurements with various types of counters and various casings (coefficient of infinite layer).

Just as in the case of radiometric sampling, in γ-ray bore-hole testing it is expedient to measure the intensity of the hard γ-rays only, so as to exclude the dependence of the coefficient on the average atomic number of the rock.

In standard γ-ray testing outfits (KRT, KRL) the counters used are type MS with copper cathode, enclosed in an iron casing of thickness 4-5 mm. For such a detector the conversion coefficient is practically independent of the average atomic number of the rock. According to determinations made with rocks of various compositions it is equal to 115-125 $\mu r/hr$ for 0.01% uranium in radioactive equilibrium. This provides a basis for the use of a single coefficient for rocks of various compositions. Only for ore with uranium content above ~7% the conversion coefficient will be smaller because of the change of spectral composition of the γ-radiation owing to the decided increase of the average atomic number of such ore as compared with ordinary rocks.

A knowledge of the coefficient for an infinite layer enables one to determine the linear total of uranium along the boring (given that radioactive equilibrium is maintained between uranium and its decay products) directly from the area of the γ-ray test diagram.

Methods for determining the thickness of an ore body from the γ-ray test curve have been developed for the case of a uniform distribution of the ore and for the case of gradual change of concentration with depth (V. A. Shpak, A. K. Ovchinikov, and others). But the use of these methods in the interpretation of γ-ray tests in cases of nonuniform ore distribution provides only a rough value for the thickness of the ore body.

An approximate determination of the thickness can also be carried out by estimating the positions of the boundaries of the ore body, using the shape of the γ-ray test curve and the dimensions of the region of influence of the radioactive ore body.

For the use of the results of quantitative interpretation of γ-ray tests for the purpose of computing reserves, a moderate amount of error in determining the thickness is of no importance, since increasing or decreasing the thickness does not affect the linear total along the boring, which remains constant. This property is of very great importance for the interpretation of γ-ray test data in cases of nonuniform ore distribution, when an exact determination of the thickness of the ore body is impossible.

Because of nonuniform ore distribution, values of the linear total of radioactive elements for individual borings, as determined from interpretation of γ-ray test data and from core sampling (when good cores are obtained) do not come out the same. Agreement between these results can be obtained only by averaging the linear totals obtained from a number of borings. The same is true of the comparison of the results of interpretation of γ-ray tests and those of gross sampling of the ore body at the place where it is penetrated by the boring. The difference is only that in this latter case agreement is found by averaging over a smaller number of borings, because of the more representative nature of gross sampling as compared with core sampling.

In the uranium series practically all of the γ-radiation belongs to the decay products of radon. On this account γ-ray bore-hole testing, like radiometric sampling using γ-rays, can give a correct notion of the uranium content only if the radioactive equilibrium between uranium and its decay products is maintained in the ores.

In regions of oxidation of ore deposits disturbance of the radioactive equilibrium between uranium and radium is encountered rather frequently. In this connection a distinction must be made between local disturbances of the equilibrium in either direction and one-sided regional disturbances of the equilibrium, which take in whole zones or districts of an ore deposit.

In the case of local disturbances of the equilibrium the resulting errors have the same effect as an additional nonuniformity in the distribution of the ore. When the results from a number of samples or borings are averaged, the influences of local disturbances of equilibrium cancel each other, if on the average the radioactive equilibrium is maintained in the sampled region.

A regional disturbance of the radioactive equilibrium leads to systematic errors in the interpretation of γ-ray bore-hole tests or in radiometric sampling. But regional disturbances of the equilibrium are rarely encountered, and therefore in the majority of cases γ-ray testing and radiometric sampling give reliable results.

LITERATURE CITED

[1] Yu. P. Bulashevich, Bull. Acad. Sci. USSR (Geophysical Series) 1955, No. 3.

[2] V. L. Shashkin, Atomic Energy (USSR) 2, 157 (1957) (T.p. 177).

Received July 10, 1956

ON THE PROBLEM OF THE METABOLIC EXCHANGE OF CESIUM, STRONTIUM, AND A MIXTURE OF β-EMITTERS IN COWS

D. I. Ilyin and Yu. I. Moskalev

The results are presented of an investigation of the distribution and excretion of the radioactive isotopes Cs^{137}, $Sr^{89,90}$, and of a mixture of β-emitters in 6 cows after peroral administration. It is shown that cesium and strontium are resorbed well from the intestines and that a considerable portion of the amount of emitters resorbed is excreted into milk. Resorbed cesium is almost exclusively deposited in the muscles, while strontium is in the skeleton. The results of the work indicate the danger of widespread application of radioactive fertilizers and of the maintenance of cows in pastures contaminated by the radioactive particles resulting from fission. The results can be used in calculating the maximum permissible contents of cesium, strontium, and mixtures of β-emitters in products intended for feeding cows.

The change in the radioactive background of the earth's surface which is occurring as a result of tests of nuclear weapons necessitates a knowledge of the distribution and redistribution of radioactivity in the biosphere, in particular, in the system of agricultural animals, including large cattle.

Practically lacking in the literature is information regarding the metabolic exchange of cesium, strontium, and some other radioactive elements in cows. Analysis of the regular distribution and excretion of these verysame isotopes appears expedient in connection with their high resorption from the gastrointestinal tract and respiratory system.

According to the observations of Hood and Comar [1], cesium is eliminated from the blood stream very quickly after intravenous administration; with administration by mouth, the maximum in the blood is reached after 20 hours. Initially, the cesium concentration is higher in plasma than in whole blood; after 22-30 hours an equalization occurs, after which the concentration becomes less in the plasma than in the whole blood. The cesium concentration in blood cells is 6.5 times higher than in plasma. Considerable amounts of cesium are eliminated in milk and urine. After intravenous administration, 13% of the cesium is eliminated in milk in the course of 30 days, while after peroral administration 9.6% is; 28 and 39%, respectively, is eliminated with the urine. The greatest concentration of cesium was found in the muscles, kidneys, liver, spleen, lungs, thyroid gland and the least in the bones and blood. The cesium concentration proved to be 5-20 times higher in the bone marrow of the rib cage than in the bone marrow of the femur. The total cesium content of the basic organs of the cow was not determined.

Even scanter is the information regarding the metabolic exchange of strontium in cows. According to the observations of Erf and Pecher [2], about 10% of the administered radioactive strontium is eliminated in the course of 4-5 days after intravenous administration to cows. Data regarding the extent of strontium deposition in the cow's organs and regarding the intensity of the elimination of the isotope in the urine and feces is lacking.

Method

Six cows, weighing 350-500 kg each, were under observation. In the course of four days, four cows were given a solution to drink diluted with water of a mixture of β-emitters (pH of the solution ~ 5) with a concentration

of 0.019 mC/l. In the course of 4 days, 2.6-3.5 mC of β-emitters with the following radiochemical composition: Nb^{95} – 11%, Zr^{95} – 11%, Ru^{106} – 9%, Cs^{137} – 4%, $Sr^{89,90}$ – 10%, and the sum of rare-earth elements – 55%, was administered to each cow.

The fifth cow drank 2.45 mC of a solution of the chlorides of Sr^{89} and Sr^{90} at one time, the sixth, 2.2 mC of Cs^{137}.

The radioactivity of the milk and urine of the experimental animals was determined. Two cows, which received the mixture of β-emitters, were killed on the 14th and 70th days after the beginning of the experiment, while the cows which received strontium and cesium were killed on the 32nd day. The test samples for measurement by a counter tube were prepared from the ash left after burning the organs and tissues in a muffle furnace. The radioactivity of the organs, milk, urine, and feces is expressed in percentages of the amount of the radioactive materials which was administered.

In the case of the four-day administration of the mixture of β-emitters, the beginning of the experiment was calculated from the first day of supplemental feeding. With these cows, the radioactivity of the urine, feces, and milk during the period of supplemental feeding (first four days of the experiment) was expressed in percentages of the radioactivity of the mixture of emitters which had been administered during the elapsed time, and after the fourth day in percentages of the total amount of radioactive substances administered in the course of the experiment.

The values shown on the drawings of the content of the mixture of β-emitters in excretions represent the arithmetic averages obtained from three or four cows correspondingly. Samples of milk from one of the experimental cows of this group were not tested since she was pregnant and gave no milk.

A correction for K^{40} is included in the results. It was established that the natural radioactivity of the organs and excretion is a very small value (up to several tens of thousands of fissions/minute/kg) in comparison with the radioactivity of the organs of the experimental animals, measurable in hundreds of thousands and millions of fissions/minute/kg.

In calculating the radioactive content of the entire skeleton, the weight of the latter was taken as equal to 10% of the body weight, the weight of the muscles as 43%, of the skin 12.4%, of the blood 7% [3], urine excretion as 10 l per day.

The intensity and total elimination of radioactivity in the feces were determined after the inclusion of corrections for the balance. In these calculations it was assumed that the cows eliminated the same amount of feces daily in the course of the experiment.

By graphic representation of the experimental results, data for the values of the elimination of radioactivity, lacking for individual periods of time, were found by extrapolation, which is quite permissible when materials are on hand regarding the elimination of the isotope at close intervals during the experiment and with a knowledge of the general shape of the curve. This method of analysis of the experimental results is frequently used in work on distribution [4].

Results

Elimination. In Fig. 1 are presented comparative data on the elimination of cesium, strontium, and the mixture of β-emitters in milk. It can be seen from these data that cesium was eliminated with the greatest intensity in milk. This is explained basically by its greater resorption from the intestines and its comparatively rapid exchange in comparison with other elements, including also the alkaline earths.

The greatest intensity of elimination of the isotopes in milk was observed in the course of the first days of the experiment. During five days the total elimination of cesium, strontium, and the mixture of β-emitters was: 4.0, 0.05, and 0.01%, while during 32 days it was 7.47, 0.88, and 0.09%, respectively. The intensity of the elimination of the radioactive elements in milk decreased gradually, reaching the lowest values after 3-4 weeks. The cesium concentration in milk, as a rule, was 10-20 times higher than the strontium concentration and 100 times higher than the concentration of the mixture of β-emitters. These differences were preserved throughout the course of the experiment. The greatest concentration of cesium, strontium, and the mixture in milk was observed on the second-fourth day and reached at this time 0.2, 0.03, and 0.002-0.005% of the amount administered per liter, respectively. On the 31st day the concentration of emitters in milk equalled 0.0044%

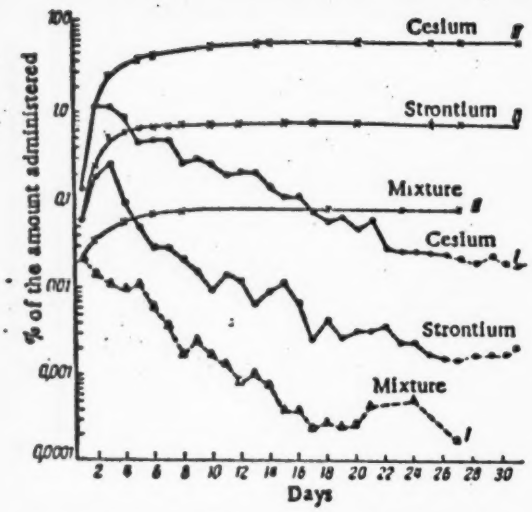

Fig. 1. Intensity (I) and total (II) elimination of cesium and of the mixture of β-emitters in milk after peroral administration.

TABLE 1

Periods of Half-Elimination of Radioactive Products in Milk (in Days)

Element	T_1	T_2	T_3
Strontium	0.4	2.4	350
Cesium	1.1	3.3	50
Mixture of β-emitters	1	3.1	46

for cesium, 0.00032% for strontium, and 0.0001% for the mixture of β-emitters.

There were differences in the distribution of the elements in the various components of the products obtained from milk. Thus, for example, the greatest amount of cesium was found in cottage cheese (0.158% per 1 kg) and in whey (0.069% per 1 kg) and approximately 10 times less was found in sour cream (0.006%). Strontium was also concentrated in large amounts in cottage cheese (0.025%), but in contrast to cesium its concentration in sour cream (0.0144%) was not only not less, but was even somewhat higher than in whey (0.0138%).

Radiochemical analysis of the milk of cows which received the mixture of β-emitters with water showed that 67-68% of the radioactivity of the milk is due to cesium and 33-32% to strontium.. Zirconium, niobium, ruthenium, and rare earth elements were not found in the milk, a fact which is, apparently, connected with the insignificant resorption of these radioisotopes from the gastrointestinal tract.

Analysis of the curves of the elimination of cesium, strontium, and the mixture of β-emitters in milk permitted the establishment of the existence of three periods of half-elimination and of their determining sizes (Table 1).

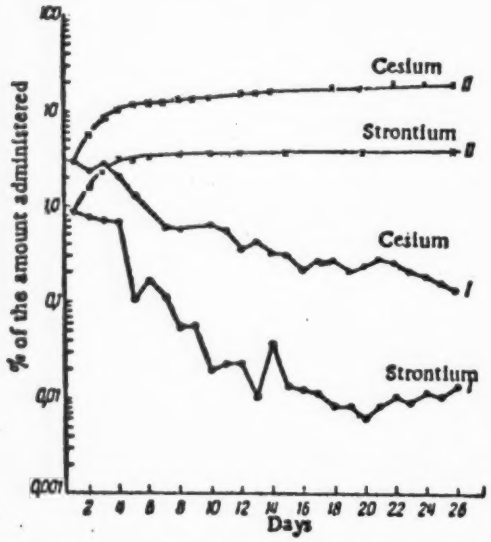

Fig. 2. Intensity (I) (in percentages per day) and total (II) elimination of cesium and strontium in urine.

The fact that the half-periods T_1 and T_2 are very small in comparison with T_3 and that they are almost equal for cesium, strontium, and the mixture of β-emitters calls attention to itself. On the contrary, T_3 of strontium is considerably higher (350 days) than the T_3 of cesium (50 days); T_2 of cesium and of the mixture of β-emitters are practically equal.

On the second day of the experiment the proportion of radioactive substances eliminated in the milk with half-periods of T_1, T_2, T_3 is in the ratio of 40: 38: 1. On the 25th day the elimination of radioactive substances occurs only with a half-period of T_3.

The hypothesis can be expressed that T_1 characterizes the portion of the radioactive element eliminated in the milk directly after its entrance into the blood stream from the intestines.

T_2, in contrast to T_3, characterizes the elimination of the portion of radioactive products from the tissues which bind the isotope weakly. T_3, apparently, characterizes the elimination of strontium from the skeleton, and of cesium from the muscles.

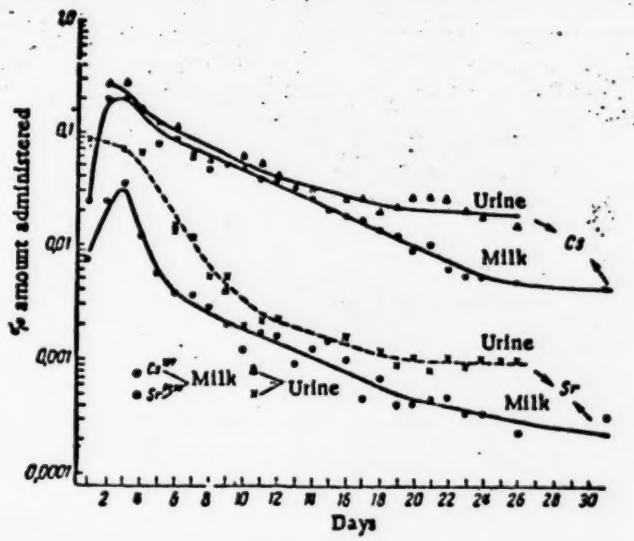

Fig. 3. Relationship of the cesium and strontium concentrations (in percentages per liter) in milk and urine at various periods of the experiment.

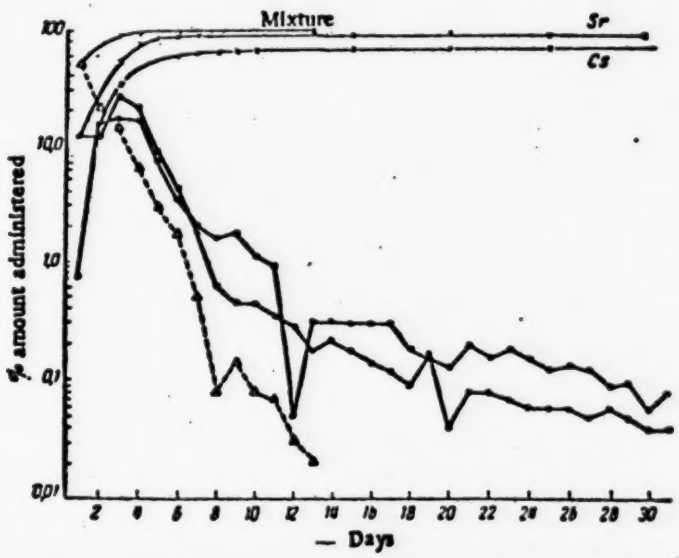

Fig. 4. Intensity (in percentages per day) and total (smooth curves) excretion of cesium, strontium, and "mixture" of β-emitters in the feces. o—o) Sr; •—•) Cs; Δ--Δ) mixture of β-emitters.

In Figs. 2 and 3 are presented data on the elimination of cesium and strontium in urine.

Cesium, strontium and the mixture of β-emitters are eliminated in the urine variously. Throughout the course of the experiment the cesium concentration in the urine is higher than the strontium concentration: during the first 5 days it is 3-10 times higher, in the subsequent days it is 10-20 times higher. Thus, for example, a liter of urine on the 3rd, 5th, 10th, and 20th days contained 0.27, 0.12, 0.06, 0.02% of the cesium, and 0.07, 0.01, 0.002, and 0.0006% of the strontium. During 26 days 17.6% of the cesium and 3.6% of the strontium were eliminated in the urine, 11.4% and 3.1% of these during the first five days.

TABLE 2

Content (% of the Administered Amount Per Organ) and Concentration(% of Administered Amount Per 1 Kg) of Cesium, Strontium, and the Mixture of β-Emitters in the Organs of a Cow and the Total Data on the Elimination of Isotopes in Milk and Urine During the Experiment

	In the whole organ				In 1 kg of tissue			
time during experiment	32 days		14 days	70 days	32 days		14 days	70 days
isotope	Cs	Sr	mixture of β-emitters		Cs	Sr	mixture of β-emitters	
Weight of cow, kg	350	388	320	503	—			
Liver	0.035	0.0025	0.004	0.0014	0.009	0.0004	0 0011	0.0003
Kidneys	0.007	0.0026	0.0015	0.0002	0.006	0.021	0.001	0.0002
Spleen	0.002	0.0009	0.0007	0.00013	0.002	0.0009	0.0008	0.0001
Lungs	0.007	0.009	0.001	0.0017	0.0013	0.0023	0.0005	0.0003
Heart				0.0002				0.00016
Muscles (gastrocnemias)	4.15	0.048	0.143	0.164	0.0282	0.0003	0.0011	0.0004
Skin	0.086	0.048	0.0022	0.13	0.002	0.001	0.0005	0.002
Blood	0.014	0.0035	0.0007	0.0008	0.0006	0.00013	0.00003	0.00002
Brain	0.0012	0.0001	0.0001	0.00005	0.0024	0.0002	0.0002	0.00007
Bone marrow					0.0006	0.0016		
Skeleton (femur)	0.081	1.45	0.125		0.0023	0.038	0.004	
Skeleton (according to the tibia)			0.125				0.004	
Epiphysis of the femur			0.274	0.234			0.0086	0.0047
Udder	0.008	0.0013	0.0015	0.0009	0,003	0,0003	0.0007	0.0003
Fetus (5 months) skeleton (femur)				0.00011				0.0003
Milk	7.473	0.884	0.050	0.136				
Urine	17.62	3.65						

The concentration of the mixture of β-emitters in the urine was 4-8 times less than the concentration of strontium and decreased during the first 10 days of the experiment from 0.018 to 0.0015%. The presence of equal concentrations of the radioactive elements in the urine of different cows receiving the mixture of β-emitters draws attention.

The concentration of cesium and strontium in the urine was higher than in milk (see Fig. 3). The decrease in the concentration with time occurs at about the same speed.

The basic amounts of the radioactive mixture, strontium, and cesium were eliminated in the feces (Fig. 4). During the first three days of the experiment the total elimination of cesium, strontium, and the mixture of β-emitters in the feces consisted of ~ 33.1, 54.0, and 93.7%.

Distribution. As is evident in Table 2, comparatively small amounts of cesium, strontium, and the mixture of β-emitters were contained in the organs of cows killed on the 14th, 32nd, and 70th days.

The basic amount of cesium found in the organs of the cow was contained in the muscles (4.15%), which is 95% of the total radioactivity found in the organs. 0.035% of the cesium was found in the liver, 0.007% each in the kidneys and lungs, 0.002% in the spleen, 0.086% in the skin, 0.08% in the skeleton and 0.0012% in the brain.

Strontium is primarily deposited in the skeleton: 1.45% of the administered amount or 94% of that found in the organs. Its content in the soft tissues was very low: on the 32nd day 0.0025% of the strontium was contained in the liver, 0.026% in the kidneys, 0.0009% in the spleen, 0.009% in the lungs, 0.048% in the muscles, 0.0001% in the brain.

With administration of the mixture of β-emitters through the gastrointestinal tract, the radioactivity of the organs proved to be even lower than with administration of cesium and strontium. The basic amount of

radioactive substances – up to 96.1% of their total content – was also found in the muscles and skeleton in this case.

The rare earth elements (Ce^{144}, Pr^{144}, Pm^{147}), as well as Zr^{95}, Nb^{95}, and Ru^{106} are practically not resorbed from the gastrointestinal tract of rats [5]. Knowing the composition of the solution of the mixture of β-emitters and the size of the deposition of strontium and cesium in the organs of the cow, it is not difficult to calculate the expected extent of strontium and cesium deposition in the skeleton and muscles from the mixture of β-emitters. Calculations indicate that when the mixture of β-emitters, containing 4% cesium and 10% strontium, is administered into the intestines, 0.145% of cesium and 0.167% strontium should be contained in the muscles and skeleton, respectively. These values are close to those found in the experiment – 0.13% for the skeleton and 0.143-0.164% for the muscles. The difference in the experimental variables (single administration of cesium and strontium, quadruple administration of the mixture of β-emitters) did not influence the total amount of absorption of cesium and strontium from the mixture of β-emitters in the intestines.

Hood and Comar pointed out the considerable difference in the action of cesium in animals with a unicameral stomach (pigs, rats) and with a multicameral one (goats, cows). Ruminants retained less cesium and eliminated relatively more in the feces than nonruminants. An experiment specially set up by us with cesium on five rats confirms this observation. Thus, the cesium content in all the organs, including the muscles, proved to be higher (14.7%) in rats than in cows (4.15%). Rats eliminate cesium primarily in the urine; the urine/feces coefficient equals 6-9. Cows, on the contrary, eliminate the greater amount of radioactivity in the feces, especially during the first week of the experiment. On subsequent days the intensity of cesium elimination in the urine and feces proves to be approximately the same. During the 32 days of the experiment a cow excreted 17.6% of the cesium in the urine, 71% in the feces, while rats eliminated 69.3% and 10.9%, respectively.

On the basis of the experimental results a general appraisal of the amount of resorption of cesium, strontium, and the mixture of β-emitters from the gastrointestinal tract of cows can be made.

The amount of cesium resorption from the intestines of cows, apparently, is 50%. This value is obtained if it is assumed that the resorbed portion of cesium is excreted in equal amounts in the urine and feces (17.6% each). The probability of this hypothesis is substantiated by the fact that the urine/feces coefficient for cesium in cows is equal to approximately one. Remember that cesium is completely resorbed from the intestines of rats.

About 10% of the strontium (the skeleton contains 1.45%, the internal organs 0.14%, 0.88% was excreted in milk, 3.65% in the urine) was absorbed from the intestines. The amount of resorption of the mixture of β-emitters from the intestines is equal to approximately 1% (milk – 0.1%, urine – 0.5%, skeleton – 0.13 and 0.24%, other organs – 0.13-0.01%, muscles – 0.15%).

The results of the present investigation allow the danger of widespread use of radioactive fertilizers containing cesium, strontium, or other isotopes which are easily resorbed and of the maintenance of animals on pastures and reservoirs contaminated by radioactive substances to be stressed.

LITERATURE CITED

[1] S. L. Hood and C. L. Comar, Arch. Biochem. and Biophys. 45, 2, 423 (1953).

[2] Erf and C. Pecher, Proc. Soc. Exptl. Biol. Med. 45, 762 (1940).

[3] B. K. Bol, Pathological Anatomical Autopsy of Agricultural Animals (Selkhozgiz, Moscow, 1953).

[4] R. M. Fink, Natl. Nuclear Energy Ser. Div. IV, 3 (1950).

[5] J. G. Hamilton, Radiology 49, 325 (1947).

Received March 29, 1956

LETTERS TO THE EDITOR

EXCITATION FUNCTIONS FOR THE REACTIONS $Mg^{24}(d, \alpha)Na^{22}$, $Fe^{54}(d, \alpha)Mn^{52}$ $Fe^{54}(d, n)Co^{55}$, and $Zn^{66}(d, 2n)Ga^{66}$

N. A. Vlasov, S. P. Kalinin, A. A. Ogloblin, V. M. Pankramov, V. P. Rudakov, I. N. Serikov, and V. A. Sidorov

A series of measurements of excitation functions have been carried out using the well-known method in which a stack of foils is placed in the deuteron beam from the cyclotron. A diagram showing the arrangement of the foil stack in the beam is shown in Fig. 1. After passing through the exit window of the cyclotron, which is covered by an aluminum foil 25 μ thick, the deuteron beam strikes the target (a stack of foils of magnesium, iron or zinc). To measure the deuteron flux, the target was insulated from the remainder of the system and connected to a current integrator. The effect of secondary electron emission on the deuteron current measurements was avoided by covering the face of the target with a layer of mica 15μ thick on both sides of which there was a thin layer of aluminum. The outer layer was grounded and the internal layer was connected to the target.

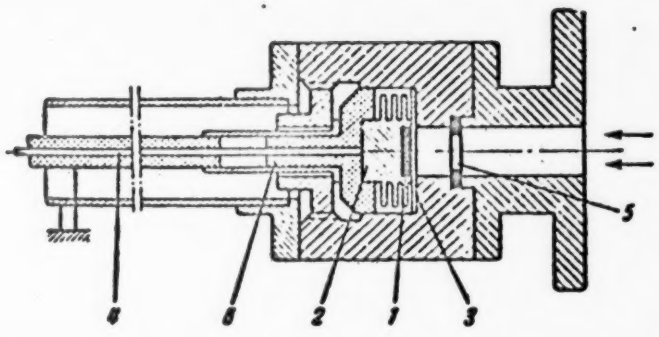

Fig. 1. Diagram of a target. 1) Foil stack; 2) current collector; 3) mica window; 4) lead to the current integrator; 5) diaphragm; 6) insulator.

The neutron energy in each foil was determined from the range-energy curve given by Rybakov [1]. Any error in the energy determination is due chiefly to the uncertainty in the initial energy of the deuteron beam (± 0.2 Mev). This error, which increases as the deuterons are slowed down, reaches ± 0.3 Mev for an energy of 8 Mev and ± 0.5 Mev at an energy of 4 Mev.

The activity of the irradiated foils was measured with an end-counter. The absolute measurements of the activity were based on the β-particle count in a special "absolute" instrument, the geometry of which is known, and in which the effects due to absorption and scattering are small and known. The samples were very thin so that self-absorption could be neglected.

The relative errors in the excitation curves may be determined from the spread of points in the different series of measurements. The errors in the absolute measurements, which were determined on the basis of the errors in the measurements in the deuteron current and in the determination of the geometry of the "absolute" instrument, as well as instabilities of the counting instruments, were ± 15%.

1. The Reaction $Mg^{24}(d, \alpha)Na^{22}$

A magnesium foil 50 μ thick was obtained from a rolled sheet of magnesium, type MG1 (purity 99.9%). When a natural isotopic mixture of magnesium is bombarded by deuterons, Na^{22} is obtained not only as a result of the (d, α) reaction in Mg^{24} (78.60% by content) but also as a result of the (d, αn) reaction in Mg^{25} (10.11% by content). The energies for these reactions are, respectively, +1.9 and −5.4 Mev. The half-life of Na^{22} (2.6 years) exceeds by a large factor the half-life of the other radioactive materials which are produced when magnesium is bombarded by deuterons.

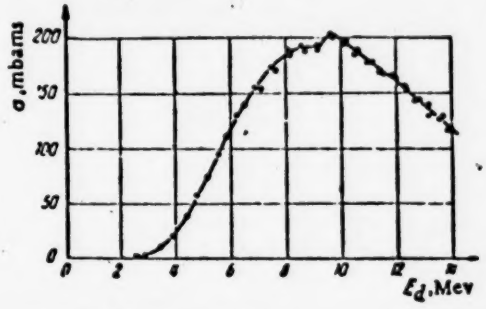

Fig. 2. Yield curve for Na^{22} in the bombardment of magnesium by deuterons.

The measurements were carried out one month after irradiation at which time all spurious radioactivity had completely decayed. The activity in Na^{22} was measured from the γ-radiation in which case the window of the counter was covered with a lead foil 1 mm thick. Samples of Na^{22} for calibrating the counter were fashioned by applying to an organic film, a thin layer of sodium, which was chemically separated from the irradiated magnesium foils; these were measured in the "absolute" instrument. In determining the absolute values of the cross section, it was assumed that 11% of the Na^{22} nuclei decay via the capture of orbital electrons [2].

The excitation function, obtained from 2 irradiated foils, is shown in Fig. 2. The cross section is calculated on the basis of a natural isotopic mixture. The curve exhibits a small narrow maximum in the region of 10 Mev. It is interesting to note, that although in similar work carried out by Irvine and Clark [3], the authors presented smooth curves, the actual experimental points in this region showed some irregularity. Comparing the experimental points of Irvine and Clark with two series of the present measurements it seems reasonable to assume that the observed maximum is real. It appears the maxima of this type have been observed by Kinsey in proton scattering in carbon and oxygen [4]. It is not very likely that the maxima, which correspond to a very high excitation energy for the intermediate nucleus, can be explained by the existence of some individual excitation level of this nucleus.

The yield of Na^{22} obtained by bombarding a thick magnesium target by 14 Mev deuterons is $6.0 \cdot 10^{-4}$ atoms per deuteron or 3.1 μcurie/μamp·hr. Irvine and Clark [3] have reported a value of 1.8 μcurie/μamp·hr for this same quantity [3]. The discrepancy in the results is greater than the limits of error but its origin is not clear.

2. The Reaction $Fe^{54}(d, \alpha)Mn^{52}$

Foils 30 and 15 μ in thickness were obtained from rolled laminated Armco iron. Since iron has four stable isotopes, in deuteron bombardment a large number of radioactive species with different decay periods are obtained. Mn^{52} formed only as a result of the reaction $Fe^{54}(d, \alpha)Mn^{52}$ in the ground state and in metastable states (half-life 6.0 days and 21 minutes).

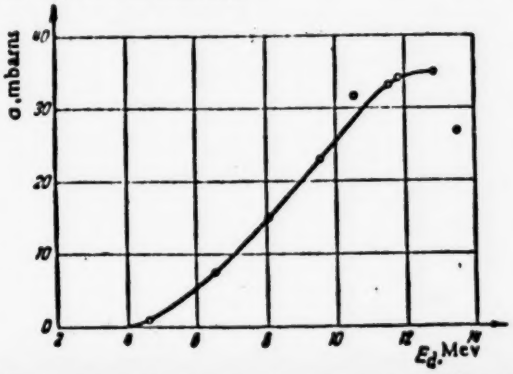

Fig. 3. Excitation function for the reaction $Fe^{54}(d, \alpha)Mn$ with the production of Mn^{52} in the ground state.

In the present work the yield of Mn^{52} in the ground state was investigated. The manganese was separated chemically from each foil of the irradiated stack in the form of the pyrophosphate ($Mn_2P_2O_7$). The decay curves for the activity of these samples were checked for a period of 2,000 hours. The measurements indicate that along with the activity which has a half-life of six days, there is an activity with a period of approximately 100 days, which is apparently due to impurities such as the long-lived cobalt isotopes (half-life of 80 and 270 days).

The decay curves for each sample were analyzed by a least square method for the two calculated periods – 6.0 and 100 days. The absolute value of the cross section was determined for a deuteron energy of 11.4 Mev. The

manganese, separated chemically from the foil associated with this deuteron energy was deposited in a thin layer (0.2 mg/cm^2) on organic films. The activity of the samples prepared in this way was measured with the "absolute" instrument. In calculating the cross section it was assumed that 65% of the Mn^{52} nuclei decay via capture of orbital electrons [5].

The excitation function obtained from two irradiated foils, is shown in Fig. 3. The yield of Mn^{52} obtained in bombarding a thick iron target by 14 Mev deuterons is $4.6 \cdot 10^{-5}$ atoms per deuteron or 34 μcurie/μamp·hr.

3. The Reaction $Fe^{54}(d, n)Co^{55}$

Co^{55} is formed in the bombardment of iron by deuterons only as a result of the reaction $Fe^{54}(d, n)Co^{55}$. It has been established that when the foil stack is irradiated for 30 min, the main part of the activity which appears is due to this isotope (half-life 18.2 hours). However, along with this effect, there is observed a noticeable long-lived activity. Thus, in each foil three decay curves were measured, which were then analyzed by a least squares method for 3 half-lives: 18.2 hours, 6.0 days and 80 days. The absolute value of the cross section was determined for deuteron energies of 6.2, 7.2, 8.9, and 10.0 Mev. In calculating the cross section it was assumed that 40% of the Co^{55} nuclei decay via capture of orbital electrons [5].

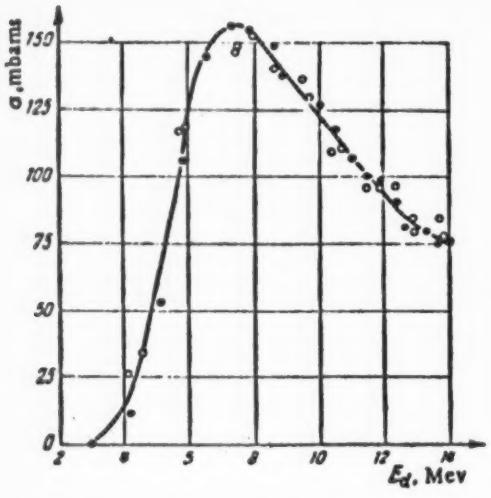

Fig. 4. Excitation function for the reaction $Fe^{54}(d,n)Co^{55}$.

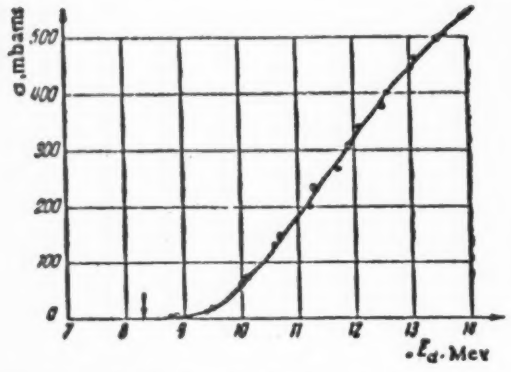

Fig. 5. Excitation function for the reaction Zn^{66} (d, 2n) Ga^{66}.

The excitation function obtained from 3 irradiated foils is shown in Fig. 4. The yield of Co^{55} obtained by bombarding a thick iron target by 14 Mev deuterons is $2.4 \cdot 10^{-4}$ atoms per deuteron or 1.5 μ curie/μamp·hr.

4. The Reaction $Zn^{66}(d, 2n)Ga^{66}$

A zinc foil 15 μ thick was obtained from a sheet of laminated zinc type TsO (purity 99.9%). Since zinc has 5 stable isotopes, neutron bombardment results in the production of many activities with different half-lives. Ga^{66} is produced only as a result of the (d, 2n) reaction in the isotope Zn^{66} (content of this isotope is 27.81%, the energy of the reaction is 8.1 Mev).

It was found possible to measure the activity of Ga^{66} against the background of other activities because of the presence in its β-spectrum of high-energy positrons (E_{max} = 4.15 Mev). An aluminum filter, 2 mm thick, was set up in front of the counter window; this transmitted about half the Ga^{66} positrons but completely attenuated all β-particles of the other activities. Moreover, the fact that the hard part of the spectrum was used made it possible to neglect self-absorption in the foils. To measure the background of γ-radiation an aluminum filter 8 mm thick was set up in front of the counter window. Continuous measurements over the course of several days indicated that the activity measured in this fashion decayed with a half-life of 9.4 ± ± 0.2 hours (the tabulated value we used is 9.45 hours [5]).

To obtain the samples which were used to calibrate the counter, Ga^{66} was obtained by bombarding copper foils with α-particles using the reaction Cu^{63} (α, n) Ga^{66}. The irradiation was carried out inside the cyclotron chamber at a radius of 52 cm where the α-particle energy is 18 Mev. This method of forming Ga^{66} is convenient in that only 2 radioactive materials, Ga^{66} and Ga^{68} are produced. The latter has a half-life

of 66 min and several hours after irradiation it has almost completely disappeared. Thin samples, (0.1 mg/cm^2) were obtained by dusting the irradiated copper on organic films or by applying the chemically separated gallium on organic films. In determining the absolute value of the cross section it was assumed that 40% of the Ga^{66} nuclei decay via capture of orbital electrons [5].

The excitation function obtained from the irradiation of 2-foil stacks is shown in Fig. 5. The yield of Ga^{66} obtained in bombarding a thick zinc target with 14 Mev deuterons is $8.5 \cdot 10^{-5}$ atoms per deuteron or 1.0 mcurie/μamp·hr.

The authors are indebted to their colleagues at the cyclotron laboratory who made it possible to carry out this work.

LITERATURE CITED

[1] B. V. Rybakov, J. Exptl.-Theoret. Phys. 28, 651 (1955).

[2] W. E. Kreger, Phys. Rev. 96, 1554 (1954).

[3] J. W. Irvine and E. T. Clarke, J. Chem. Phys. 16, 686 (1948).

[4] B. B. Kinsey, Phys. Rev. 99, 332 (1955).

[5] G. Seaborg, I. Perlman, and J. Callender, Table of Isotopes (Foreign Lit. Press, 1955)(Russian translation).

Received October 15, 1956

EXCITATION FUNCTIONS FOR THE REACTIONS $Li^7(p, n)Be^7$, $B^{10}(p, \alpha)Be^7$, AND $B^{11}(p, n)C^{11}$, AND ENERGY LEVELS IN Be^8, C^{11}, AND C^{12} NUCLEI

S. P. Kalinin, A. A. Ogloblin, and Yu. M. Petrov

The various existing models of the nucleus have been formulated on the basis of various experimental data among which the data concerning the energy level spectrum in light nuclei are of great importance. One of the methods of studying the energy levels is the measurement of the excitation functions for various nuclear reactions. The presence of resonances in the excitation curve is an indication of the existence of a level at the corresponding energy in the intermediate nucleus.

The present work reports the results of measurements of the excitation functions for the reactions $Li^7(p,n)Be^7$, $B^{10}(p, \alpha)Be^7$, and $B^{11}(p, n)C^{11}$ at a proton energy of 12 Mev. In these reactions the intermediate nuclei are Be^8, C^{11}, and C^{12}. The available data on levels in these nuclei and the excitation energy region which is attainable using 12-Mev protons are extremely poor: it is doubtful that there is a series of levels, but, in general, comprehensive studies over wide energy regions have not been carried out [1]. The excitation curves for the reactions $Li^7(p, n)Be^7$, $B^{10}(p, \alpha)Be^7$, and $B^{11}(p, n)C^{11}$ have been measured at low proton energies; the absolute value of the cross section has been measured only for the reaction $Li^7(p, n)Be^7$ at a proton energy of 2.6 Mev [2].

The excitation functions were measured by the well-known stack method in which a stack of thin samples of the material being investigated is irradiated; measurements of the activity of each sample are then carried out. The irradiation was performed in the external proton beam of the cyclotron at a proton energy of 12.2 ± ± 0.1 Mev.

In measuring the excitation functions for the reactions $B^{11}(p, n)C^{11}$ and $B^{10}(p, \alpha)Be^7$ the target, consisting of samples of boron-polystyrene films with thicknesses ranging from 3.5 to 16 mg/cm², was fabricated from natural boron. In studying the reaction $B^{10}(p, \alpha)Be^7$ use was also made of a thinner target obtained by dusting boron anhydride B_2O_3 on an aluminum foil 10 μ thick. In the measurements of the excitation curve for the reaction $Li^7(p, n)Be^7$ the target was a layer of LiF 2-10 mg/cm² thick which was applied to a 10 μ aluminum substrate.

The proton energy in the targets was determined from the range-energy curve which was plotted by extrapolating known range-energy curves for paraffin, air, and aluminum.

The irradiation of the stack was carried out in the setup described in [3].

The excitation functions for the reactions $Li^7(p, n)Be^7$ and $B^{10}(p, \alpha)Be^7$ were measured from the γ-activity of Be^7 while the excitation function for the reaction $B^{11}(p, n)C^{11}$ was measured from the annihilation radiation in C^{11}.

The Be^7 activity measurement was carried out with a scintillation counter using a NaI(Tl) crystal and a FEM-12 photomultiplier with an 8-channel pulse-height analyzer. In addition, the activity of the Be^7 obtained in the reaction $Li^7(p, n)Be^7$, was measured with an end-counter. In all stacks the results were independent of the method of measurement.

The activity in C^{11} was measured from the annihilation γ-radiation using an end-counter, in front of which was placed a lead filter 1 mm in thickness which completely attenuated decay positrons. Measurements of the decay curves of several samples yielded a half-life, $T_{1/2}$ = 20.3 min which is in good agreement with the tabulated values (20.42 min).

To measure the absolute value of the cross sections the Geiger counters were calibrated for γ-radiation using samples of Au^{198} of known activity. Since the gold line (E_γ = 0.412 Mev) has an energy which is close to the energy of the γ-quanta of Be^7 (E_γ = 0.480 Mev) and the annihilation γ-quanta of C^{11} (E_γ = 0.511 Mev) the counter efficiency in the measurements of all three activities was approximately the same. The absolute value of the activity of the gold samples was measured using the β-particles in a special "absolute" instrument [3] with known geometry and with a well-defined and small effect due to scattering and absorption. The samples were very thin so that it was not necessary to make corrections for self-absorption and back-scattering.

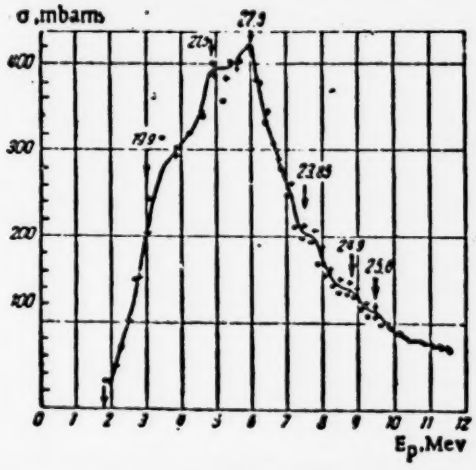

Fig. 1. Excitation function for the reaction $Li^7(p, n)Be^7$. The crosses and dots indicate the results of measurements of different stacks. The arrows designate the location of levels of the intermediate nucleus. The solid arrows indicate known levels while the dotted arrows indicate levels the existence of which has not been definitely established (in [1] these were designated by solid and dashed lines), the heavy arrows indicate levels first found in the present work.

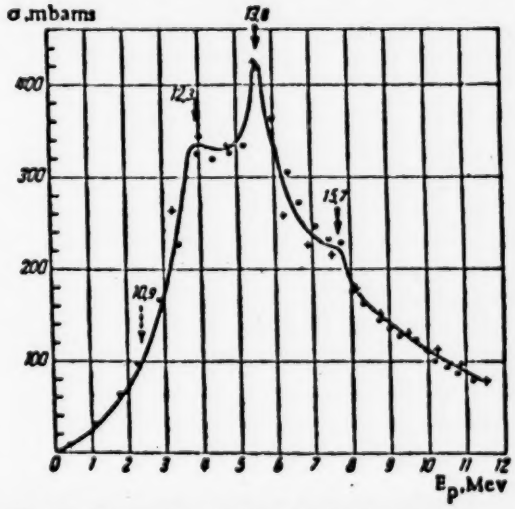

Fig. 2. The excitation function for the reaction $B^{10}(p, \alpha)Be^7$. The notation is the same as in Fig. 1.

In measuring the absolute value of the cross section for the reaction $Li^7(p, n)Be^7$ the activity of the gold samples was compared directly with the activity of the various stack samples. In making the measurements on the absolute cross sections for the reactions $B^{10}(p, \alpha)Be^7$ and $B^{11}(p, n)C^{11}$ specially prepared thin samples were irradiated in which the boron content was known more accurately than in the films. The sample thickness was such that the entire proton range was covered. Thus, the total yields of Be^7 and C^{11} were measured in the reactions indicated and then the excitation functions, measured in relative units, were normalized.

The accuracy of the measurement of the absolute cross section was ± 20%.

In Fig. 1 is shown the excitation function for the reaction $Li^7(p, n)Be^7$ as obtained from two foils. The excitation function exhibits maxima at proton energies of 4.9, 6.0, and 7.6 Mev which correspond to known levels in Be^8 with excitation energies of 21.5, 22.5, and 23.85 Mev, respectively. Furthermore, at proton energies of 8.8 and 9.5 Mev and in the region around 3.5 Mev there are kinks in the excitation function. The kinks at 8.8 and 9.5 Mev, although weakly defined, appeared in both series of measurements. It would seem that these may be explained by the presence in Be^8 of hitherto unknown levels with excitation energies of 24.9 ± 0.2 Mev and 25.6 ± 0.2 Mev. The kink in the region of 3.5 Mev may possibly be due to the known level in Be^8 at an energy of 19.9 Mev. Some of the energy discrepancy may be explained by the rather broad energy spread in this region. Because of the poor resolving power at low proton energies, the excitation function differs sharply from those which have been published in [2]. In particular, the well-known resonance at E_p = 2.25 Mev is not completely defined. This situation is explained by the fact that in the present measurements the spread in the beam at E_p = 2.25 Mev amounts to 600 kev, which is considerably greater than the width of the level.

The excitation function for the reaction $B^{10}(p, \alpha)Be^7$ (Fig. 2) exhibits well-defined maxima at proton energies of 4.0 and 5.6 Mev. The first of these resonances corresponds to the well-known level in C^{11} at an energy of 12.3 Mev. The second resonance may be explained by the existence in C^{11} of a hitherto unknown level with

an excitation energy of 13.8 ± 0.2 Mev. At a proton energy of 7.8 Mev, the excitation function exhibits a weakly defined maximum which is associated, apparently, with a hitherto unknown level in C^{11} with an energy of 15.7 ± 0.2 Mev.

The known levels in C^{11} at energies of 9.7 and 10.06 Mev, which could be excited at proton energies of 1.1 and 1.5 Mev, were not found because of the poor energy resolution in this region. The level at an energy of 10.9 Mev, predicted in the survey in [1], was also not found.

In Fig. 3 is shown the excitation function for the reaction $B^{11}(p, n)C^{11}$ measured from 3 stacks. The curves are different in the energy region 9-12 Mev for different foils; this would appear to be due to some systematic errors which have not been taken into account in determining the boron content in the films of each stack. However, in all three series of measurements there are clearly visible three maxima at proton energies of 6.6, 8.8, and 10.1 Mev as well as a kink in the curve at a proton energy of 4.5-5 Mev. The maximum at an energy of 6.6 Mev corresponds, evidently, to the 2 well-known levels in C^{11} at energies of 21.79 and 22.4 Mev. The maxima at proton energies of 8.8 and 10.1 Mev correspond to levels with energies of 24.3 and 25.36 Mev predicted in the survey in [1]. The kink in the excitation function in the region of 4.5-5 Mev probably corresponds to a group of levels in C^{11} with energies of 19.7-20.7 Mev.

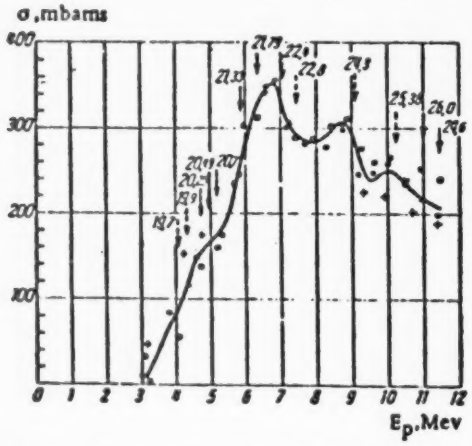

Fig. 3. The excitation function for the reaction $B^{11}(p, n)C^{11}$. The notation is the same as for Fig. 1.

It should be noted that in the cases in which the proton energy was greater than 6-7 Mev, the cross sections for the reactions $Li^7(p, n)Be^7$ and $B^{10}(p, \alpha)Be^7$ were measured from the Be^7 yield and do not represent the total cross section for the (p, n) and (p, α) reactions in Li^7 and B^{10}.

This is connected with the fact that Be^7 may be produced in states in which it may break up into He^3 and He^4. An estimate of the probability of this process is rather difficult; generally speaking, however, it may be large. Thus, for example, the cross section for inelastic scattering of protons on Li^7 with the production of the residual nucleus Li^7 in similar excited states, from which it may break up into H^3 and He^4, is large. In one report, which is to be published shortly by this laboratory, it has been found that for proton energies from 8 to 12 Mev this cross section is approximately 200 mbarns and that it starts to increase sharply at 6.5 Mev. If the breakup of Be^7 in the reactions $Li^7(p, n)Be^7$ and $B^{10}(p, \alpha)Be^7$ goes with the same probability, then the measured cross sections are considerably smaller than the total cross sections for (p, n) and (p, α) reactions in Li^7 and B^{10}.

The high probability for the breakup of Be^7 may explain the sharp reduction in the cross section for the production of Be^7 at proton energies above 6 Mev. The ratio of the cross sections at the maximum to the cross section at 11.5 Mev is 6.0 in the reaction $Li^7(p, n)Be^7$ and 5.3 for the reaction $B^{10}(p, \alpha)Be^7$. This change in cross section over an energy interval of 5-6 Mev is considerably greater than one might expect for (p, n) and (p, α) reactions on the basis of the intermediate-nucleus theory.

The excitation function for the reaction $B^{11}(p, n)C^{11}$ in this same energy region was found to have a considerably greater slope. The ratio of the cross section at the maximum to the cross section at 11.5 Mev is 1.7. The threshold for the breakup of the residual nucleus C^{11} into Be^7 and an α-particle is 8.2 Mev. However, the importance of this process may be less than it is in Be^7 since C^{11}, in contrast with Be^7, has many levels between the ground state and the level from which particle disintegration can occur. Hence, the inclusion of new levels should not have any great effect on the distribution of the cross sections for (p, n) reactions in B^{11}.

The possibility of the breakup of C^{11} should, however, be taken into account in measuring the excitation function for the reaction $B^{10}(p, \alpha)Be^7$ for proton energies greater than 8.2 Mev since in this case the production of Be^7 in the reaction $B^{11}(p, n\alpha)Be^7$ is possible.

In conclusion, we wish to express our gratitude to N. A. Vlasov for discussing the results, D. A. Panov for a number of valuable comments and also to all the people at the Cyclotron Laboratory who made the execution of the present work possible.

LITERATURE CITED

[1] F. A. Ajzenberg and T. Lauritsen, Rev. Mod. Phys. 27, 77 (1955).

[2] N. A. Vlasov, Neutrons (State Tech. Press, 1955).

[3] N. A. Vlasov, S. P. Kalinin, A. A. Ogloblin, V. M. Pankratov, V. P. Rudakov, L. N. Serikov, and V. A. Sidorov, J. Atomic Energy 2, 169 (1957). *

Received October 13, 1955

* Original Russian pagination. See C. B. translation.

MEASUREMENT OF THE ANGULAR DISTRIBUTION OF 0.9-MEV NEUTRONS ELASTICALLY SCATTERED ON Bi, Pb, Sn, Fe, AND Al

G. N. Lovchikova

This report contains the results of measurements of the angular distribution of neutrons from a Na-γ-Be source scattered elastically in bismuth, lead, tin, iron, and aluminum which were carried out by the author in 1953-1954. The experiment was carried out using a circular geometry (Fig. 1). The change from one scattering angle ϑ to another was realized by changing the source-scatterer and scatterer-detector distances. The geometrical angular resolution varied from ± 7° to ± 12°.

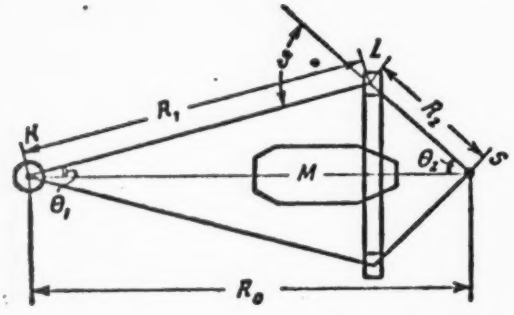

Fig. 1. Diagram of the experimental layout. S) Source; K) detector; L) scatterer; M) shielding cone; ϑ) scattering angle.

In this work a spherical photo neutron source Na-γ-Be (the thickness of the Be sphere was 8 mm) with a mean energy of 0.9 ± 0.1 Mev was used. The neutron detector was a spherical ionization chamber the output of which was fed to a linear amplifier and recorded on a 20-channel analyzer.

Of all the fillers which were tested (H_2, He, BF_3, N_2) helium was found to be most suitable for detecting neutrons of the desired energy: in the resonance region (around 1 Mev) its total cross section is relatively large; as the neutron energy is reduced, the cross section falls off sharply, hence the sensitivity of the detector was small for neutrons which were scattered from the walls. The helium chamber was more sensitive to elastically scattered neutrons than to inelastically scattered neutrons; this was essential in the present work. Because of the spherical detector geometry, the efficiency was independent of neutron direction. The pressure which was chosen (7 atmos) provideda reasonable efficiency with small cutoff effects. The scattering ring was rectangular in cross section. The number of atoms in the ring was determined by weighing.

In [1-3] the angular distribution of neutrons elastically scattered in helium has been measured for various incident-neutron energies. The angular distribution of elastically scattered neutrons in the center-of-mass system $\sigma(\theta)$ is related to the energy distribution of recoil nuclei in the laboratory system P(E) by the relation

$$\sigma(\theta) = \frac{E_{max}}{4\pi}\,\sigma_t\,P(E), \tag{1}$$

where θ is the scattering angle in the center-of-mass system; E is the energy of the recoil nucleus; σ_t is the total cross section; E_{max} is the maximum energy of the recoil nucleus.

Using Eq. (1) and the well-known relation

$$\cos\vartheta = 1 - 2\frac{E}{E_{max}}, \tag{2}$$

G. R. Poze, with the aid of the curves given by Adair[1] for the angular distribution of scattered neutrons, obtained the spectra for recoil nuclei at the same neutron energy (Fig. 2). Analyzing these spectra, Poze reached the conclusion that in the energy region from 0.3-0.9 Mev, the energy distribution curves for recoil nuclei are generally linear. It may be assumed that in this energy region the distribution function for recoil nuclei is independent of the energy of the incident neutrons. After applying the required corrections, the measured spectrum for recoil nuclei in the helium chamber for neutron energies of 0.9 Mev agrees, within the limits of the experimental errors, with the spectrum obtained from the measurements given by Adair. This feature of the recoil-nuclei spectrum in a helium chamber was also used in the present work.

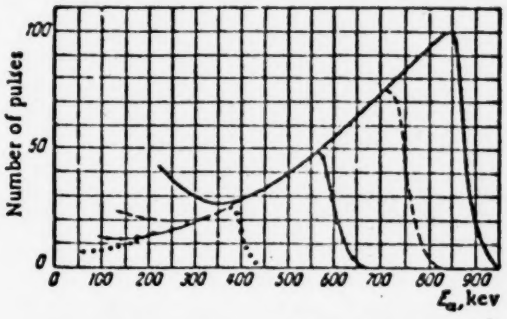

Fig. 2. Spectrum of the recoil nuclei in helium obtained from the measurements of Adair [1]. —) E_n = = 865 kev; – – –) E_n = 750 kev; – · –) E_n = 600 kev; ····) E_n = 400 kev.

The differential cross section for elastically scattered neutrons was taken as the ratio of the total number of counts in all channels of the analyzer (corresponding to the linear section of the spectrum) for measurements with the scattered flux to the total number of counts in the same channels for measurements with the direct flux. To determine the cross section, the following quantities were measured: a) the spectrum of scattered neutrons and the background (A_3); b) the spectrum of background neutrons with the scatterer removed (A_2); c) the spectrum of the direct neutron flux without the scatterer and without the shielding cone (A_1).

Thus,

$$\sigma(\vartheta)=\frac{A_3-A_2}{A_1}\cdot\frac{R_1^2R_2^2}{R_0^2N}, \qquad (3)$$

where N is the number of nuclei in the scatterer; R_1 is the distance from the detector to the scatterer; R_2 is the distance from the scatterer to the source; R_0 is the distance from the detector to the source (cf. Fig. 1).

Equation (3) is valid under the following assumptions: a) the neutron source is spherically symmetric, this obtains in the present case; b) the detector efficiency is the same for direct and scattered neutrons; in the present case the use of the linear portion of the recoil nuclei spectrum in helium automatically ensures the same detector efficiency for the direct and scattered neutron flux; c) the detector sensitivity is independent of the counting rate; this applied for the intensity of the present source; d) the detector sensitivity is independent of the direction of incident neutrons; this was guaranteed by the spherical shape of the chamber; e) the samples of the scattering material are sufficiently thin so that attenuation of the incident flux and multiple scattering can be neglected in the scatterer; inasmuch as the experiment made use of samples of thickness of the order of a free path length for the neutron, in calculating the cross sections the appropriate corrections were introduced.

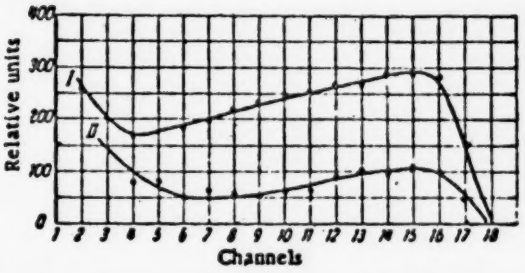

Fig. 3. Spectrum for the recoil nuclei in helium obtained in the present work. I) Typical spectrum for the direct neutron flux; II) typical spectrum for inelastically scattered neutrons in lead at an angle 120° (the background A_2 is excluded).

In Fig. 3, are shown curves of the spectra of recoil nuclei in helium. In calculating the differential cross section it is important to establish correctly the limits of the linear portion of the spectrum. The upper limit of this region was determined from the maximum in the neutron recoil-nuclei spectrum. These maxima coincide only for heavy elements, in which the losses due to elastic collisions are small. In the light elements such as aluminum, the maximum is shifted by the magnitude of the loss in elastic collisions. Part of the right-angle section of the spectrum

in the low energy region may be distorted due to inelastically scattered neutrons and recoil electrons from γ-radiation. The limit for electron recoil was determined experimentally with a γ-source, Na^{24}, and calculated for inelastically scattered neutrons.

All the measured cross sections are for elastic scattering. The measurements at a given angle in each element were repeated several times, at different times, depending on the intensity of the source and the scattering angle. A control on the proper operation of the system as a whole was realized through the spectrum of the direct flux, which was measured at the beginning and at the end of the measurement. To measure the spectrum of scattered neutrons, paraffin was used as a shield from the direct flux; inside the paraffin there was a lead cylinder which acted as a shield against the γ-radiation of the source. To measure the direct flux, the neutron source was placed in a lead sphere with wall thickness equal to the length of the lead cylinder in the paraffin shield in order to achieve the same attenuation of γ-radiation in both cases. Experiments with lead spheres of different thickness for measuring the direct flux have shown that the recoil-nuclei spectrum in the region being investigated does not change. However, the measured direct flux is too low because of inelastic scattering due to the level at an energy of 540 kev in lead, so that corrections were required.

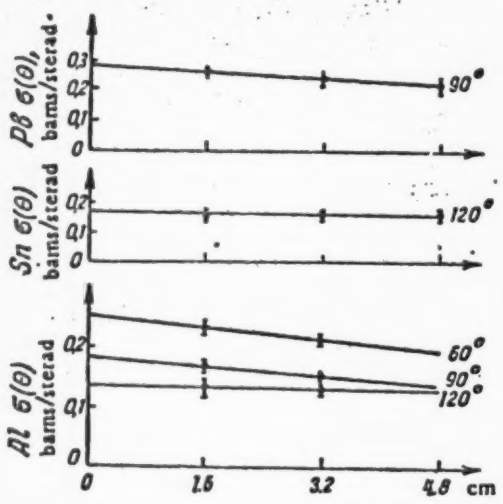

Fig. 4. Characteristic curves obtained in measurements with different ring thicknesses for extrapolating σ(θ) to zero thickness.

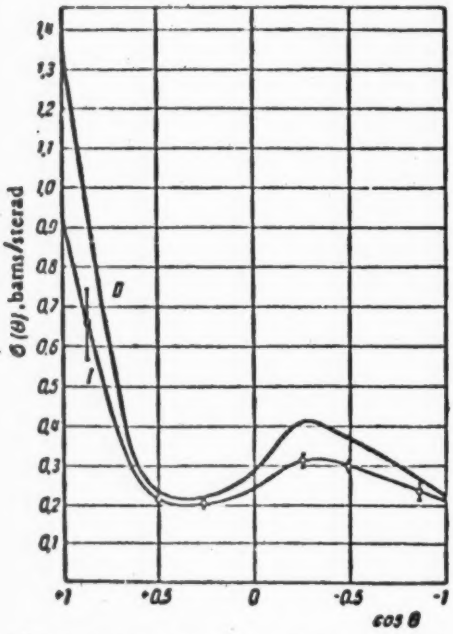

Fig. 5. Angular distribution of neutrons with energies of 0.9 Mev scattered in bismuth.

Measurements were performed to determine the background of neutrons scattered from the walls and ends of the chamber, and neutrons which entered on the detector after being scattered in the paraffin cone and then in the scattering ring. Both effects were insignificant (less than 1%) so that corrections were not required.

The corrections for the attenuation of the neutron flux and multiple scattering were calculated using the method given by Turchin [4].

To verify the calculated correction for multiple scattering and attenuation of the neutron flux, the measurements were carried out with different ring thicknesses in order to extrapolate σ(ζ) to zero thickness. In Fig. 4 are shown curves which give the dependence of the cross section on the thickness of the ring for aluminum, lead and tin. A comparison of the experimental and theoretical data shows that these coincide within the limits of statistical errors.

The results of the measurements of the angular distribution of elastically scattered neutrons are shown in Figs. 5-9. Curve I shows the experimental results without the introduction of corrections and Curve II shows the experimental results corrected for attenuation of the direct flux in the ring and for multiple scattering. In all elements a maximum in the angular distribution was observed in a forward direction and in lead and bismuth an additional maximum was noted at an angle of ~105°.

Elements with very different atomic numbers exhibit a different angular distribution whereas neighboring elements – lead and bismuth – have similar angular dis-

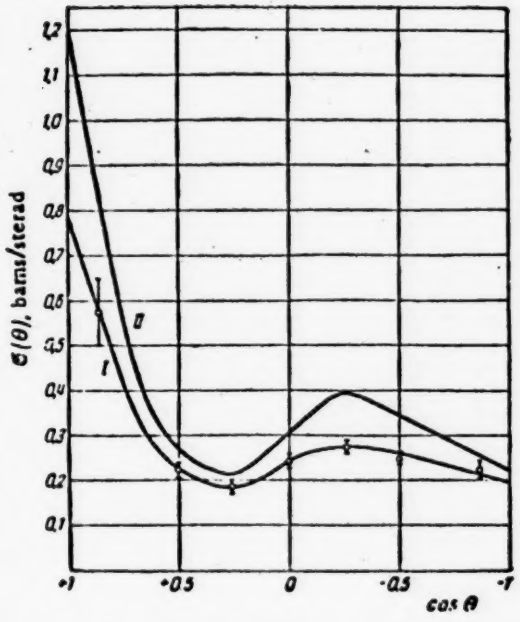

Fig. 6. Angular distribution of neutrons with energies of 0.9 Mev scattered in lead.

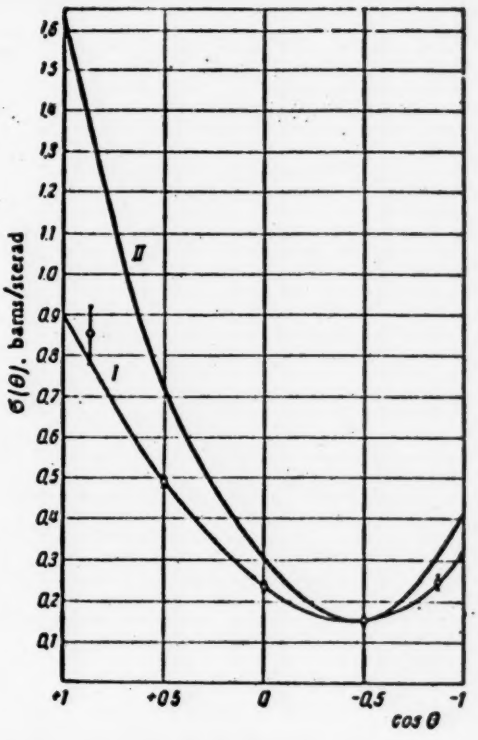

Fig. 7. Angular distribution of neutrons with energies of 0.9 Mev scattered in tin.

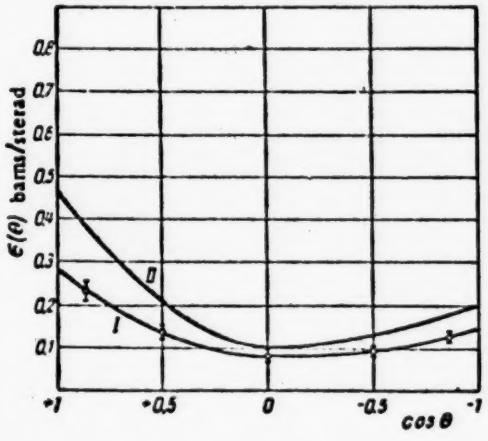

Fig. 8. Angular distribution of neutrons with energies of 0.9 Mev scattered in iron.

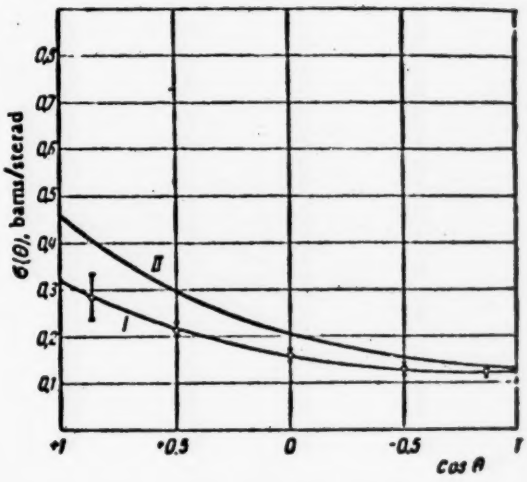

Fig. 9. Angular distribution of neutrons with energies of 0.9 Mev scattered in aluminum.

tributions. Thus, the results corroborate the anisotropy indicated by the theory.

The literature contains no data on the angular distribution of neutrons from a Na-γ-Be source. Angular distributions for neutron energies E_n = 1 Mev (the closest to the present case) have been measured by Walt and Barschall [5]. The shape of the cross section curves for lead, bismuth, tin, and iron obtained in the present work agrees with those in [5] and the numerical values of the cross section are close. Data on the angular distribution of neutrons scattered in aluminum for energies close to E_n = 0.9 Mev have not been published.

In conclusion, the author wishes to express his gratitude to V. F. Turchin for acquainting us with the method of calculating multiple scattering of neutrons developed by him and to Prof. G. R. Poze for help in this work.

The author wishes to thank Act. Member Acad. Sci. Uk. SSR A. L. Leipunsky for continued interest in the work.

LITERATURE CITED

[1] R. K. Adair, Phys. Rev. 86, 155 (1952).

[2] T. A. Hall and P. G. Koontz, Phys. Rev. 72, 196 (1947).

[3] P. Huber and E. Baldinger, Helv. Phys. Acta 25, 4, 435 (1952).

[4] V. F. Turchin (Private Communication).

[5] M. Walt and H. H. Barschall, Phys. Rev. 93, 1062 (1954).

Received May 29, 1956

STRONG FOCUSING IN LINEAR ELECTRON ACCELERATORS

K. N. Stepanov and A. A. Sharshanov

In linear electron accelerators in which a travelling wave is used, radial focusing for particles, the velocity of which v is not very close to the velocity of light c, is usually realized by means of a longitudinal magnetic field. For $v \to c$ the defocusing force which acts on the electron due to the radio-frequency field tends to zero. The departure r of particles from the axis of the accelerator (z-axis) in this case slowly increases with energy

$$r(z) = r(0) + r'(0)\,\frac{\epsilon(0)}{eE_0}\,\ln\frac{\epsilon(z)}{\epsilon(0)}, \qquad (1)$$

where $\epsilon(z)$ is the electron energy, E_0 is the intensity of the electric field, $\epsilon(z) = \epsilon(0) + eE_0 z$, $r' = \frac{dr}{dz}$ is the angle of inclination of the particle trajectory with respect to the accelerator axis. If a beam is formed with values of $r(0)$ and $r'(0)$ such that at exit from the accelerator the quantity r is small, then obviously no supplementary focusing is required. However, in cases in which $r(0)$ and $r'(0)$ are large or in those cases in which it is desired to make the value of r smaller, then it is necessary to add an additional focusing term in Eq. (1).

The additional focusing may be realized by a system of quadrupole magnetic (or electric) lenses which cause alternate focusing and defocusing in a given direction (strong focusing [1, 2]).

We will assume that a system of paired magnetic quadrupole lenses is set up along the accelerator in such a way that each nth sector of the system consists of two quadrupoles of length l_n forming a magnetic field

$$H_x = \pm H'_n y,\quad H_y = \pm H'_n x,\quad H_z = 0. \qquad (2)$$

The + sign in Eq. (2) is taken for the first lens and the − sign for the second lens. The first lens causes defocusing in the y-direction and focusing in the x-direction while the second lens causes focusing in the y-direction and defocusing in the x-direction. The quadrupoles are separated by a space d_n, the distance from the second lens to the next $(n+1)$ sector is D_n. The length of the nth sector is $L_n = 2l_n + d_n + D_n$.

We will also assume that the energy increment of the particle in the nth sector $\Delta E_n = eE_0 L_n$ is small compared with the energy of the particle at the beginning of the nth sector ϵ_n, that is,

$$\sigma_n = \frac{eE_0 L_n}{\epsilon_n} \ll 1.$$

If, moreover, the lens parameters are slowly varying functions of the number n then the equations of motion of the particle become differential equations with coefficients which are almost periodic. The solution of these equations has been given in [3] (cf. also [5, 6]). The oscillation amplitude of the particles is found to be

$$y_{max} = \sqrt{\frac{\epsilon_0\gamma_0}{\epsilon_n\gamma_n}}\,y'^{(0)}_{max}, \qquad (3)$$

$$y'^{(0)}_{max} = \left[y_0'^2 + \frac{(y_0' + \eta_0 y_0)^2}{\gamma_0^2}\right]^{1/2}, \qquad (4)$$

where y_0 and y_0' are the initial values of $y(z)$ and $\frac{dy}{dz}$.

$$\chi_n^2 = \frac{\mu_n^2}{L_n^2}\left(\frac{1}{3} + \frac{2}{3}\frac{d_n}{l_n} + \frac{2}{3}\frac{D_n}{l_n} + \frac{d_n D_n}{l_n^2}\right). \tag{5}$$

$$\eta = \frac{\mu_n^2}{L_n}\left(1 + \frac{d_n}{l_n}\right). \tag{6}$$

$$\mu_n = \sqrt{\frac{eH_n'}{\varepsilon_n}}\, l_n. \tag{7}$$

The maximum value of the angular divergence is

$$y'_{max} = \sqrt{\frac{\varepsilon_0 \chi_0 \chi_n}{\varepsilon_n}}\left\{\left(\frac{y_0' + \eta_0 y_0}{\chi_0} - \frac{\eta_n}{\chi_n} y_0\right)^2 + \left[y_0 + \frac{\eta_n (y_0' + \eta_0 y_0)}{\chi_0 \chi_n}\right]^2\right\}^{1/2}. \tag{8}$$

Equations (3)-(8) are valid if $\mu_n \ll 1$ and

$$H_n' l_n \gg E_0 \frac{\frac{L_n}{l_n}\left(1 + \frac{d_n}{l_n}\right)}{\frac{1}{3} + \frac{2}{3}\frac{d_n}{l_n} + \frac{2}{3}\frac{D_n}{l_n} + \frac{d_n D_n}{l_n^2}}. \tag{9}$$

Let $H'_n = H'_0$; $l_n = l_0$; $d_n = d_0$; $D_n = D_0$. Then

$$y_{max} = y_{max}^{(0)}; \tag{10}$$

y'_{max} increases in proportion to ε_n^{-1}. These same formulas apply if $H'_n = H'_0 \frac{\varepsilon_0}{\varepsilon_n}$, $\frac{l_n}{l_0} = \frac{d_n}{d_0} = \frac{D_n}{D_0} = \frac{\varepsilon_n}{\varepsilon_0}$.

For $H_n = H_0$; $\frac{l_n}{l_0} = \frac{d_n}{d_0} = \frac{D_n}{D_0} = \sqrt{\frac{\varepsilon_n}{\varepsilon_0}}$

$$y_{max} = \sqrt[4]{\frac{\varepsilon_0}{\varepsilon_n}}\, y'^{(0)}_{max}. \tag{11}$$

In this case, $y'_{max} \sim \varepsilon_n^{-3/4}$.

If $H'_n = H'_0 \frac{\varepsilon_n}{\varepsilon_0}$ and $l_n = l_0$; $d_n = d_0$; $D_n = D_0$, then

$$y_{max} = \sqrt{\frac{\varepsilon_0}{\varepsilon_n}}\, y'^{(0)}_{max}, \tag{12}$$

y'_{max} increases in proportion to $\varepsilon_n^{-1/2}$.

The results in Eqs. (10)-(12) are in agreement with those given in [4].

An estimate indicates that to focus electrons in a linear accelerator by means of lenses one required magnetic fields with gradients of $H'_n \sim 10$-100 gauss/cm for a quadrupole length $l_n \sim 20$-200 cm. It is convenient to arrange the lenses with large distances between them so that $D_n \gg l_n$ and $D_n \gg d_n$.

LITERATURE CITED

[1] E. D. Courant, M. S. Livingston, and H. S. Snyder, Phys. Rev. 88, 1190 (1952).

[2] J. P. Blewett, Phys. Rev. 88, 1197 (1952).

[3] A. A. Sharshanov, Report Phys. Tech. Inst. Akad. Sci. Ukrainian SSR (1954).

[4] E. L. Ginzton, W. W. Hansen, R. L. Kyhl, R. B. Neal, and W. K. H. Panofsky, Rev. Sci. Instr. 26, 2, 134 (1955).

[5] V. O. Kononenko, Proc. Acad. Sci. U.S.S.R. 105, 229, 664 (1955).

[6] E. L. Burshtein and L. S. Solovyev, Proc. Acad. Sci. U.S.S.R. 109, 721 (1956).

Received September 19, 1956

HEAT TRANSFER IN NONBOILING WATER AT HIGH THERMAL LOADS

V. V. Yakovlev

This paper presents the preliminary results of an experimental investigation* of the heat transfer in nonboiling water in turbulent flow in a tube at high thermal loads.

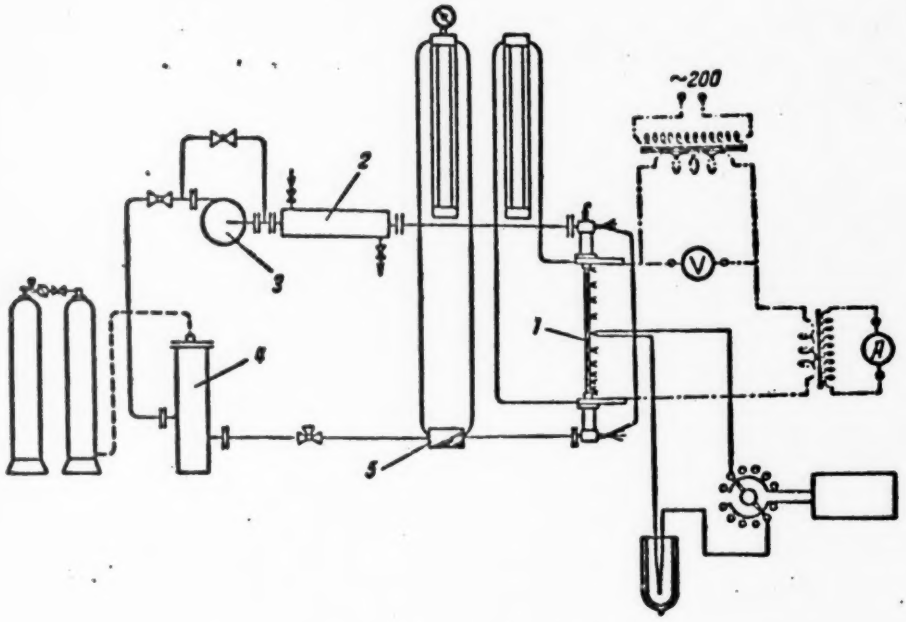

Fig. 1. Diagram of the experimental setup.

The most important results of the calculations of heat transfer under these conditions have been given in an empirical formula by Mikheev:

$$Nu_l = 0.021 \cdot Re_l^{0.8} \cdot Pr_l^{0.43} \left(\frac{Pr_l}{Pr_w}\right)^{0.25}. \qquad (1)$$

where Nu_l, Re_l, Pr_l, and Pr_w are the Nusselt, Reynolds and Prandtl numbers, respectively. The subscripts "l" and "w" refer to the parameters for the liquid, taken for the average temperature of the liquid, and to the walls.

* The work was carried out at the Department of Heat Physics of the Moscow Engineering-Physics Institute.

** M. A. Mikheev, Izv. Akad. Nauk SSSR No. 1 (1952).

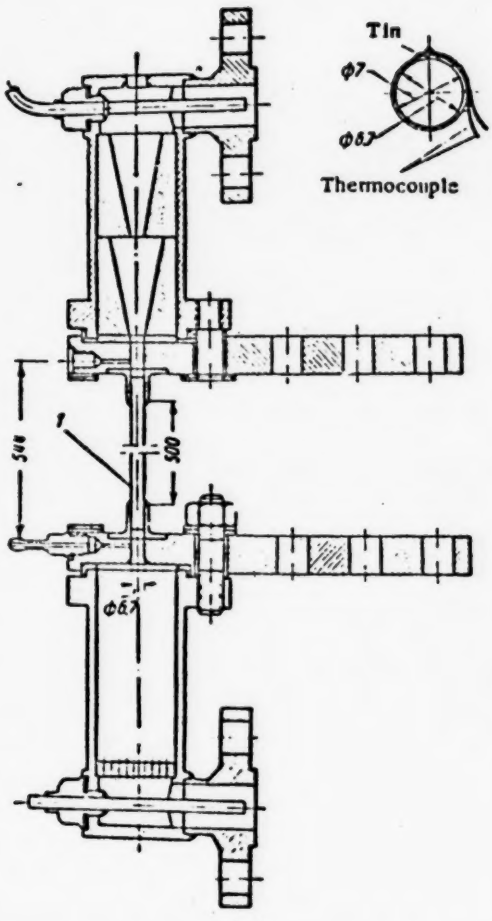

Fig. 2. Working section.

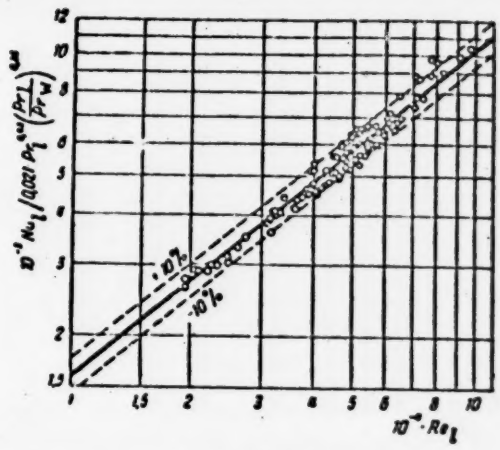

Fig. 3. Variation of Nu_l as a function of Re_l.

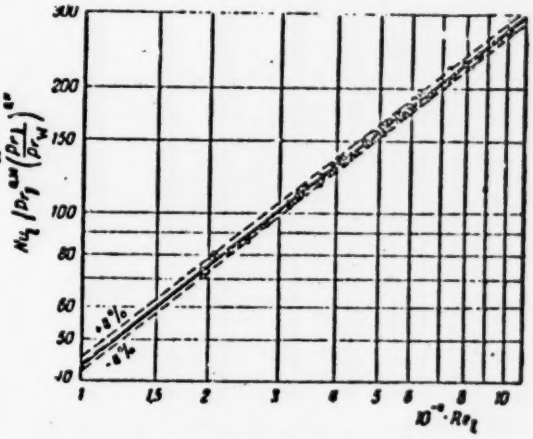

Fig. 4. Variation of Nu_l as a function of Re_l.

Equation (1) was obtained from the experimental data for heat transfer for liquids having $Pr \geq 0.6$ with $Re \geq 10^4$, $1 \leq \frac{Pr_l}{Pr_w} \leq 2$ and a thermal flux $q \leq 0.5 \cdot 10^6$ kcal/m²·hr. The last condition is a limitation on the region of applicability of the formula since in nuclear reactors and in reactor engineering the heat loads reach $\sim 10^6$ kcal/m²·hr and higher. Because of this situation it was decided to undertake the present investigation.

A schematic diagram of the experimental layout is shown in Fig. 1. A circulating pump 3 forces distilled water through a pressure tank 4 and a calibrated diaphragm 5 into the working section 1 and finally through the heat exchanger 2 whence the water returns to the pump.

A diagram showing the construction of the working section is shown in Fig. 2. The working section 1 is a vertical copper tube 6.7 mm in diameter and 500 mm long which is heated by alternating current from a stepdown transformer. The voltage in the secondary of the transformer can be varied from 3 to 18 volts. The heat balance is maintained within an accuracy of ± 1.5%.

The results of the measurements of the average (over the length of the tube) heat transfer for the water are shown in Fig. 3 in the form of the function $\frac{Nu_l}{0.021} \cdot Pr_l^{-0.43} \left(\frac{Pr_l}{Pr_w}\right)^{-0.25} = f(Re_l)$. The solid line in this same figure is a plot of Eq. (1). It is evident from these curves that the experimental data obtained for heat loads $q \leq 4.2 \cdot 10^6$ kcal/m²·hr vary by 10% from the data obtained according to Eq. (1).

In order to obtain more accurate data measurements, the proportionality factor and the value of the exponent in Eq. (1) were determined again. The results of these calculations are shown in Fig. 4 in the form of the function $\frac{Nu_l}{Pr_l^{0.33}}\left(\frac{Pr_l}{Pr_w}\right)^{0.11} = F(Re_l)$. In this same curve, the solid line is a plot of the equation

$$Nu_l = 0.0274 \cdot Re_l^{0.8} \cdot Pr_l^{0.33}\left(\frac{Pr_l}{Pr_w}\right)^{0.11} \qquad (2)$$

It is apparent from Fig. 4 that Eq. (2) gives an accuracy of ± 4% and is suitable for calculations of heat transfer in nonboiling water in tubes for $2 \cdot 10^4 \leq Re_l \leq 10^5$; $3 \leq Pr_l \leq 12$; $1 \leq \frac{Pr_l}{Pr_w} \leq 5$ and $q \leq 4.2 \cdot 10^6$ kcal/m^2·hr.

Under these conditions, Eq. (1), which describes heat transfer for different liquids in turbulent flow in tubes of irregular or circular cross section, retains its universal applicability.

In conclusion, we wish to express our gratitude to Prof. L. L. Novikov and K. D. Voskresensky for their interest in the work and valuable comments.

Received November 5, 1956

RADIATION FIELD OF A RECTANGULAR SOURCE

E. E. Kovalev, V. I. Popov, and L. N. Smirennyi

Sources of γ-radiation are widely used in various fields of science, engineering, and medicine. Sources of rectangular shape have definite advantages for irradiating certain objects, cold sterilization, etc. One of these advantages is the fact that it is possible to produce a uniform radiation field; this is important in many cases.

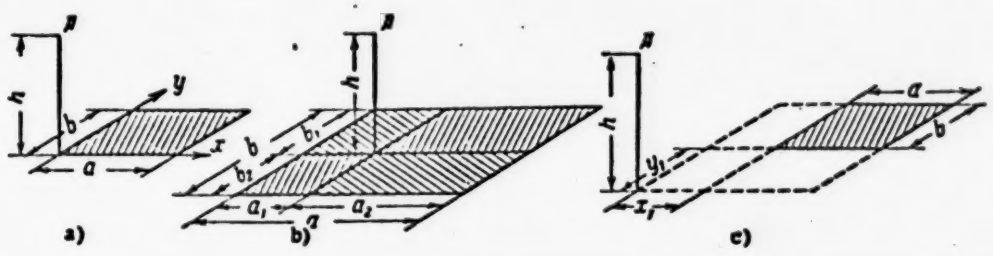

Fig. 1. Diagram for calculating the dose of γ-radiation at a point A as a function of the configuration of the point and source.

Calculations of the radiation field for a rectangular source of arbitrary dimensions have been carried out using the following assumptions: 1) the radioactive material is uniformly distributed over the entire surface of the source; 2) self-absorption and self-scattering in the source may be neglected.

Using these conditions it is not difficult to show that the dose of γ-radiation at the point A (Fig. 1) due to a rectangular source with sides a and b and with surface activity-density σ depends only on the relative dimensions of the source $n = b/a$ and the relative distance to the point $m = h/a$.

The values of n may be limited to the region $0 \leq n \leq 1$, without reducing the generality of the calculation since side a can always be taken as the larger of the two sides of the rectangular source.

The calculations, the results of which are shown in Fig. 2 in the form of a nomogram suitable for practical use, were carried out for the most frequently encountered relative distances m ($0.01 \leq m \leq 5$) and relative source dimensions n ($0.025 \leq n \leq 1$) for $\sigma = 1$ mg-equiv. Ra/cm².

Using the nomogram, the dose P_A of γ-radiation from a rectangular source with any surface activity-density σ can be easily calculated from the formula

$$P_A = \sigma \cdot P\left(\frac{h}{a}, \frac{b}{a}\right), \qquad (1)$$

where $P\left(\frac{h}{a}, \frac{b}{a}\right)$ is found from the nomogram. This relation makes it possible to find the radiation field for the case shown in Fig. 1a in which the projection of the point A coincides with the vertex of one of the angles of the rectangle. In any other case in which a system consisting of the source and point A are considered, in cal-

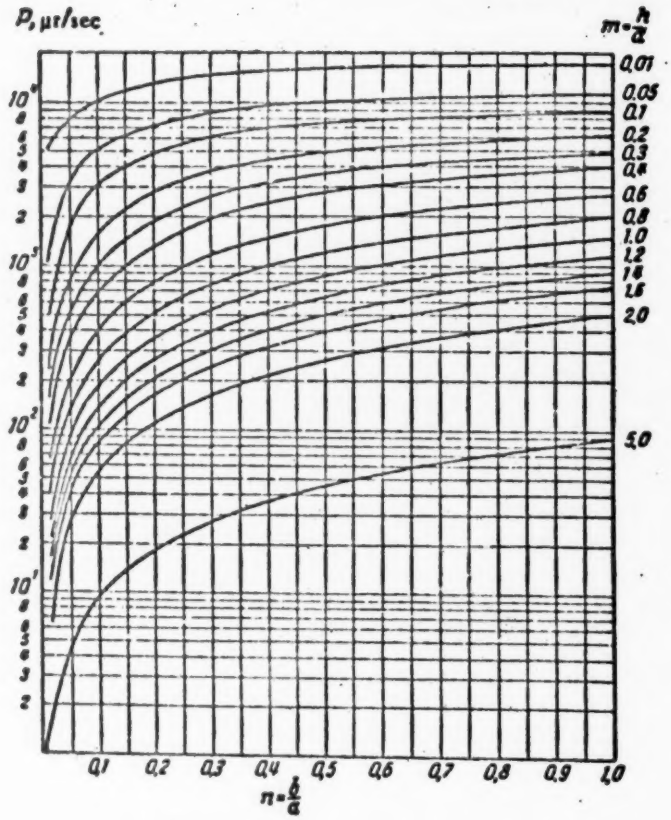

Fig. 2. Nomogram for calculating the dose for γ-radiation from a rectangular source (σ = 1 mg-equiv. Ra/cm²).

culating the dose level of γ-radiation the following approach may be used. If the projection of point A falls within the boundaries of the source (Fig. 1b) it is easily seen that

$$P_A = \sigma\left[P\left(\frac{h}{a_1}, \frac{b_1}{a_1}\right) + P\left(\frac{h}{a_2}, \frac{b_1}{a_2}\right) + P\left(\frac{h}{a_2}, \frac{b_2}{a_2}\right) + P\left(\frac{h}{a_1}, \frac{b_2}{a_1}\right)\right]. \quad (2)$$

All terms can be found from the nomogram since Eq. (2) makes it possible to reduce the case being considered (Fig. 1b) to the previous case (Fig. 1a).

In a similar fashion it is easy to find the dose of γ-radiation at a point whose projection in the source plane does not fall within the boundaries of the source (Fig. 1c). In this case,

$$P_A = \sigma\left[P\left(\frac{h}{x_1+a}, \frac{y_1+b}{x_1+a}\right) - P\left(\frac{h}{x_1}, \frac{y_1}{x_1}\right) - P\left(\frac{h}{x_1}, \frac{b}{x_1}\right) - P\left(\frac{h}{a}, \frac{y_1}{a}\right)\right] =$$
$$= \sigma\left[P\left(\frac{h}{x_1+a}, \frac{y_1+b}{x_1+a}\right) - P\left(\frac{h}{x_1}, \frac{b}{x_1}\right) - P\left(\frac{h}{x_1+a}, \frac{y_1}{x_1+a}\right)\right]. \quad (3)$$

Thus, the calculations which have been carried out for the field of γ-radiation can be applied to any configuration of the rectangular source with respect to the point of interest. In the case of a rectangular source with a nonuniform distribution of active material over the surface of the source, the source may be divided into rectangular sections characterized by constant values of σ and then the γ-radiation can be calculated using Eqs. (2) and (3).

Received August 1, 1956

INTENSE γ-SOURCE WITH AUTOMATIC CONTROL

V. G. Firsov

Intense sources of γ-radiation are frequently required in scientific and engineering research work. Below is given a description of a convenient and easily constructed Co^{60} source with an activity of 1,000 curies (1600 g-equiv. Ra).

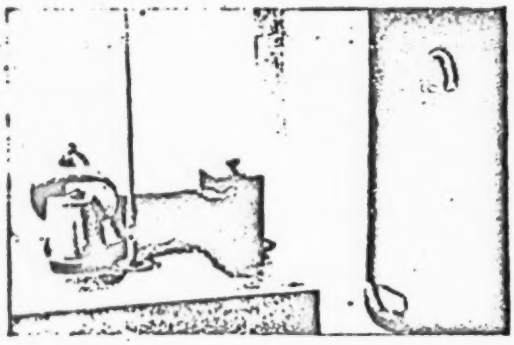

Fig. 1. General view of the apparatus.

A general view and a section through the source are shown in Figs. 1 and 2. The source 9 is a cylinder of metallic cobalt 100 mm high with an internal diameter of 25 mm which is placed in the vertical tube 3. The cobalt is covered by a layer of pure aluminum 0.7 mm thick. Shielding against the radiation is provided by tube 4 with an internal diameter of 23 mm and the barium cement 7. Because of this shielding, only a narrow beam of scattered radiation reaches the level of the upper slab 6. Irradiation of the samples is carried out in the ampule 8 which is hinged to the rod 5 formed of dural tubes which move inside each other thus providing stable control of the distance from the source to the object. The clearance space in the tubes can be used for leads to the thermocouple in a sample, a heater, etc.

Raising and lowering are performed by a reversible motor MUN-1 with a special reducer 2 which provides 3 speeds. Limit switches which are set up in the reducer automatically cut out the motor when a desired level is reached in the raising or lowering operation. The beam of scattered γ-rays which emerges in an upward direction is absorbed in the lead block 1 which is moved by motor.

The source is transported and set up by means of the container shown in Fig. 3. A small inner container 2 has a bottom which moves in a horizontal plane 5 and is moved by means of a remotely controlled pulley and placed on the shoulder 6 on the upper slab of the installation (Fig. 2, 6). When the door 5 is moved the source 4 is lowered through the guiding tube. This method does not require extensive shielding and is convenient.

The control of the operating mechanism is realized by means of an electronic circuit which is connected to a control panel.

The source geometry which has been chosen makes possible maximum use of the flux of γ-radiation. The level of energy absorption in a sample with a volume of 5 ml, placed in the center of a cylinder, measured with a ferric sulfate dosimeter, was found to be $1.28 \cdot 10^{21}$ ev/l · min or 365 r/sec. We may note that the source described in a paper by Hochanadel,* with an activity of 1,500 curies produced an intensity of ~ 225 r/sec.

The field of γ-radiation is very uniform in the horizontal plane and falls off quickly in a vertical plane. Because of the stable control of the length of the rod, it is possible to obtain identical conditions in various experiments.

* C. J. Hochanadel and J. A. Ghormley, J. Chem. Phys. 21, No. 5, 880-885 (1953).

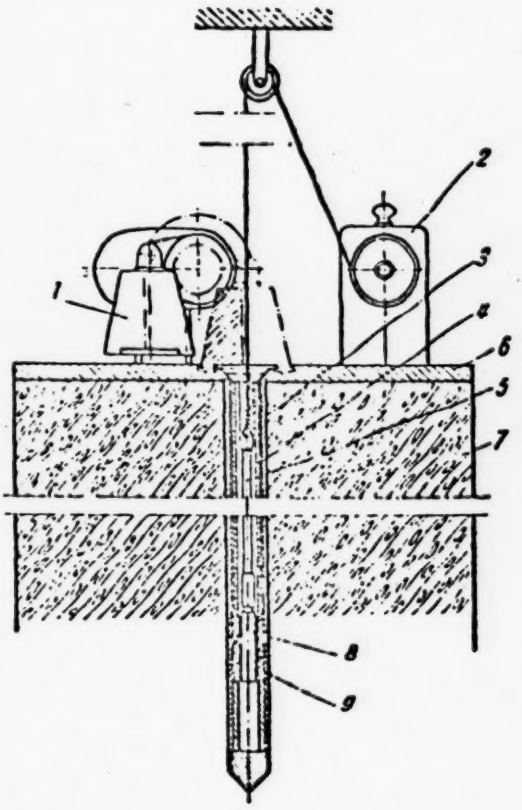

Fig. 2. Section of the source. 1) Lead block; 2) reducer; 3) outer tube; 4) inner tube; 5) rod; 6) upper slab; 7) concrete; 8) ampule; 9) source.

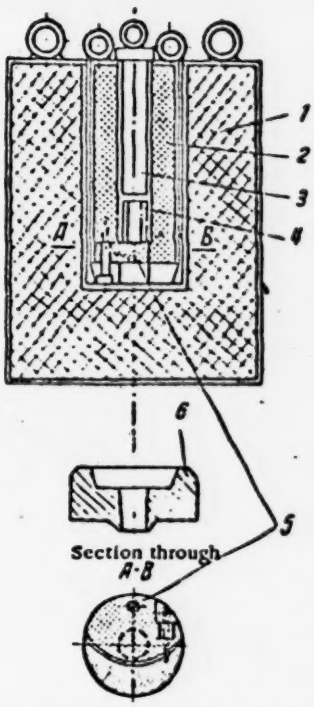

Fig. 3. Section through the container. 1) Outer container; 2) small container; 3) block; 4) source; 5) movable door; 6) shoulder.

The source is safe in operation. With the covering block in place at any point in the operating space the dose is less than 0.01 μr per sec; when the block is removed a narrow beam emerges with a dose level of approximately 27 μr per sec which, at a distance of 15 cm, falls off to 0.05 μr per sec.

The rate at which the irradiated sample can be raised (that is, the time from the end of the exposure to the time at which it is raised to a height at which the intensity falls off by a factor of 100) is a function of the gear ratio in the reducer and varies from 0.1-1 sec.

The temperature at the center of the source as measured with a chrome-alumel thermocouple is 16.5°C with a daily variation less than 1°. It may be pointed out that the temperature of the surroundings is 5-6° lower.

The author is indebted to B. V. Ershler for valuable advice and consultation and also to G. A. Barysheva and A. P. Besschetnova for help in the construction of the apparatus.

Received July 9, 1956

USE OF DK-0.2 POCKET DOSIMETERS FOR INDIVIDUAL FAST-NEUTRON DOSIMETRY

V. V. Bovin and A. I. Mosharov

From information given in the literature, based on work carried out with an 8 Mev deuteron beam [1], it is known that the main component of the ionization observed in thimble chambers placed near a cyclotron with a beryllium target is due to neutrons.

It has been found, that in work with a cyclotron using a beryllium target bombarded by 8-13 Mev deuterons, it is possible to use thimble chambers with an air-equivalent wall for practical fast-neutron individual dosimetry. In this work use was made of DK-0.2 chambers manufactured at the "Geological-Prospecting" plant and designed for measuring x-rays and γ-rays [2]. The ratio of the ionization due to the neutron component (from recoil nuclei, mainly protons) to the total effect of neutron and γ-radiation was determined in the chamber through the use of lead filters (thickness up to 17 cm) and paraffin filters (thickness 25 cm). Three measurements were carried out: without the filters, with the lead filter, and with the two filters. In a chamber, oriented at an angle of 105° to the neutron beam, this ratio was 0.80.

The absolute sensitivity for fast neutrons was determined from an experiment with a Ra-Be source with an activity of 318 μcuries and a lead filter. Although the neutron spectrum from the Ra-Be source differs from the neutron spectrum in the reaction $Be^9(d, n)B^{10}$, this is not of importance inasmuch as the spectrum of the Ra-Be source has a wide maximum around 4 Mev and extends to 13 Mev, falling to zero linearly as the energy is reduced below 3 Mev. Moreover, the dose for neutrons with energies from 3 up to 20 Mev is almost independent of energy whereas below 3 Mev it falls off as the energy is reduced. In thimble chambers the ionization is proportional to the dose regardless of the energy of the recoil protons since, in these chambers, the Gray conditions are fulfilled at all neutron energies which have been indicated and even more so at energies below 3 Mev (to 0.3-0.5 Mev). Thus, in calibration the contribution to the ionization due to neutrons with energies below 3 Mev constitutes a small part of the total ionization effect.

The thickness of the lead was chosen (25 cm) so that the main contribution to the ionization due to radiation which passed through the filter would be that of fast neutrons. In a separate experiment in which a fast-neutron dosimeter was used (a "Tiss" type instrument with a scintillation element of paraffin and ZnS activated with Ag) which had been calibrated beforehand with the same source the attenuation of the neutron flux in the lead filter was determined. Taking the limiting allowable radiation level for fast neutrons to be, in accordance with the normally accepted practice, $6.5 \cdot 10^6$ fast neut./cm^2 per working week, we determined the sensitivity of the DK-0.2 chamber to fast neutrons. It was found that $6.5 \cdot 10^6$ fast neut./cm^2 corresponds to 25 mr on the scale of the pocket dosimeter.

The spread in the readings of the dosimeter for exposures under identical conditions was ± 6%. The uncertainty in the calibration because of errors in determining the neutron flux from the source was less than ± 26%. Hence, the total error for an individual count in the determination of the neutron doses by means of a DK-0.2 dosimeter cannot be greater than ± 32%; in calibration with a more accurately known neutron flux (with an accuracy, for example, of ± 8% [3]) it should be possible to reduce the error for a count to ± 14%.

Observations on the self-discharge of DK-0.2 chambers under typical laboratory conditions indicate that many of these chambers have an electrical insulation whose leakage causes a reading on the scale of the dosimeter which is less than 10-20 mr per month when they have been first exposed in a charged state. Thus, one charging of the DK-0.2 suffices for a minimum of two months of normal operation at allowable radiation limits.

In making measurements one requires corrections for only the γ-radiation and for self-discharge.

In a copper target from a different experiment, similar to the present one, using these same chambers the neutron contribution in the ionization was found to be 0.18 instead of the value 0.80 obtained in beryllium.

The foregoing indicates that it is completely feasible to use DK-0.2 pocket dosimeters for individual fast-neutron dosimetry in work with cyclotrons under the conditions indicated for both beryllium and copper targets.

LITERATURE CITED

[1] P. C. Aebersold, Phys. Rev. 56, 714 (1939); 69, 1 (1946).

[2] Description and Operating Instructions for the DK-0.2 Pocket Dosimeter, Ministry of Geology and Mineral Conservation USSR, Leningrad (1955).

[3] F. Seidl and S. P. Harris, Rev. Sci. Instr. 18, 897 (1947).

Received September 24, 1956

SCIENCE CHRONICLE

THE CONFERENCE ON THE USE OF TAGGED ATOMS IN CHEMICAL RESEARCH AND PRODUCTION CONTROL

The first city-wide conference on the application of radioactive indicators in chemistry and in industry, which was called on the initiative of the D. I. Mendeleev All-Union Chemical Society and the scientists of the chemical faculty of the A. A. Zhdanov Leningrad State University, was held in Leningrad from the thirtieth of October to the first of November.

The first day of the conference was devoted to the application of tagged atoms to analytical chemistry and was opened with the report of V. M. Vdovenko on the subject of "The application of radioactive methods in analytical chemistry."

The speaker emphasized that radioactive isotopes have found wide application in solving many analytical problems (the investigations of solubility, of co-precipitation and of new separation methods, the analysis of mixtures of substances which are poorly separable, the analysis of the natural radioactive elements, and so forth). The technique of applying tagged atoms in analytical chemistry is superior on two counts: the high sensitivity makes it possible to measure amounts of a substance of the order of fractions of a microgram and the analysis itself can be carried out without separating the substance which is being determined.

V. M. Vdovenko, characterizing the development of research connected with methods based on radioactive transformations, marked out three basic trends: the evolution and the application of methods resting on the analysis of natural radioactivity; activation analyses; and the method of tagged atoms.

In each of these fields the Soviet scientists, including those of Leningrad, have scored great successes, instances of which can be found in the works of: I. P. Alimarin, Yu. V. Yakovlev, and A. M. Zhabin on the radioactive determination of the contaminants in metallic germanium and germanium dioxide; A. P. Ratner,* G. R. Rik, and L. A. Shebashev on the determination of cadmium in tin alloys through the adsorption of slow neutrons; A. A. Grinberg and F. M. Filinov on the radioactive determination of iridium in platinum; I. E. Starik on the determination of lead in granites down to 10^{-10} g by the technique of isotopic dilution; B. A. Nikitin* and G. M. Tolmachev on the solubility of radium sulfate in water; A. E. Polesitsky and G. M. Tolmachev on the solubility of radium iodate; V. P. Shvedov on a refinement of the oxalate method for the separation of calcium and magnesium, and so forth.

The speaker also went into details concerning the requirements in regard to radiochemical purity which are imposed on the employed radioactive isotopes, the special features of the isolation of radiochemically pure isotopes and the techniques for the identification of such isotopes.

Following this survey report there were communications on the original investigations which are being carried out in the various Lengingrad institutions.

A. P. Perovsky reported on the results of S. E. Bresler, A. I. Egorov, V. M. Kolikov, and A. P. Perovsky (Leningrad Polytechnic Institute) who have investigated with the aid of tagged atoms (Zr^{95}, Hf^{181}) the extractional separation of zirconium and hafnium.

L. M. Korenman and G. A. Shatalina, associates of the State Institute of Applied Chemistry, presented a report on the subject of "The radiometric determination of certain difficultly soluble iodides." Using the radioactive isotope Cs^{134}, these authors studied the composition of the complex iodides of cesium and bismuth and of cesium and antimony, these having great significance for the microcrystalloscopic detection of cesium, bismuth, and antimony, and for certain drop reactions as well.

* Deceased.

B. K. Preobrazhensky (The Radium Institute of the Academy of Sciences of the USSR) for himself and O. M. Lilova, and A. V. Kalyamin reported on "The rapid separation of the active rare earth elements on the cation exchanger KU-2 without the use of a pH meter."

During the second day of the conference there were heard reports on researches in the field of organic chemistry and also on the synthesis of various organic and inorganic compounds.

A survey paper on "The possibilities for the study of molecular structure and reaction mechanisms with the aid of tagged atoms" was read by N. A. Domnin.

He distinguished three fundamental problems to the solution of which most of the work with tagged atoms has been devoted: the study of the chemical bond in organic compounds (bond equivalence, bond stability, and weakness, and so forth), the study of the molecular structure of organic compounds, and the study of the mechanisms of organic reactions.

The speaker stated that in the near future the members of the chemical faculty of the Leningrad State University will carry out a variety of investigations utilizing tagged atoms. Among these will be: a study with the aid of C^{14} of the mechanism of the interaction of ethyl diazoethanoate with allyl bromide; a study, using heavy oxygen, O^{18}, of the mechanism of the rupture of oxide rings; a demonstration of the structures of isomeric dibromides, utilizing radioactive Br^{80}, and so forth.

V. I. Kurov spoke of the researches which are being carried on in the analytical chemistry laboratory of the S. M. Kirov Leningrad Textile Institute. With the isotope C^{14} there have been studied the reactions of thermal decomposition of the alkyl carbonates. By synthesizing ethyl sodium carbonate and methyl sodium carbonate with tagged C^{14}, V. I. Kurov obtained direct confirmation of the earlier proposed hypothesis according to which the carbon monoxide liberated during the thermal decomposition of the alkyl sodium carbonate is formed from the carbon of the carbonate group.

N. V. Sadikova outlined for the conference one of a series of researches with tagged atoms which is under way in the I. P. Pavlov Institute of Physiology.

Starting from $BaC^{14}O_3$, N V. Sadikova carried through an involved synthesis of glutamic acid, tagged at the third or the fourth carbon atom. Such method opens wider possibilities for following the behavior of glutamic acid in metabolism and is more effective than the introduction of C^{14} into the labile carboxyl groups of the amino acids.

The associates of the State Institute of Applied Chemistry reported on their work with the synthesis of tagged compounds.

N. B. Vinogradova, V. R. Budanova, N. N. Zatsepina, and E. E. Polikarpova have developed methods for synthesizing many organic compounds tagged with C^{14} including various acids, alcohols, esters, and so forth.

O. L. Andreeva, G. P. Okatova, V. S. Tsvetkov, and A. N. Krasner have synthesized a number of inorganic compounds tagged with S^{35}, P^{32}, Fe^{59}, and Cr^{51}.

The methods of synthesis of organic and inorganic compounds which have been developed in the State Institute of Applied Chemistry give good yields of tagged products of high specific activity and purity and at the present time these are being introduced into production.

The final day of the conference was devoted to methods of applied radiochemistry with certain examples of their application.

A. N. Murin (Leningrad State University) read a paper on the applications of scintillation and mass-spectrometric methods in applied radiochemistry.

In his report A. N. Murin outlined the principles and the prospects of the utilization of scintillation and mass-spectrometric methods in radiochemistry.

The speaker noted that with the aid of scintillation counters it is possible to study the spectra of the radiation from radioactive preparations of very low activity (down to 10^{-9} curies), which permits the identification of radioisotopes at infinitesimal concentrations, the control of the radiochemical purity of preparations and, in a series of cases, the spectral analysis of complicated radioactive mixtures.

A. N. Murin also presented a number of examples of the use of the scintillation method in the work of the Leningrad scientists, including that of Yu. A. Nemilov and the author of the report.

Speaking of the mass-spectrometric methods, A. N. Murin pointed out two of the sources of the superiority of this method: the possibility of registering short-lived isotopes (with half-life periods less than 0.1 sec) and the possibility of determining, with sensitive electrometric procedures, extremely small amounts of long-lived radioactive isotopes (as low as 10^{-14} g in the case of the alkali metals) in mixtures of these with stable isotopes.

It is, moreover, possible to carry out mass-spectrometric analysis in numerous cases without a chemical separation into fractions of the elements undergoing determination. By way of illustration A. N. Murin told of the work performed in his laboratory on the determination of the yields of a series of products resulting from the fission of plutonium by thermal neutrons and of the work of other Leningrad scientists.

The two following papers were devoted to the application of the scintillation technique.

V. M. Gavrilov (State Institute of Applied Chemistry) reported on the possibility of the application of scintillation spectrometry for the determination of radioactive contaminants. The identification of the type of contamination is indispensable in choosing the correct technological process for purification. If the contaminants are γ-radiators, then this problem can be solved through the study of the γ-spectrum.

V. M. Gavrilov has determined the contaminants in two preparations, Mo^{99} and P^{32}. Analyses of the γ-spectra of samples from irradiated molybdenum blocks showed that Mo^{99} is contaminated with Zr^{95}, Nb^{95}, Nb^{92}, and Fe^{59}. These data permitted the improvement of the purification of the Mo^{99} which was used for the production of Tc^{99}. The study of the γ-spectra of additives to the pure β-radiator P^{32} made it possible to establish that P^{32} is contaminated, not with Fe^{59}, as has been supposed up to the present, but with Zn^{65}.

G. M. Gorodinsky and V. N. Pokrovsky (The Radium Institute of the Academy of Sciences of the USSR) have applied the scintillation method for the identification of the rare earths. The radioisotopes of the rare earths which result from the reaction of deep fission of Ta induced by its irradiation with protons of 680-Mev energy were chromatographically separated into various fractions. There were studied the γ-spectra of 11 fractions of the rare earths: Ce, Nd, Eu, Gd, Tb, Ho, Er, Tu, Yb, Dy, and Lu. Despite the presence in these fractions of several isotopes of a single element, it was possible to identify, not only the separate fractions, but also the individual isotopes, and then, with a certain modification of the technique, to obtain data on the relative content of the isotopes in the fraction. G. M. Gorodinsky and V. N. Pokrovsky have discovered two new radioisotopes, Gd^{147} and Gd^{145}.

Through reports the participants of the conference became acquainted with the applications of the method of tagged atoms in various fields of science and technology.

In the paper of B.P. Nikolsky, E. A. Materova, and V. V. Moiseev on "An investigation of the glass electrode with the aid of tagged atoms" there were presented certain results from a study of the interaction of electrode glasses with salt solutions and a comparative investigation of the electrochemical and the exchange properties of these glasses. The application of radioactive indicators made it possible to study in detail the mechanism of the formation of potential differences at the glass-solution interface and opened the way for conjectures as to the mobility of the ions in the glass and in the process of the interaction between the glass and the solution.

N. P. Peregudov, an engineer from the steel rolling-mill, reported on the application of tagged atoms in industry. In place of the system which is in use at the present time for gaging cold rollings, at the mill there has been developed, in collaboration with the scientific personnel of the Institute of Physics of the Academy of Science of the Latvian SSR, and introduced into production a new gaging method based on radioactive isotopes, in particular P^{32}. This method possesses, according to the speaker, a number of advantages in comparison with the former one.

At this conference, which aroused great interest among the scientists and workers of the Leningrad industry, a resolution was adopted in which there was emphasized the necessity of periodically arranging conferences of this kind.

L. A. Skulsky

DELAYED EFFECTS OF DISEASES CAUSED BY IONIZING RADIATION

(From Material Presented at a Conference of the USSR Academy of Medical Sciences)

A conference on the delayed effects of ionizing radiation sickness was held in Moscow on the 20th and 21st of November, 1956. Over twenty scientific papers were read at the conference.

Data obtained by Soviet researchers in recent years were presented in one of the papers read: "Delayed Effects of Diseases Caused by Ionizing Radiation", by D.I. Zakutinsky.

The author paid particular attention to the question of radiant energy influence on the progeny of animals which had received radioactive substances internally. New facts were presented indicating that normal response to a series of medicinal preparations was disturbed in the case of animals which had been exposed to radioactive substance action.

Much space was given in this paper to the problem of malignant growth due to the entry of various radioactive substances.

In a series of papers many new facts were presented regarding the condition of the hematopoietic organs long after the onset of acute or chronic radiation sickness.

Data obtained from a study of dogs and rabbits 6-12 months after their one-time exposure to large doses of fast neutrons showing the renewal of blood cell formation processes to take from 2-6 months for red corpuscles to 1.5 years for white corpuscles was presented by V.V. Sokolov. In dogs with acute radiation sickness, the fur turned gray, loss of weight occurred, and sterility developed.

A paper by L.K. Petrovich, which traced the development of disease in dogs over periods of 5-59 months after the administration of $Sr^{89,90}$, Po^{210} and uranium nitrate, reported changes in the blood picture of the animals long after the entry into the body of radioactive substances. Pronounced changes in the white corpuscle content were observed in a few months after the dogs' injection with uranium fission products. The peripheral blood regeneration phase occurred 5-6 months after the administration of Sr^{90}.

The most profound changes in the blood picture resulted from the administration of Po^{210}.

A.A. Kanarevskaya and S.Yu. Posherstnik presented data on hematopoietic disturbance at a late phase of Po^{210}, RdTh and Rn chronic radiation sickness. Hematopoietic stimulation, supplanted by periods of depression, was observed after administration of radioactive substances.

In a paper by M.S. Lapteva Popova, an analysis of the blood picture resulting from long chronic exposure to small doses of roentgen rays was presented. The author divided the course of chronic radiation sickness into four periods. The characteristic changes for each of these four periods were described.

S.M. Mikhailovich showed in his report that the length of time between the experiment and the animals' death apparently depended on the various individual susceptibilities of the animals. Loss of weight, decrease in hemoglobin content and number of red corpuscles occurred in 2-2.5 years after the administration of radiothorium.

Very pronounced pathological body condition changes (high ESR, pronounced azotemia) were observed to be present when the animals died.

L.N. Byrykina disclosed that, in chronic poisoning from small doses of radioactive strontium, the death of the animal sometimes occurs after a period of apparent health.

The earliest changes resulting from chronic sickness caused by small doses of uranium fission products were determined by studying the dynamics of change in the blood, weight, bone structure, and substance distribution in the various organs (E.I. Klimova).

A.P. Novikova presented extensive material concerning morphological change in animals long after the injection of uranium fission products. Changes extremely varied in degree and character were observed in simple forms of radiation sickness. Epilation, loss of weight, anemia, atrophy of the gonads, development of bronchiectasis, i.e., the symptoms characteristic of extreme old age, were observed in the animals.

Besides the above-mentioned changes, pneumonia and skin mycoses were present in complex cases of chronic radiation sickness. The growth of tumors was observed in a series of cases, localized chiefly where the substances had been injected.

L.L. Vannikov traced the changes in dog brain glia* for periods of 7 months to 2 years after acute radiation sickness. Increasing gliosis** of the brain was observed in all of the animals.

Material characterizing the morphological changes in animals at late periods after the injection of radiothorium in small doses was presented in a paper by E.V. Erleksova.

Atrophy of the lymph nodes and dystrophic changes in the parenchymal organs were observed parallel with pronounced emaciation in the animals. Radiography showed RdTh and RdTh decomposition products to be present in all organs and tissues. Injection of RdTh in 0.0001 millicurie doses led to the formation of bony tissue tumors – after 8-16 months for white rats and after 3 years for dogs.

The conference discussed the very important problem of malignant neoplasmic growth. V.N. Streltsova and Yu.I. Moskalev presented a detailed report on this problem. The authors studied delayed effects resulting from single and repeated entry via the gastro-intestinal tract of the radioactive isotopes Ce^{144}, Ru^{106}, $Sr^{89,90}$ and of a mixture of beta-radiators.

The elements studied were localized differently in the body. Those isotopes which were evenly distributed throughout the body (Ru^{106}) caused tumors in the soft tissues only: the gastro-intestinal tract, kidneys, and thymus glands; those isotopes absorbed mainly by the skeleton ($Sr^{89,90}$) caused osteosarcomas and leukoses.

The isotopes that concentrated in the liver caused tumors to develop in the gastro-intestinal tract, mammary glands, endocrine glands, and liver. Tumors caused by isotopes poorly absorbed out of the intestine formed mainly in the gastro-intestinal tract.

L.L. Khamaide injected rabbits subcutaneously and intravenously with uranium fission products in small concentrations and, after a year, observed that tumors developed, located at the place of injection. The developing sarcomas caused multiple metastases in the internal organs.

R.I. Makarycheva presented interesting data concerning the onset and development processes of osteogenic sarcomas in an experiment.

By skeletal serioscopy of rats affected by Sr^{90}, the author traced the dynamics of change in bony tissue and showed tumor development to be preceded by bone structure change.

N.N. Litvinov's report presented the dynamics of bone tumor onset and development in radioactive strontium and yttrium diseases.

The influence of ionizing radiation on spermatozoal activity in dogs was presented in a paper by N.E. Trusova. A study made on the sperm of dogs 3-6 and 30 months after a radiation dose of 600 r showed the presence of azoospermia, decrease in ejaculated quantity and the appearance of immature sperm. Where radioactive substances had been injected into the body, the disturbance of spermatogenesis was less marked.

S.P. Voskresensky and A.N. Novikova presented clinical and pathomorphological studies made on the progeny of dogs which had been exposed to the action of uranium fission products.

The injection of small doses of uranium fission products into females produced disturbances of the sexual cycle and mammary gland function, and caused the number of offspring to decrease in each subsequent litter.

---

*Fibrous tissue of the brain.

**Fibrosis.

In the first litter, radioactive substances were found to be present in the bodies of the puppies, and the mortality rate was observed to be higher than in subsequent litters.

Blood picture changes in given experiments were presented by T.A. Ivanova. The author showed certain temporary aberrations in the development of hematopoietic tissue.

E.N. Antipenko defined reactions peculiar to animals with acute radiation sickness by experimentally induced neurosis.

Experimentally induced neurosis showed that, even three years or more after an animal's clinical recovery from acute radiation sickness caused by external exposure, the body reactions were not completely normalized. In these animals were observed the development of leukopenia, increase of vasal permeability, blood pressure decline, and other changes which did not occur from experimentally induced neurosis in healthy dogs not previously exposed.

The conference recorded in a resolution all known facts obtained to date concerning the delayed effects of ionizing radiation sickness.

However, the biological effect of an elevated natural background has not yet been sufficiently studied; there has been almost no research on genetic problems, and very little work on early biological diagnosis of radiation diseases or on comparative evaluation of different kinds of radiation action.

One of the factors retarding the development of work on delayed effects is the country's lack of a master research plan for a given problem.

The conference considers that special attention must be given both to the question of the direct influence of ionizing radiation in small doses and to the question of its genetic influence. More detailed investigation must be made of trophic disorders in the body and of the blastomogenic action of ionizing radiation, and work must be continued on the experimental determination of the permissible dose range for the various radioactive substances.

A master plan of research on the delayed effects of ionizing radiation diseases must be drawn up.

V.V. Shikhodyrov

STOCKHOLM CONFERENCE ON PROGRESS IN RADIOBIOLOGY *

Michael Ebert and Alma Howard

The Fifth International Conference on Radiobiology met in Stockholm during August 15-19, under the chairmanship of Prof. George de Hevesy. About 180 scientists from nineteen countries were present, and eighty contributions read and discussed. In comparison with previous meetings, emphasis was placed more on the haemopoietic and genetic effects of radiation, and less on its primary physical or chemical action.

During the past year, it was shown that haemopoietic cells injected into heavily irradiated animals of the same, or even of a different, species can colonize the blood-forming tissues of the hosts. This explains how animals can survive lethal doses of radiation if part of their blood-forming tissue is shielded, or if they receive after irradiation an injection of haemopoietic cells of another animal. The hypothesis that recovery is promoted by some humoral or subcellular factor is now unnecessary, and at this meeting it was reported that the 30-day survival of CBA mice after 950 r. depends on the number of intact spleen cells inoculated, and is independent of the number of nuclei of damaged cells (D. W. H. Barnes, M. P. Esnouf and L. A. Stocken). The effectiveness of a given inoculum is greatest when the graft is least different genetically from the host (J. Soska, V. Drasil and Z. Karpfel; J. A. Cohen, O. Vos and D. W. van Bekkum). After 950 r. whole-body irradiation to mice and subsequent injection of spleen cells, the entire blood-forming tissue was taken over by the graft. No reversions to tissue of host origin was observed up to 157 days after grafting from another mouse. With heterologous (rat) grafts, reversion may occur (C. E. Ford, J. L. Hamerton, D. W. H. Barnes and J. F. Loutit).

Of medical interest was a more sensitive assessment of haemopoietic damage in persons exposed to low occupational doses, by means of a new method of collecting and treating blood-count data (M. Helde). The great sensitivity of red-cell precursors was seen after 50 r. whole-body x-irradiation of rats, when the number of late and intermediate normoblasts in the bone marrow fell to less than 50 per cent in 24 hr. (E. V. Hulse). It now seems established that exposure to radiation increases the risk of leukaemia in man (W. M. Court-Brown). Study of 828 case histories of leukaemia from the Danish cancer register (M. Faber) leads to the conclusion that both chronic myeloid and acute leukaemia can be induced by radiation, and that part of the increased incidence is due to diagnostic x-ray procedures in which bone marrow is exposed. The absorption, retention and removal were described of the decay products of radium and thorium (K. Aurand, W. Jacobi and A. Schraub), of strontium-90 in bone (M. Owen and J. Vaughan) and of yttrium (R. Lewin, B. Rosoff, H. Hart, K. G. Stern and D. Laszlo).

Work done on chemical protectors has failed to reveal a common mechanism for their action. Some earlier observations on cysteamine have not been confirmed (Z. M. Bacq); it was ineffective when given to chicks or administered orally to rats. It was suggested that cysteine and cysteamine act by inducing anoxia (J. F. Duplan and H. Marcovitch; J. A. Cohen, O. Vos and D. W. van Bekkum). Cysteine protected Glis glis from mortality if administered twenty-one days after irradiation, provided the animals were kept meanwhile at 4°C. in their hibernating state (H. Künkel, G. Höhne and H. Maass). It is difficult in this case to see how the protector could interfere with primary radicals or exert its influence by specific reactions involving —SH or —S-S— groups of

*A slightly abridged Russian translation of this paper is presented in the original issue of Atomnaya Energiya. The original paper as it appeared in Naure, Vol. 178, pp. 842-843, is reprinted here, with the permission of the editors of Naure and the authors. The Russian abridged translation was credited to S. L.— Publisher.

target molecules (A. Pihl and L. Eldjarn; U. Hagen). We are reminded of the specificity of protectors by the fact that α-thiolaminoacids are protective, whereas β-thiolamino-acids enhance radiation effects in mice (R. Koch). Dose-reduction factors of cysteamine and of β-aminoethylisothiouronium change with the dose of radiation. Critical damage is thought to occur at different sites after different doses, and the efficiency of protection to vary from site to site (A. Catsch).

Among agents which increase radiosensitivity, oxygen has retained its interest. The sensitivity of E. coli irradiated in buffer solution increased with oxygen concentration in the bubbling gas, and reached almost full sensitivity at 3 per cent oxygen (T. Alper). The sensitivity change in Ehrlich ascites tumour cells from anoxia to full oxygenation occurs at lower concentrations of oxygen than previously reported (O. C. A. Scott), and a similar pattern of sensitivity was found in the ascites form of the Yoshida rat sarcoma (W. Dittrich). The sensitivity typical of the anoxic state was attained 3 sec. after stopping the circulation in mouse tails (P. Howard-Flanders). Cooling mice to 0-0.5°C afforded a dose-reduction factor of 2·8, an effect largely attributed to the anoxic condition of hypothermic animals (S. Hornsey). Organic peroxides produced by x-rays seem to be implicated in mutagenesis in Drosophila, since it is potentiated by pretreatment with dihydroxydimethyl peroxide or formaldehyde, or with cyanide or azide (F. H. Sobels).

The question of the contributions of the direct and indirect effects to biological damage received some attention. The direct effect in polythene and dry bovine serum can be influenced by oxygen or temperature, but seems to be independent of small amounts of water (P. Alexander). In contrast, it was claimed that the radiosensitivity of enzymes in wet yeast cells is 2-50 times higher than in dry cells, suggesting a high contribution from the indirect effect (F. Hutchinson).

The respiratory system of mouse-liver slices is affected by doses higher than 10^6 r. Sensitivity is determined by cytochrome c, which is destroyed by indirect action (B. Rajewsky, G. Gerber and H. Pauly). Yoshida ascites cells 20 min. after 20,000 r. show a drop in respiration and in aerobic and anaerobic glycolysis, and changing relative levels of adenosine di- and triphosphate. These differences become less pronounced at 40 min. (G. Höhne, H. A. Künkel and H. Maass). Incorporation of di-phenylalanine-^{14}C into cell components of mouse liver is higher after 500 r. whole-body exposure (J. A. V. Butler, P. Cohn and A. R. Crathorn). The rate of incorporation of phosphorus-32 into rat thymus deoxyribonucleic acid is reduced to half within 3 min after 1,000 r to the whole body (M. G. Ord and L. A. Stocken). Increased incorporation of tracers after irradiation may be due to reduced size of body pool (F. Sherman and A. B. Almeida).

A single sub-sterilizing dose of 1,050 r. given to rabbit ovaries is less damaging to late primordial follicles than if given in fractions of 210 r. every 48 hr. (P. Desalve). The sterilizing dose for female mice, on the other hand, does not seem to be dependent on dose-rate, whether delivered at 2·5 r. daily or in one exposure (H. and U. Langendorff).

In a session on genetic effects in Drosophila, H. J. Muller and L. I. Oster presented new evidence that true reversals of the original forked (f^+) mutation can be induced by x-rays. They believe that point mutations of whatever origin are indistinguishable in principle, and are due to qualitative chemical changes in the gene locus. Alkylating agents were reported to have produced a large number of point mutations in loci that have not been observed to mutate under x-irradiation, and the distribution of chemically and x-ray induced mutations on the x-chromosome has been found to vary with the mutagen used (O. G. and M. J. Fahmy). Chromosomes of spermatids are at least twice as sensitive to the x-ray induction of lethals and translocations as those of mature sperm in inseminated females (L. I. Oster). Crossing-over in spermatogonia can be induced by injection of formaldehyde (F. H. Sobels). Chromosome breaks, and possibly also intragenic changes, induced by x-rays in mature sperm, are thought to undergo recovery if the sperm are retained for one day in the male (K. Nordback and C. Auerbach). At least five times as many small-effect detrimental mutations as recessive lethals are induced in male Drosophila by x-rays (K. G. Luning and S. Johnsson). The reduced viability of flies receiving irradiated chromosomes is accompanied by a decreased rate of development, and it was suggested that growth-rate studies might be useful in assessing genetic damage due to radiation in mammals (G. Bonnier).

Two films were shown illustrating the effect on mitotic behaviour of irradiating parts of cells in tissue culture with α-ray microbeams. Sensitivity increased by a factor of 10 from prophase to metaphase (M. I. Davis, L. Simon-Reuss and C. L. Smith), and irradiation of chromosomes was much more effective in producing anaphase and telophase abnormalities than irradiation of cytoplasm only (R. Munro). When roots of Vicia faba are irradiated with very high intensities of x-rays, in the range 600-1,200 r/min., a class of chromosome breaks becomes

apparent which rejoin very rapidly and which may be due to breakage of ionic bonds. These breaks are to be distinguished from those others regarded as due to the breakage of covalent bonds, which remain open for a relatively long time (S. Wolff).

Under the appropriate chairmanship of Prof. A. Gustaffson, a special session met on the last day to discuss the application of the mutagenic effects of radiation to plant breeding. Facilities and techniques were described for the Brookhaven Laboratory (H. J. Curtis) and plans outlined for the improvement of the rice crop in India (A. R. Gopal-Ayengar). Of 427 radiation-induced mutations in soya beans, only 1 per cent seem to be of some economic value (M. Zacharias). In black currants, selection of mutated shoots from irradiated cuttings was reported to have given promising results (R. Bauer). A review was given of the work of the Swedish group in utilizing "directed" mutations produced in barley by various physical and chemical agents (D. von Wettstein).

BLANK
PAGE

IN THE SOVIET UNION

IN THE ATOMIC PAVILION OF THE ALL-UNION INDUSTRIAL EXHIBITION (ATOMIC RAW MATERIAL SECTION)

The section "Atomic Raw Material" in the pavilion "The Peaceful Uses of Atomic Energy" of the All-Union Industrial Exhibition has a big collection of uranium minerals and ores on display.* Equipment for uranium prospecting and for the analysis of uranium ores under laboratory and field conditions is demonstrated.

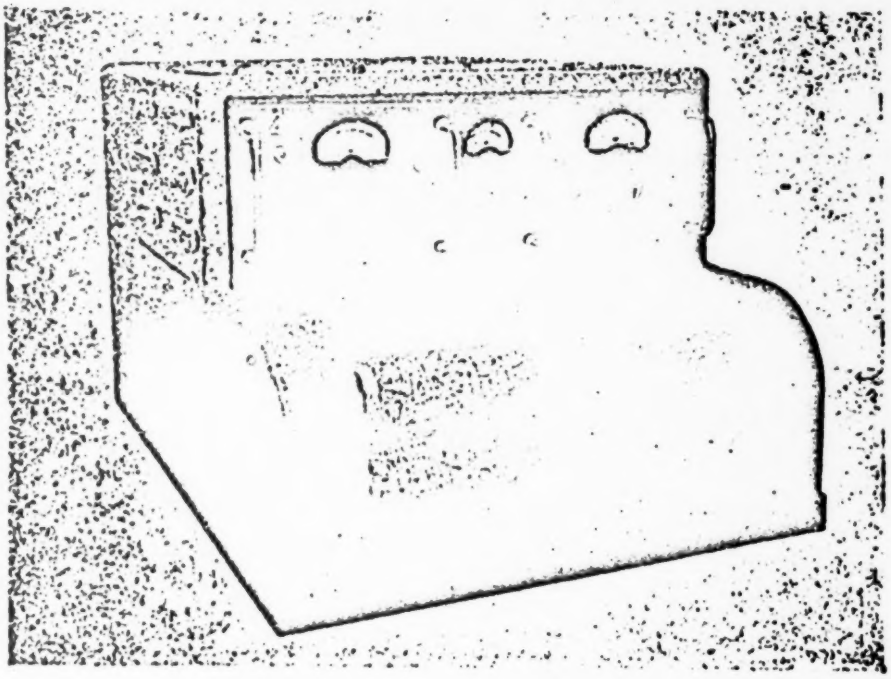

Fig. 1a. A general view of the control unit of the equipment ASGM-25. 1) γ-radiometer channel; 2) magnetometer channel.

The methods used in prospecting for radioactive ores can be divided into γ-detection and emanation detection.

γ-detection is carried out by various methods with the help of special radiometric equipment. At the exhibition several types of equipment, being produced industrially at present, are exhibited. The equipment used is classified according to the method of transportation: γ-detection by air, by car and on foot.

* J. Atomic Energy (USSR) 2, 1, 81 (1957).

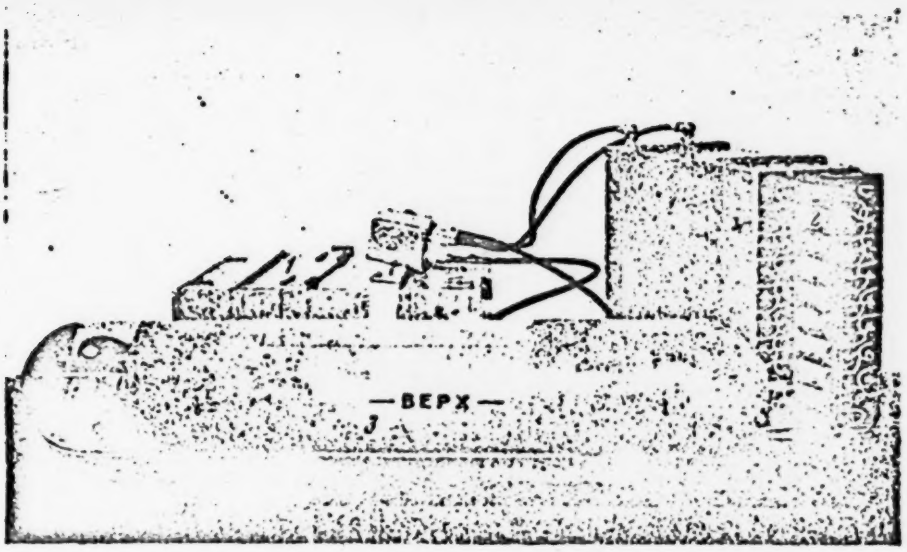

Fig. 1b. γ-radiation detector and the magnetosensitive element of the equipment ASGM-25. 1) Containers with gas discharge counters; 2) type VS-9 gas discharge counters; 3) magnetosensitive element.

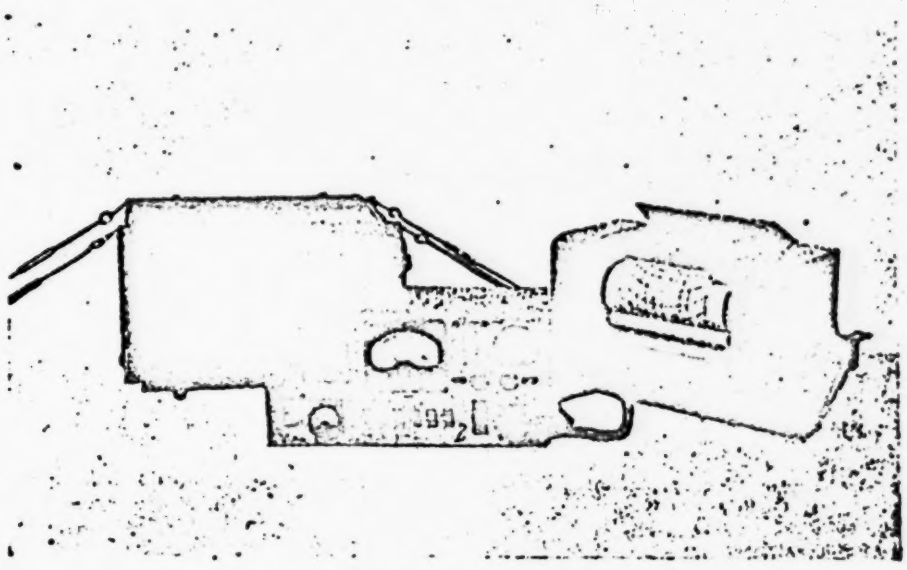

Fig. 2. γ-Radiometer SG-14 for cars. 1) γ-radiation detector (container with gas discharge counters of type AMM-9); 2) amplifying and measuring section; 3) recording section.

For aerial γ-detection the complex geophysical equipment ASGM-25 (Figs. 1a,1b), produced by the factory "Geological Prospecting," is used. The equipment is intended for the rapid simultaneous prospecting for ore deposits and the deposits of useful minerals by observing the radioactive and magnetic properties of rocks. The search for the ore locations with the help of this equipment is made by the continuous automatic measurement and recording of the γ-radiation and geomagnetic field intensities, together with the simultaneous recording of the true flying height. The equipment is installed in aeroplanes AN-2 or helicopters MI-4. One operator looks after the equipment. The γ-detector consists of two containers, each of which has 36 gas discharge counters VS-9. To lower the cosmic-ray background the counters are arranged in four rows and are connected in parallel through quenching resistors (Fig. 1b). The counters are completely enclosed by their walls to prevent the influence of electrical interference on the measurements. Power is supplied to the equipment from the aircraft circuit. The total weight of the equipment is 160 kg, and the flight weight is 132 kg.

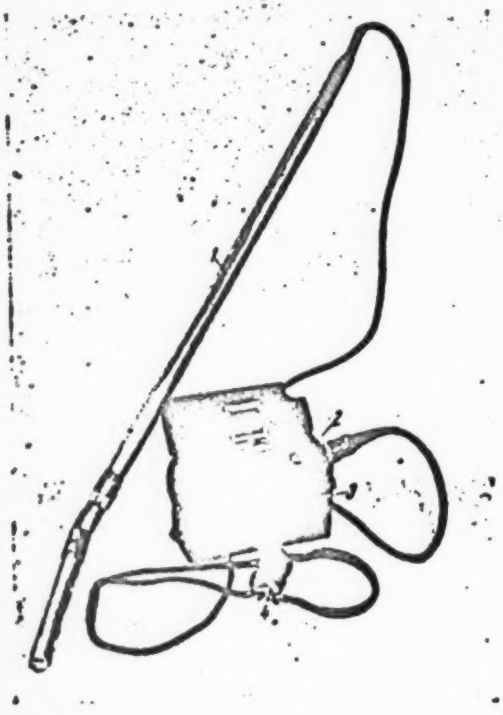

Fig. 3. A general view of the radiometer UR-4M. 1) Radiometer probe; 2) control panel; 3) supply batteries; 4) earphones.

Fig. 4. A γ-radiometer with the scintillation counter SG-42. 1) Counter and case; 2) control panel; 3) supply batteries.

γ-Detection from cars is carried out with the γ-detector SG-14 (Fig. 2), which is also manufactured by the factory "Geophysical Prospecting." The automobiles most suitable for the equipment are the GAZ-67 and GAZ-69, which have a high maneuverability and penetrability. The measuring equipment SG-14 is adapted from the airborne equipment SGM-10. The detector consists of a container with 36 counters of type AMM-9. The power supply is the automobile accumulator or 6 batteries of type BAS-G-90. The total weight of the equipment is about 25 kg.

There is on display at the exhibition a large number of counters suitable for γ-detection on foot, for example, the explosion-proof counter UR-4M (Fig. 3), which can be used in the underground working of mines. The radiometer employs STS-8 or STS-1 gas discharge counters. The range of measurement is 0.015-10 mr/hr. The range of temperature is from −20°C to +50°C. The probe can be extended telescopically from 1.14 m to 1.74m for the examination of difficult locations.

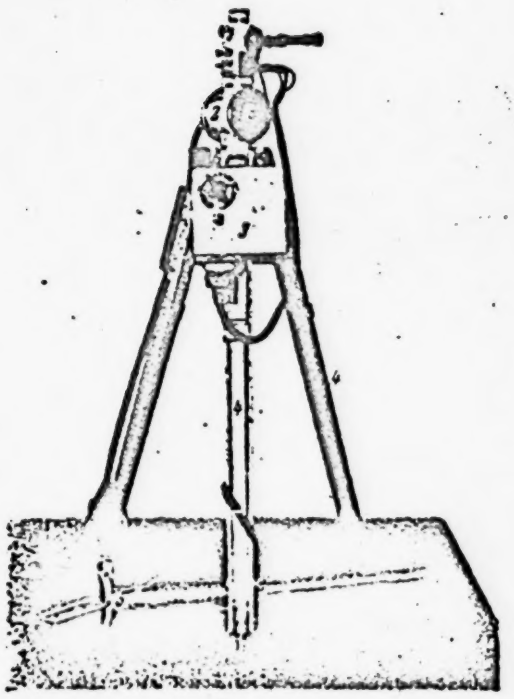

Fig. 5. The field emanation meter SG-11. 1) Electrometer; 2) ionization chamber; 3) control panel; 4) tripod; 5) sampling probe.

The detectors RP-1 and RGR have waterproof counter cases and during use can be lowered into water. The detector RP-1 has a straight case which is intended for the STS-6 and STS-8 counters. The detection of radiation is made simultaneously with an acoustic and a visual indicator. The detector RGR uses an STS-1 counter which is situated in the rotating head of the probe. The rotating head enables the counter to be placed at an angle to or along the axis of the probe.

The portable acoustic counters PRS and the scintillation counter SG-42 (Fig. 4) on display at the exhibition deserve attention. The portable acoustic detectors are made in two varieties PRS-R and PRS-P having differently-shaped probes and different ranges of measurement. The radiometer PRS-R has a straight probe with one γ-counter; PRS-P has a T-shaped probe with 7 counters. The total weight of the assembly, including batteries, is less than 2 kg. The radiometer probes are waterproof and the control boxes are splashproof.

The detector SG-42 uses a scintillation counter which has a number of advantages over a gas discharge counter: a higher sensitivity to γ-rays and a comparatively short resolving time which allows high counting rates without serious errors.

The emanation meter SG-11 (Fig. 5), on display at the exhibition, is used for the rapid analysis, under field conditions, of the emanation concentration in samples of air. The equipment allows the measurement of the radioactivity of air samples with a concentration of emanation from several tenths to several thousand emanation units. The emanation analysis is made at locations where radioactive deposits are covered by soil.

One of the stands in the section introduces the visitor to γ-ray bore-hole testing. Two bore-hole-testing radiometers, KRL-m and KRT, are on display at the exhibition. The light bore-hole-testing radiometer, KRL-m, is intended for the measurement of γ-rays in bore holes up to 120 m deep. The radiometer is made in two forms — of light and explosionproof construction. The range of measurement is from 10 to 1000 mr/hr. The heavy radiometer KRT allows the measurement of γ-ray intensity in bore holes of up to 1000 m in depth with an automatic recording of the variation of intensity with depth. The range of measurement is from 5 to 20,000 mr/hr.

F. Musaev

THE USE OF ISOTOPES IN CHEMICAL RESEARCH IN THE D. I. MENDELEEV INSTITUTE

In a number of departments of the D. I. Mendeleev Chemical and Technological Institute in Moscow radioactive and stable isotopes are used for the solution of various problems.

Under the direction of Professor G. K. Boreskov work is being carried out in which isotopes are used for the study of catalysts and catalytic processes.

G. K. Boreskov and L. A. Kasatkina have investigated the exchange of molecular oxygen and oxygen from steam and vanadium pentoxide and material made by the fusion of vanadium pentoxide with potassium sulfate and potassium hydroxide (these additions increase the catalytic action of vanadium pentoxide).

Vanadium pentoxide begins to exchange with oxygen at 450°C. Exchange with steam occurs at a lower temperature. The addition of K_2SO_4, and also of KOH, to V_2O_5 increases the rate of exchange with steam as well as with oxygen. In this way it is shown that an increase of the catalyst activity results in an increase of the speed of the isotope exchange.

The same authors have investigated the exchange between CO_2 and MnO_2 at temperatures from 18 to 150°C, and also the exchange between CO_2 and O_2 over MnO_2 at 100, 150, and 250°C. Exchange was observed at all these temperatures. The kinetics of the exchange between CO_2 and MnO_2 does not obey a linear relation and is described by the equation

$$\frac{dx}{d\tau} = ks^{-ax}$$

which, similarly, describes the exchange between manganese dioxide and oxygen and steam.

The process of exchange between CO_2 and O_2 over MnO_2 is of the first order.

Investigation of the exchange between CO_2 and steam over MnO_2 and between V_2O_5 and SO_3 are being carried out.

V. V. Popovsky, under the supervision of Professor G. K. Boreskov, is studying the isotopic exchange between molecular oxygen and several solid metallic oxides:

$$CuO, Fe_2O_3, Co_3O_4, NiO, Cr_2O_3, Sc_2O_3.$$

The aim of the work is to determine the role played by the oxygen of the oxide catalysts in the catalytic oxidation processes. In addition, the effect of oxygen pressure and temperature on the rate of isotopic exchange will be studied, and a correlation will be made of the catalytic activity with the oxygen mobility of the oxides, listed above, in connection with the oxidation of hydrogen. The work of A. I. Gorbunov concerns the study of the isotopic exchange reaction in molecular nitrogen, ($N_2^{15} + N_2^{14} \rightarrow 2N^{14}N^{15}$) catalyzed by the transition metals of group IV. The investigation is carried out with the aim of clarifying the connection between the catalytic properties of metals and their electronic structure. The heavy nitrogen isotope, with a 42% concentration of N^{15}, was obtained by the thermal-diffusion separation of molecular nitrogen enriched to 10% N^{15}.

The usual methods for the study of liquid-vapor equilibrium are not suitable in the case of dilute solutions, especially if the components have very nearly equal boiling points. Meanwhile, the region of low concentrations is both of theoretical interest, as well as of practical use in connection with the problem of the separation of

valuable materials from dilute solutions. Further, dilute solutions are the most useful for the testing of fractionating columns. Ya. D. Zelvensky and V. A. Shalygin have developed techniques for the study of the liquid-vapor equilibrium in dilute solutions. The method consists of distilling the solution, which has been labelled by radioactive oxygen or sulfur, and measuring the activity before and after distillation. The activity of the solution is directly measured with a cylindrical counter placed with its window uppermost against the bottom of a thin-walled cell. The calculations are made using Rayleigh's equation.

The method described has been successfully used to study the liquid-vapor equilibrium of a series of dilute solutions: acetic acid in water, thiophene in benzol and trichloroethylene, isopropanol in ethanol and ethyl acetate in carbon disulfide.

The same authors are studying the isotopic exchange of radiosulfur S^{35} between elementary sulfur and the simplest sulfur compounds (thiocyanogen, carbon disulfide, carbon oxysulfide, thiophene, ethyl mercaptan, and dimethyl sulfide) to examine the possibility of using this method to obtain labelled compounds. The isotopic exchange method allows the simplest and most efficient solution to the problem of obtaining pure organic compounds labelled with radioactive sulfur. On the other hand, the study of the isotopic exchange gives information about the mobility of sulfur atoms in organic compounds. Data on this subject are either absent in the literature or indicate that exchange with elementary sulfur does not occur.

Ya. D. Zelvensky and V. A. Shalygin have established that at temperatures higher than 200°C elementary sulfur exchanges the isotope S^{35} with all of the compounds listed above. This method of obtaining labelled compounds consists of heating the substance and radiosulfur together, with or without solvents, for a period of a few hours. At a temperature of 260°C, a practically complete exchange with elementary sulfur is reached for carbon bisulfide in 2 hours, for carbon oxysulfide and a solution of thiocyanogen in ethanol – also in 2 hours, for ethyl mercaptan in 10 hours; for dimethyl sulfide $^1/_3$ of the sulfur is exchanged in 10 hours, while thiopene exchanges 30% of its sulfur in 300 hours.

The kinetics of the isotope exchange has been studied for the above substances.

In the department of cement production, V. V. Timashev, under the supervision of V. N. Young,* has used a radioactive calcium isotope for the study of cement clinker structure. The reaction between the clinker minerals was investigated during their baking at 1450°C. For this, mixtures were prepared, each of which contained one mineral and radioactive CaO. The melts were then heat-treated in a current of hydrogen. The activity of the lime, formed by the decomposition of the melt, served as an indicator and a measure of the transformation.

The nature of the CaO bond was also investigated in one of the main clinker ingredients – $3CaO \cdot SiO_2$. It was established that one of the molecules is bound weaker than the others because it is more readily liberated.

The same authors used radioactive calcium in the form of oxalate for investigating the uniformity of mixing of small quantities of lime (6-12%) with a large amount of soil (88-94%). Using radiography and measuring the activity of sample sections it was possible to obtain a sufficiently clear picture of the mixing.

V. N. Young,* A. E. Fedorov, and V. V. Timashev made an attempt to use radioactive sulfur, in the form of a 5% solution of Na_2SO_4, to study the diffusion of the $SO_4^{=}$ ion into cement.

In the course of this work it was established that the method gives qualitative results. Reliable quantitative data could not be obtained because of the sorption of the SO_4 ion by the cement gel.

In the department of organic product and dye technology, Professor N. N. Vorozhtsov and V. A. Koptyug are studying the isomers of α-naphthalenehalide with the help of radioactive carbon. Work has started on the synthesis of aromatic compounds labelled with C^{14}, among them being 1-naphthol.

Ya. Z.

*Deceased.

AN EXPERIMENTAL GAMMA-RAY IRRADIATOR (EGO-2)

In the USSR Academy of Medical Sciences in Moscow an experimental γ-unit has been constructed and put into use.

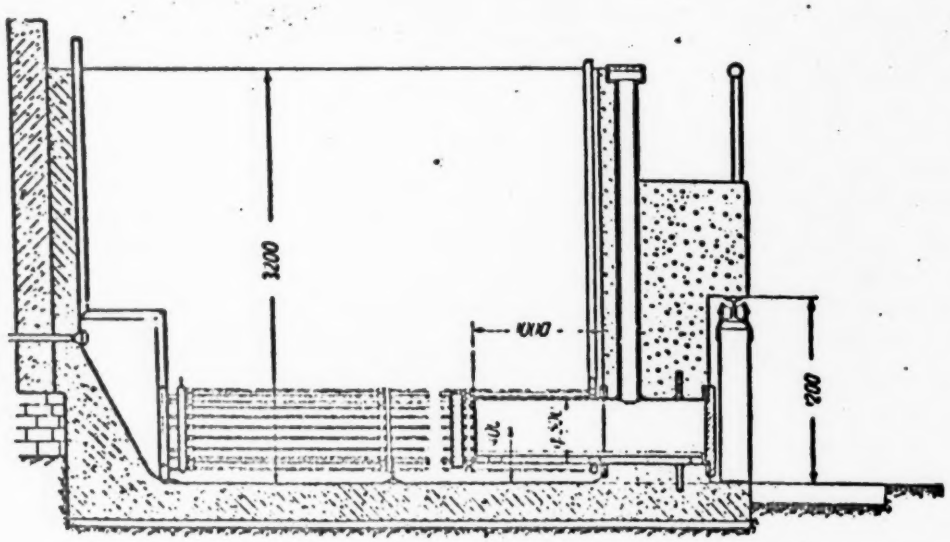

Fig. 1. The experimental γ-irradiator. Layout of the main tank.

The main purpose of the unit is the irradiation of laboratory animals with the aim of studying the biological effects of γ-radiation. In addition, the unit can be used for the study of "cold sterilization" and the effect of radiation on chemical processes in various media.

A number of radioactive cobalt (Co^{60}) preparations are used in the unit, with a total activity of 5 kC. These preparations are arranged so as to allow a uniform irradiation of a cylindrical volume 70 cm long and 30 cm in diameter.

Less uniform irradiation can be made of a cylindrical volume 50 cm in diameter and 100 cm long.

The unit allows different irradiation doses: 200 r/min, 400 r/min, and 600 r/min.

The unit is of a fixed construction, consisting of two adjacent, water-filled tanks which serve as radiation shields. The tank walls are made of concrete with a density of 3.5 t/m^3. The wall thickness lowers the intensity of the γ-ray background to a safe level.

The first small rank is used for the reception, processing, and measurement of the radioactive preparations.

A cylindrical chamber, intended for the objects to be irradiated, is placed together with the radiation sources in the bigger second tank.

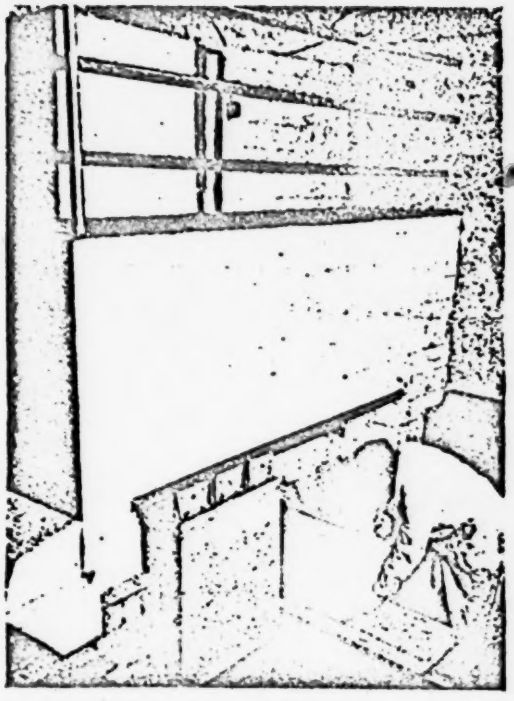

Fig. 2. The experimental γ-irradiator. Chamber for objects to be irradiated (front view).

The cylindrical chamber is fixed into the front wall of the big tank and is equipped with a massive cast-iron protective door. The unit with the radiation sources is placed in the opposite part of the tank. In the nonworking position the chamber is shielded from the radiation by two meters of water and a lead disc. This permits the chamber to be loaded under safe conditions.

The transfer of the radioactive preparations into the working position (for irradiation) is made hydraulically. For this, the preparations move along guiding tubes and are arranged around the cylindrical chamber. The preparations are transferred in 2 sec. The transfer of the preparations into the working position and their return into the storage position is made by remote control.

The γ-irradiator constructed has several advantages over standard units used for radiobiological research. The arrangement used allows the irradiation of large animals by radiation which is uniform throughout the whole useful volume. In addition a comparatively bigger dose can be given. In contrast to the x-ray units normally used for radiobiological research, the γ-irradiator guarantees very stable conditions for irradiation. At the present time, the γ-irradiator is used to conduct numerous experimental investigations in the fields of radiobiology, physical chemistry, and dosimetry.

M. P. Domshlak and V. G. Khrushchev

FOREIGN SCIENTIFIC AND TECHNICAL NEWS

HOMOGENEOUS RESEARCH REACTOR*

North American Aviation subsidiary – Atomics International – with the financial participation of 24 other interested companies, has built a homogeneous reactor (APRR) with interesting features. The reactor is located at the Illinois Institute of Technology (Chicago) and is of 50 kw power rating, which is entirely sufficient for use of the reactor as a source of neutrons and gamma rays for physical and biological research, and for obtaining short-lived isotopes.

Fig. 1. The core of the reactor.

The fuel of the reactor is enriched uranium in the form of a solution of uranylsulfate in common water.

Basic parameters of the reactor core:

Design thermal power	50 kw
Critical mass at zero power	850 g U^{235}
Maximum thermal neutron flux	$1.7 \cdot 10^{12}$ n/cm^2·sec
Mass coefficient of reactivity	.031 % per g
Temperature coefficient of reactivity	.029% per 1°C
Energy coefficient of reactivity	.006% per 1 kw
Temperature of the core solution at rated power	80°C
Excess reactivity at 20°C and zero power	3%
Absorbing action of the control and safety rods (in % reactivity)	8% (2% per rod)
Nuclear density ratio H: U^{235}	350
Density of U^{235}	75 g/liter
Maximum power density	5.5 w/cm^3

The core of the reactor forms a sphere of stainless steel of 31.6 cm outside diameter (Fig. 1). The sphere has bushings for four vertical control rods and a horizontal test hole passing through its center. Into the core are also mounted coils for the coolant, a fuel charging and draining pipe, and a gas removal pipe.

The core is surrounded by graphite blocks of the reflector which form a rectangular prism measuring 198 × × 165 × 165 cm^3.

The cooling system of the reactor consists of two loops. The coolant of the first loop is distilled water, which passes in a spiral tube through the core. (The coil through which the coolant removing the core heat is pumped, is seen in Fig. 1.) In the second loop common water is used. Distilled water temperature at entrance into the core is 26.7°C, at exit 43.3°C. The circulating pump ensures flow of the coolant through the core, amounting to 32.7 cubic meters per hour with a pressure drop of 3.5 atmospheres.

In a special space under the reactor, next to the cooling system, is located the gas elimination system (recombiner) and a drain tank-reservoir for the liquid fuel, surrounded by lead shielding (Fig. 2).

* Nucl. Eng. 1, 5, 198 (1956); Mech. Eng. 78, 8, 725 (1956).

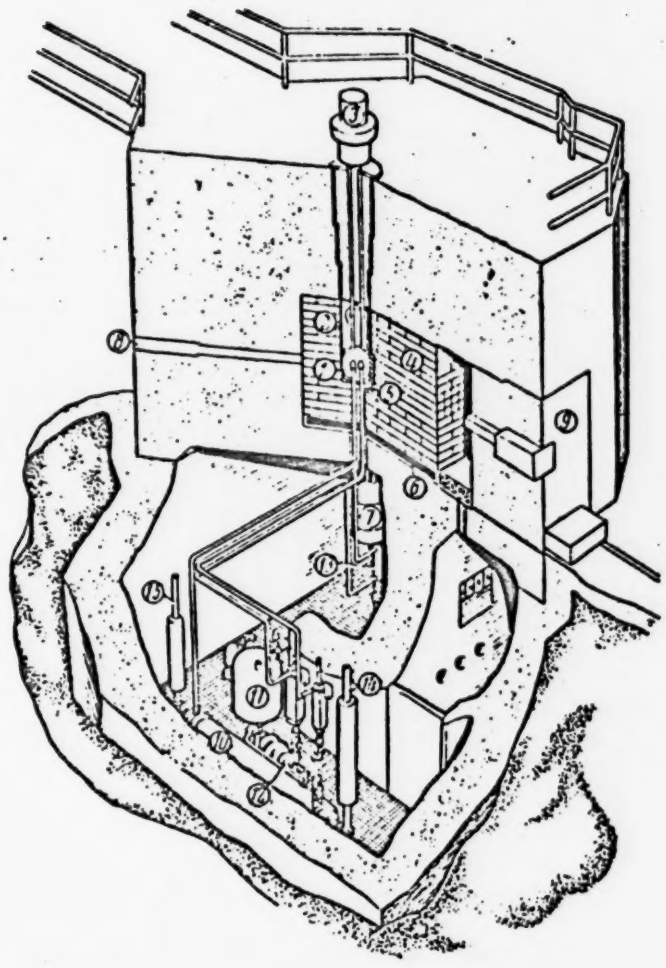

Fig. 2. Over-all view of the reactor installation. 1) Core shell; 2) secondary core enclosure; 3) control and safety rod drives; 4) graphite thermal column; 5) lead shielding; 6) ionization and fission chambers; 7) gas recombiner; 8) test hole for neutron irradiation; 9) removable concrete shield door; 10) primary heat exchanger; 11) expansion chamber; 12) circulating pump; 13) recombiner heat exchanger; 14) entrance for water of the secondary loop; 15) exit for water of the secondary loop.

Control of the reactor is accomplished through four rods of boron carbide (each 406 mm long and 15.9mm in diameter) which are enclosed in stainless steel. One of these rods serves for automatic control of reactor power, and is moved by a servo mechanism. The rate of travel of the rods is about 2.54 mm per second, the length of free travel being 305 mm.

Scramming of the rods occurs at increase of the neutron flux to levels exceeding preset values.

Serving as safety indicators are instruments for measuring gas pressure, hydrogen concentration in the fuel solution, fuel temperature in the core, and liquid level in the drain tank. Power level is measured by fission chambers, and also ionization chambers with gamma compensation.

Biological shielding of the reactor (thickness 155 cm) is made of heavy concrete with density of 3.5 g/cm^3, and with additives of limonite, colemanite and sinter. The shielding contains windows of lead glass and bismuth glass.

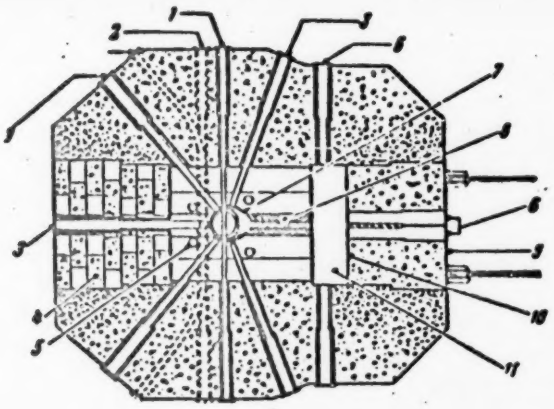

Fig. 3. Horizontal section through the reactor. 1) Central test hole for irradiation of samples; 2) test hole for pneumatic handling of samples; 3) beam hole for neutron and gamma rays; 4) blocks of the concrete shielding; 5) exits of the vertical beam holes; 6) passage for introduction of samples; 7) bismuth shielding in aluminum cladding; 8) removable graphite bars of the thermal column; 9) movable concrete door; 10) borated facing; 11) air gap.

For irradiation of materials and provision of emanant beams the reactor has the following: 5 horizontal holes 7.6 to 10.2 cm in diameter, 4 vertical holes each 10.2 cm in diameter, 2 holes with pneumatic handling of samples 5.1 cm in diameter, and a central test hole for irradiation of materials 3.8 cm in diameter. There is a thermal column, .46 square meters in area, along whose axis runs a hole which can be filled in when necessary with graphite bars of square section measuring 10×10 cm^2.

Between the exterior surface of the thermal column and the concrete shield door there is a gap from which emerge four test holes 152 mm in diameter for irradiation of samples.

The thermal column and basic test holes are shown in Fig. 3.

O. Shch

RESEARCH REACTOR OF THE WESTINGHOUSE CORP.*

The Westinghouse Corp. is assembling a reactor (WTR) 30 miles south of Pittsburgh (U.S.A.) in Waltz Mill, Pennsylvania. The reactor is intended primarily for irradiation of materials in a high neutron flux, under high temperature and pressure. This reactor will be one of the first not belonging to government agencies. It is of interest because of its vast capacities for testing materials, its compact design and small size.

The reactor is scheduled to start operation toward the end of 1957. Basic characteristics of the reactor:

Reactor type	heterogeneous, thermal neutron, pressurized core
Nominal thermal power	20 megawatts
Maximum thermal power	60 megawatts
Fuel and its critical mass	10-12 kg U^{235}
Coolant	common water
Thermal neutron flux	10^{13}-10^{14} neutrons/cm^2·sec

The reactor core is about 112 cm high and about 127 cm in diameter, and consists of a group of vertical aluminum tubes, forming the triangular grid pattern of the reactor. The aluminum tubes are designed to hold fuel assemblies, control rods, and experiment holes. The control rods and experiment holes are distributed so that each one is surrounded by six fuel assemblies (Fig. 1). All together six holes for experiments are planned, each in the form of blind aluminum tubes. In the center of the core is located a large experiment hole. The central aluminum tubes are reserved for the fuel assemblies; the peripheral aluminum tubes serve as supplementary experiment holes for irradiation of samples, which are introduced through the reactor top cover.

The blind holes are intended mainly for testing of fuel elements and various materials in a medium of flowing water or other coolants, and are designed for pressures up to 140 atmospheres and temperatures up to 315°C.

Charging and unloading of the blind holes will be performed by means of a remote manipulator which is installed under the reactor. These operations will be performed only with the reactor shut down.

The fuel assembly of the reactor consists of three coaxially assembled cylindrical fuel elements which are fastened together by a central aluminum tube (Fig. 2). The fuel used is an alloy of aluminum and uranium. Also made of aluminum is the retaining cladding of the fuel element. The fuel assemblies are made symmetrical, so that to obtain maximum fuel burn up, they can be turned over, top down. It is assumed that the burn up of U^{235} during an operating run, which lasts about four months, will reach 25%. The excess reactivity available is sufficient to permit restarting the reactor, with override of the so-called "iodine sink" for about one hour after shutdown.

The control rod is a cylinder of cadmium enclosed in aluminum, which is placed in the center of the fuel assembly and is fastened to it. Above and below the core, over each aluminum tube through which moves a control rod, is located a guide tube of stainless steel, which protects the control rod against deformation which could appear under the action of radial flow of coolant (outside the core). Movement of the control rod is produced through a rack and pinions.

---

* Westinghouse Eng. 16, 5, 138 (1956).

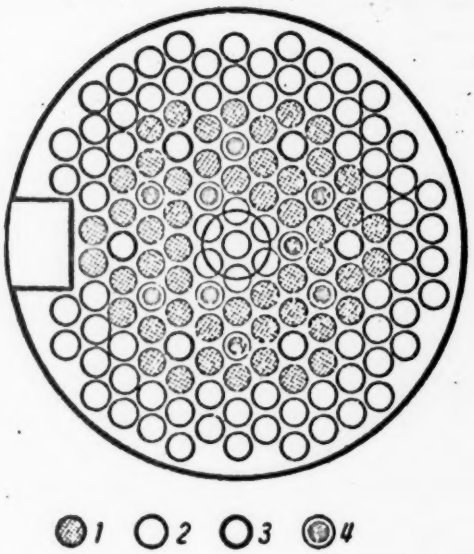

Fig. 1. Diagram of reactor passages. 1) Fuel assemblies, 2) supplementary experiment holes, 3) high pressure, blind holes for experiments, 4) control rods.

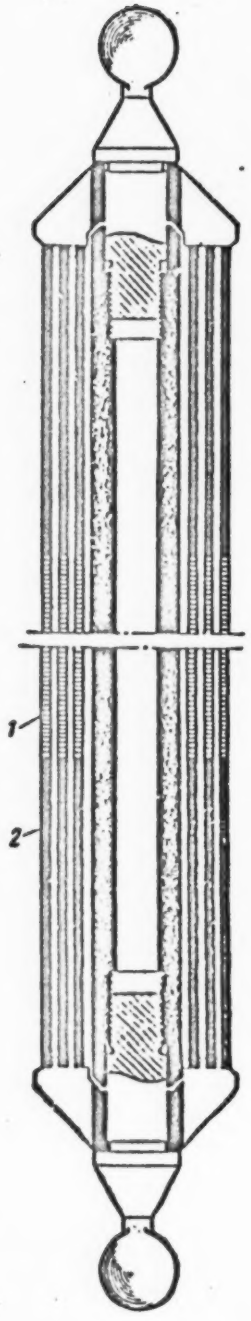

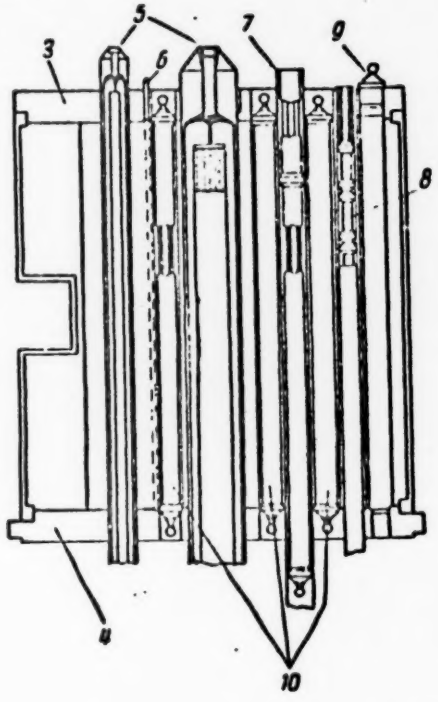

Fig. 2. Section through fuel assembly and reactor core. 1) Aluminum-uranium alloy, 2) aluminum, 3) upper support plate, 4) lower support plate, 5) high pressure, blind holes for experiments, 6) neutron source, 7) control rod, 8) hole with pneumatic feed of samples, 9) plug, 10) fuel assemblies.

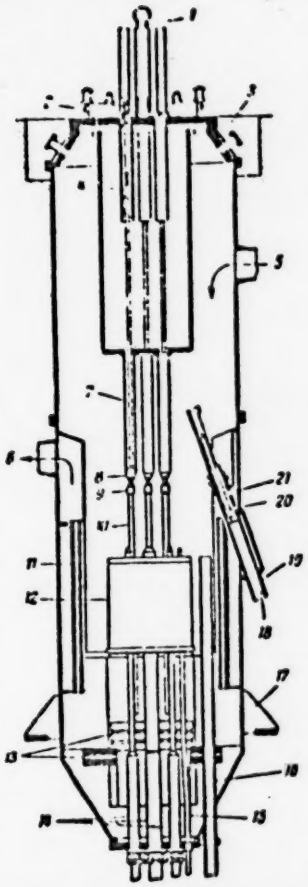

Fig. 3. Section through reactor shell. 1) Lifting eye, 2) control rod drive, 3) removable cover, 4) upper guide tube for control rod, 5) water entrance, 6) water exit, 7) control rod guide tube, 8) magnet, 9) shock absorber, 10) control rod passage, 11) thermal neutron shielding, 12) core, 13) biological shield, 14) blind holes for experiments, 15) experiment hole with pneumatic feed of samples, 16) vertical tube, 17) support bracket, 18) passage for unloading fuel, 19) guide tube, 20) fuel assembly container, 21) fuel assembly.

The safety rods are held in the raised position by electromagnets. At cutoff of electromagnet winding current, the rods fall under the action of their own weight and the pressure of the coolant flow, which is directed from the top down.

The reactor shell, designed for coolant pressure of 8 atmospheres, is a vertical sealed vessel of stainless steel, about 2.5 cm thick, and consisting of three flanged sections, bolted together (Fig. 3). The two lower sections are permanently fixed to the concrete shielding at installation. Through the conical upper section, which is the top cover of the reactor, is brought out the electric wiring of the instruments that are located inside the shell, and also are inserted the samples to be irradiated.

Around the periphery of the core are located five additional experiment holes with pneumatic feed of samples. At the ends of these holes are small openings through which flows water that cools the test samples. Since the operating pressure in these holes is somewhat higher than the coolant pressure, the test samples are held at the extreme upper end of the hole by the flow of the cooling water. When the pressure in the holes is dropped the samples return to the loading point in the pneumatic holes under the action of the water pressure in the reactor itself.

The central tube of each fuel element can also be used for irradiation of small samples of materials.

Yu. K.

NEW DATA ON METALLIC PLUTONIUM

In one of the volumes of "Progress in Nuclear Energy" [1] that recently appeared in England, there are published for the first time, a number of new data on the properties of plutonium.

The crystal structure of the α-phase of plutonium has been obtained by V. Zakhariasen from the Debye pattern (Table 1).

TABLE 1

Crystal lattice	Dimensions of elementary cell, A at 21°C	Number of atoms in elementary cell	Computed density, gm/cm^3
Monoclinic	$a = 6.1835 \pm 0.0005$; $b = 4.8244 \pm 0.0005$; $c = 10.973 \pm 0.001$ $\beta = 101.81° \pm 0.02°$	16	19.816 ± 0.006

Data on the thermal expansion coefficients of various phases of plutonium of high purity are given in Table 2.

TABLE 2

Phase	Temperature range, °C	Coefficient of linear expansion $\times 10^6$, per °C (t = °C)	Remarks
Alpha	−186—100	$(46.85 \pm 0.05) + (0.0559 \pm 0.0004)\,t$	Determined with a linear dilatometer for polycrystalline isotropic specimens [2]
Beta	133—197	(33.88 ± 0.11)	
Delta	320—440	(-8.6 ± 0.3)	Determined by x-ray method [3]
Delta-prime	465—485	$\alpha_a = (305 \pm 35)$; $\alpha_c = (-659 \pm 67)$; $\alpha_{polycr} = (-16 \pm 28)$	
Epsilon	490—550	(36.5 ± 1.1)	
Liquid	at 665	Volume coefficient $= (50 \pm 25)$	Taken from [4]

The data of Laker on the elastic properties of α-plutonium of high purity and the data on the speed of sound from which they were obtained are given in Table 3.

TABLE 3

Property	Value*	Pressure coefficient,** 10^{-6}/bar	Temperature coefficient,*** 10^{-5}/°C
Young's modulus	$(9.03\pm0.03)\times10^{11}$ dyne/cm^2	$+18\pm1$	-127 ± 8
Modulus of rigidity	$(4.34\pm0.01)\times10^{11}$ dyne/cm^2	$+14\pm1$	-145 ± 10
Poisson ratio	0.15 ± 0.01	$+27\pm7$	$+138\pm71$
Compressibility	$(2.14\pm0.02)\times10^{-6}$/bar	-28.5 ± 3	$+68\pm32$
Speed of longitudinal waves (v_l)	$(2.244\pm0.004)\times10^5$ cm/sec	$+7.8\pm0.6$	-56 ± 4
Speed of transverse waves (v_{tr})	$(1.483\pm0.002)\times10^5$ cm/sec	$+6.1\pm0.7$	-65 ± 5
Speed in infinite medium	$(2.301\pm0.003)\times10^5$ cm/sec	$+9.2\pm0.4$	-48 ± 6

*) Measured by pulse method. Specimen without micropores, pressure-treated at 300°C and 3.5 tons/cm^2 and cooled under load. $\rho_{30°C} = 19.722 \pm 0.005$ gm/cm^3.

**) $\rho_{30°C} = 19.62$ gm/cm^3. Measured by pulse method.

***) Measured by resonance method on two specimens ($\rho = 19.5$ and 19.6 gm/cm^3).

G. Z.

LITERATURE CITED

[1] Progress in Nuclear Energy, Ser. V. Metallurgy and Fuels, Vol. I (Pergamon Press, 1956) p. 387.

[2] E. M. Cramer, L. L. Hawes and F. W. Schonfeld, unpublished data.

[3] F. H. Ellinger, J. Metals 1956, October.

[4] A. A. Comstock and R. B. Gibney, US AEC report LA 1348.

ALLOYS OF PLUTONIUM WITH RARE EARTH METALS

Very little information on plutonium alloys is available. It is therefore of interest to evaluate the possibility of alloying plutonium with rare earth metals according to experimental data [1] relative to the extraction of plutonium from uranium by these metals. Plutonium forms two compounds with uranium [2] and its dissolution in uranium at 1540°C is close to ideal [3], which shows that the solubility of plutonium in liquid uranium is unlimited. The rare earth metals lanthanum and cerium do not alloy with liquid uranium, but form considerable aliquation regions [4]. Thus the solubility of cerium in uranium is only 1.2% at 1150°C [5]. The extraction of plutonium from liquid uranium by lanthanum and cerium is accompanied by considerable thermal effect while in the case of neodymium the thermal effect is close to zero. These facts can be interpreted as the result of the unlimited solubility of plutonium (assumed on the basis of certain calculations [6]) in liquid rare earth metals; lanthanum and cerium, however, have a tendency toward a stronger reaction (formation of compounds) at lower temperatures in the solid state. Thus the alloys of plutonium with rare earth metals are considerably different from analogous alloys of uranium and are more like alloys of thorium [4], which forms unlimited solutions with lanthanum and cerium in the solid and liquid state.

LITERATURE CITED

[1] D. E. McKenzie, Can. J. Chem. 34, 1176 (1956).

[2] A. S. Coffinberry and F. H. Ellinger, "Intermetallic compounds of plutonium," Report No. 875 to the International Conference on Peaceful Uses of Atomic Energy (Geneva, 1955).

[3] D. E. McKenzie, Can. J.Chem. 34, 515 (1956).

[4] H. A. Saller and F. A. Rough, BM I-1000 (1955).

[5] A. Voight, "Purification of nuclear fuel by extraction with liquid metals," Report No. 545 to the International Conference on the Peaceful Uses of Atomic Energy (Geneva, 1955).

[6] D. E. McKenzie, Can. J. Chem. 34, 749 (1956).

ALLOYS OF PLUTONIUM AND AMERICIUM WITH BERYLLIUM

New data [1] have been published on the preparation of alloys of Pu^{239} and Am^{241} with beryllium; these alloys are sources of neutrons; neutron emission in these alloys proceeds according to (α, n) reaction under various conditions.

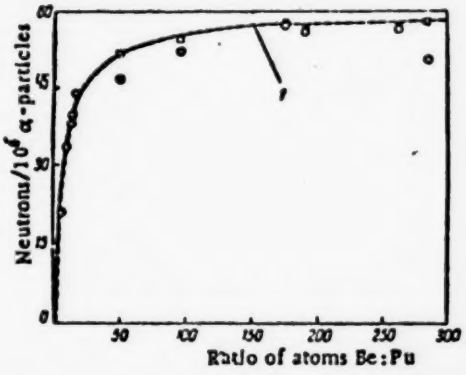

Fig. 1. Variation of neutron emission rate as the function of the composition of plutonium-beryllium alloys [1]. I) The theoretical emission rate (assuming an asymptotic maximum) is equal to 60 neutrons/10^6 α-particles; □) liquid alloys; ○) solid alloys.

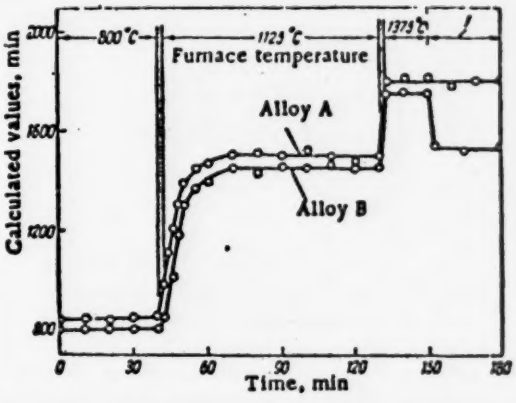

Fig. 2. Variation of neutron background during the transformation of two mixtures PuF_3 + Be, first into sintered, then into liquids alloys Pu-Be, and also during hardening [1]. I) Cooling down to 300°C.

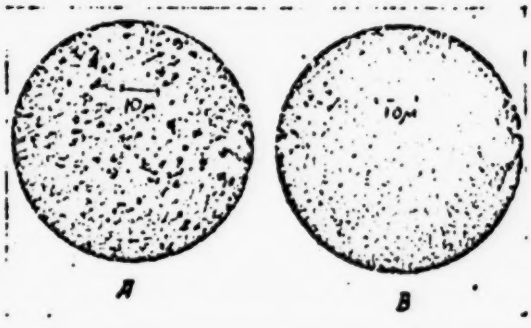

Fig. 3. Slides of Pu-Be alloys: A) with 90.0% Be by weight and B) with 91.5% Be by weight. Etching in 1% HF for 30 seconds. Dark crystals of $PuBe_{13}$ in light Be-matrix [1].

Plutonium alloys were prepared in BeO crucibles by regenerating 0.1-0.3 g of plutonium trifluoride by 99.8% pure beryllium powder at 1100-1200°C in vacuum. At this temperature the beryllium fluoride slag is easily eliminated and the pure alloy, which is rich in beryllium, is melted by heating up to 1375°C. The composition of the alloy was calculated on the basis of the PuF_3 charge, and the amount of plutonium passing into the alloy reached 99% in certain experiments. Neutron emission rate [2] was determined by comparison with a standard polonium or radium source. According to the measurements made on 11 alloys the emission rate varies with the composition of the alloy, as is shown in Fig. 1.

Figure 2 represents the variation of neutron background during the regeneration of two batches of PuF_3 (ratio of Be:Pu is 265:1 in alloy A and 285:1 in alloy B). The rapid increase of neutron background shows that the alloy starts to form rapidly beginning at 1125°C.

After 25 minutes the background becomes constant, which indicates the end of the regeneration process. At this stage the product of alloying is composed of a sintered mixture of $PuBe_{13}$ aggregates in the beryllium matrix. When the temperature is raised to 1375°C the alloy becomes liquid and the neutron background increases sharply. When the cooled alloy hardens, the neutron background of the A alloy does not change while that of the B alloy decreases considerably. Metallographic analysis (Fig. 3) shows that the dimension of the $PuBe_{13}$ crystals is ~ 2μ in alloy A and ~ 15μ in alloy B. The range of α-particles is equal to 20μ in $PuBe_{13}$. Since in alloy B the dimension of $PuBe_{13}$ crystals is of the same order of magnitude as the range of α-particles, the rate of neutron emission approaches that of $PuBe_{13}$ (mixture 1: 13) and decreases with respect to the neutron emission rate of the liquid state, where Pu is regularly distributed. In alloy A the crystals are small with respect to the range of α-particles and the distribution of Pu in the solid state approaches that in the liquid state.

It is supposed that the $PuBe_{13}$ crystals are one order smaller in the A alloy than in the B alloy, since the A alloy undergoes monotectic transformation during cooling while in alloy B, richer in beryllium, primary crystals of $PuBe_{13}$ separate during the entire cooling time.

Two alloys of americium were prepared in similar way from 0.03 g AmF_3. In the alloy with the ratio Be: Am = 263: 1 the neutron background does not decrease during hardening of the liquid [3]; the dimension of the crystals of $AmBe_{13}$ is apparently also of the order of 2μ. In this alloy the neutron emission rate was equal to 71.7 neutrons/10^6 α-particles, while in the alloy whose ratio Am: Be = 1: 14 the emission rate was 48.5 neutrons/10^6 α-particles. According to these data the maximum theoretical neutron emission rate for a homogeneous mixture of atoms is equal to 73.7-74 neutrons/10^6 α-particles.

G. Z.

LITERATURE CITED

[1] O. J. Runnals and R. R. Boucher, Can. J. Phys. 34, 949 (1956).

[2] G. C. Hanna and O. J. Runnals, Can. J. Phys. 34, 959 (1956).

[3] O. J. Runnals and R. R. Boucher, Nature 176, 1019 (1955).

EVALUATION OF THE PATHOLOGICAL EFFECTS DUE TO RADIOACTIVE PARTICLES SUSPENDED IN AIR*

Many of the methods of taking samples of air which are used at the present time are more apt to confuse than to furnish a reliable estimate of the pathological effects due to radioactive particles distributed in the air. The nature and degree of the interaction with lung tissue in all organisms can be estimated only on the basis of adequate data, obtained by suitable methods of obtaining air samples, the analysis of which should furnish information on the following: 1) the relative amount of active material precipitated in the upper respiratory tracts and in the alveolae; 2) the solubility and, in certain cases, the radiochemical structure of the absorbed material since these determine the intake and distribution of the material in the organism; 3) the decay rates, nature, intensity and energy of the radiation; 4) the number of absorbed particles per unit volume and their specific activity in microcuries per particle which must be known to determine the tissue dose. Only on the basis of these data is it possible to estimate the internal damage from a comparison of the magnitude of a given interaction with the magnitude of the allowable concentration.

An ideal method of taking samples of radioactive dust should imitate the processes which occur in the lungs. In taking the samples the process should be carried out in two successive stages: the first stage should simulate the trapping of particles in the upper respiratory tracts while in the second stage the residual activity scattered in the air should be taken up to the same extent as in the alveolae. The following can be used in the first stage: a fine filter, a modified coil, a one stage impactor and so on. In the second stage it is convenient to use an electrostatic precipitator or a molecular filter. The choice of method used in taking the sample is determined by the material being investigated.

In order to simulate the solubility conditions which are encountered by the particles in the organism it is necessary to use the different physiological solutions associated with the alveolae, the bronchae, and the gastrointestinal tract.

The determination of the dose factor in the interaction with lung tissue is based on data obtained by means of an autoradiograph of an undissolved alveolar fraction. The number of particles is determined directly by counting the spots on a plate while the distribution of activity is obtained from the size of these spots. Just as in any meaningful test, the obtained samples of air should reflect the constituency of the inhaled air and the appropriate interaction time. Since no one sample can completely correspond to all individual variations in inhalation and interaction conditions it is desirable to take a number of samples using the same procedure.

S. L.

* T. J. Barnett and T. E. Hatch, Ind. Hyg. 17, 1, 80 (1956).

RADIOLOGY WITH β-RADIATORS*

It is well known that the interaction of β-particles with matter results in the production of radiation in the x-ray region in the form of characteristic x-rays or bremstralung. However, up to the present time, no attempts have been made to exploit this effect for use in medicine as a radiological diagnostic tool.

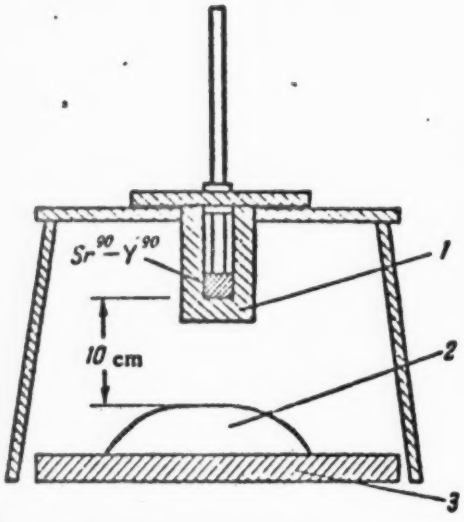

Fig. 1. Experimental arrangement.
1) Lutecium shield; 2) object being irradiated; 3) casette.

Fig. 2. X-ray picture of the body of a rat. Focal distance is 10 cm. Length of exposure 5 minutes.

In the work being reported here a medical applicator comprising of a $Sr^{90}-Y^{90}$ complex is used as a source of β-radiation. The source, with a working diameter of 5 mm, is placed at the end of a 16-centimeter rod. A circular plastic shield is used as protection against radiation when the applicator is adjusted. The Sr^{90} in the source is in equilibrium with Y^{90} in an amount such that the surface intensity of the radiation is 330 fer/sec. The radiation consists of β-particles with energies of 0.537 Mev emitted in the transmutation of Sr^{90} into Y^{90}, and β-particles with energies of 2.18 Mev emitted in the transmutation of Y^{90} into a stable isotope of zirconium. The mean energy of the β-radiation for Sr^{90} is 0.22 Mev and for Y^{90} is 0.7 Mev. The half-life for Sr^{90} is approximately twenty years and

*) Radiology 67, 3,416 (1956).

that of Y^{90} is about 62 hours.

The source has a metal shield consisting of 0.05 mm of stainless steel and 0.25 mm of aluminum, equivalent to a 100 mg/cm^2 filter. Because of the shielding, the number of β-particles produced in the decay of Sr^{90} and Y^{90} is reduced to 3 per cent and 60 per cent of the original number, respectively.

A shield of lutecium, 1.2 cm thick, is placed between the source and the object being investigated to absorb the β-radiation.

The interaction of the β-radiation with the material in the source itself and in the absorber produces bremstralung and characteristic x-ray radiation which can be used to make x-ray pictures. In Fig. 1 are shown the details of the experimental apparatus. In Fig. 2 and Fig. 3 are shown x-ray pictures of the body of a rat and a human hand.

The radiographs would seem to indicate that x-radiation is given off by ordinary medical applicators. This radiation is due to the following: a) internal bremstralung produced in the interaction of the β-particles with nuclei in the material; b) external bremstralung produced as the β-particles are brought to a stop by the nuclei in the absorber, and c) characteristic x-ray radiation due to the interaction of β-particles with orbital electrons in the material of the source, shell, and absorber. The internal bremstralung arises in the strontium-ytterbium complex; the external bremstralung in the absorbing layers of the source and surrounding material. Since only 3 per cent of the β-radiation of the strontium penetrates the shield, it may be assumed that some part of the absorbed 97 per cent of the β-particles is transformed into characteristic x-rays and bremstralung.

Fig. 3. X-ray picture of a human hand. Focal distance 10.5 cm. Length of exposure 5 minutes.

The characteristic x-rays, produced by β-particles from $Sr^{90}-Y^{90}$ in the foil amount to 1×10^{-2} photons for each β-particle while the yield of bremstralung for particles with higher energy is approximately 6×10^{-2}/β-particle. The internal bremstralung of $Sr^{90}-Y^{90}$ with energies from 10-150 kev exhibits a maximum at about 35 kev; the radiation produced by the β-particles of a preparation in tin have two maxima: 25 kev for the characteristic radiation and 55 kev for the bremstralung. The corresponding data for β-particles of Sr^{90} and Y^{90} for interaction in steel and aluminum are not known. Preliminary measurements of the emission spectrum of the radiation indicate that this radiation is nonuniform and has several hard components.

The x-ray pictures obtained with this simple and relatively weak nuclear source (300 mcuries) show very good definition and contrast in spite of the large "working diameter" of the source (5 mm) and the short focal length. Better x-ray pictures can be obtained by using a source with a smaller working diameter and using other β-radiators in conjunction with materials which emit radiation more suitable for radiology of various parts of the body. It is evident from the x-ray pictures which have been presented that pure β-radiators can be used to obtain radiation which is suitable for medical radiology.

S. L.

BRIEF REPORTS

India. In July 1956 a two-day conference on the peaceful uses of atomic energy was held in Bombay under the direction of the well-known Indian scientist H. J. Bahba. Scientists from India, Burma, Ceylon, Egypt, and Indonesia were present. A resolution was adopted to hold these conferences regularly in the future and to invite other countries from Asia and Africa. [Nuclear Power I, 4, 153 (1956)].

France. In September of 1956 construction was completed on the power section of the dual-purpose reactor G-1 at Marcooule. [Nuclear Eng. I, 8, 347 (1956)]. The generator associated with the power section of the reactor has a capacity of 5 megawatts. The power required to supply its own needs (chiefly the electrical supply for the gas blowers), however, is 8 megawatts [Atomic Energy (USSR) 1956, 2, 108].

Belgium. According to an agreement recently drawn up in Washington, Belgium is to receive 8 kg of enriched uranium from the US (up to 90% U^{235}). This uranium is to be used in a Belgian reactor designed for materials testing at high neutron fluxes. The reactor is to be built at Malo.

According to the agreement Belgium will receive from the US secret information on methods of extraction and refining of uranium and thorium and will also reprocess irradiated fuel when the equipment desigend for this purpose is approved by the US Atomic Energy Commission [Nuclear Power I, 4, 152 (1956)].

Denmark. The Atomic Energy Commission of Denmark is reported to be beginning the construction of an atomic-energy scientific research center in the vicinity of Roskilde (32 km from Copenhagen). The United States will furnish a "swimming-pool" reactor for research purposes. The design and construction of this reactor will be carried out by an American firm, Foster Wheeler. The installation and assembly of the reactor will be performed by Danish specialists. Several Danish scientific workers are being trained for this purpose at various American research centers (Argonne and Brookhaven) [Nuclear Power I, 4, 152 (1956)].

Japan. The Japanese firm "Shova Denko" which is engaged in the manufacture of artificial fertilizer is planning the construction, in the near future, of a plant for the production of heavy water. It is expected that the plant will have an output of 10 tons of heavy water per year. The experimental work required in connection with the construction of the plant was carried out in 1954. The plant will be constructed by the Japanese firm of "Zhitashi." [Atomwirtschaft 2, 6, 235 (1956)].

Federation of German Republics. Deposits of uranium ore with uranium contents up to 3.6% have been discovered near Kassel (district of Hesse). Another well-known uranium ore deposit in West Germany is in the Fichtel Mountains. The uranium content of this ore is 0.5% [Nuclear Eng. I, 8, 347 (1956)].

USA. In model studies of a nuclear reactor of one of the first atomic power stations (PWR) in the USA use will be made of a plastic tape (total length approximately 8 km) containing enriched uranium which will serve as the fuel for an experimental nuclear reactor being built by the Foster Wheeler company at its laboratory in Lynchburg, Virginia. The plastic tape, with uranium dispersed throughout its volume, will be alternated with thorium slabs. (This is the first case in which thorium has been used in a nuclear reactor.)

If the reactor power level becomes too high gas bubbles form in the plastic; these bubbles automatically cause the reactor power level to become sub-critical and prevent a chain reaction [NY Times, Nov. 11, 1956].

USA. In Arco (Idaho) land tests have been performed on an atomic aviation engine and it appears that in several years the United States will be in a position to test an atomic-powered airplane in the air.

It is probable that a sea-plane, such as the Martin Seamaster, will be used for this purpose and that an atomic turbo-reactor engine will be used. In this engine the combustion chamber, in which the air is heated, is

replaced by a nuclear reactor. Liquid metal (sodium or bismuth) is used as a reactor coolant; this material passes to a heat exchanger in which compressed air, generated by the motion of the turbine blades, serves to remove the heat.

The choice of a sea-plane for installation of the atomic engine is due to the high weight of the engine and shield; if a land plane were used for this purpose the length of the required runways would be prohibitive. Moreover, if a plane crashes at sea there is much less danger of radioactive contamination of the surrounding atmosphere (Yorkshire Observer Aug. 24, 1956).

USA. At the present time in the USA there are in operation 13 industrial reactors (designed chiefly for plutonium production); of these 8 are at Hanford and 5 at Savannah River.

There are 24 research reactors of which 12 are used for materials testing; there are 4 experimental reactors.

Thus, in all, there are 41 reactors in operation in the USA. There are also 61 reactors in various stages of design and construction. [Atomic Energy Guideletter 98, 3, 1 (1956)].

USA. It is proposed to build an atomic electric power station with a capacity of 10 megawatts at Anchorage (Alaska). The moderator will be heavy water and sodium will be used as a coolant. Since the cost of electric power is extremely high in Alaska and it is proposed to use slightly enriched uranium as the fuel in this power station, it is assumed that the power from installations of this type will be economically competitive with the power from ordinary power stations at an earlier data in Alaska than in the States.

The US Atomic Energy Commission has stated that although the problems involved in the application of sodium and heavy water have been investigated comprehensively on a separate basis there is still a good deal of research and development work to be done before these materials can be used jointly [Nuclear Power I, 7, 303 (1956)].

BIBLIOGRAPHY

NEW LITERATURE ON QUESTIONS OF THE PEACEFUL USES OF ATOMIC ENERGY

Books

Berlin, R. I. and Sakhovaler, I. I., Some Radioactive Equipment and Its Uses in the Food Industry (Food Ind. Press, 1956) 16pp., 25 kopecks.

Dzhelepov, B. S. and Zyryanova, L. N., The Influence of the Atomic Electric Field on β-Decay (Acad. Sci. USSR Press, 1956) 312 pp., 28 rubles.

Markovsky, E. A. and others, Radioactive Isotopes in the Study of Metals (State Tech. Press Uk. SSR, Kiev, 1956) 90 pp., 1 ruble, 70 kopecks.

Omelyanovsky, M. E., Philosophical Problems of Quantum Mechanics (Acad. Sci. USSR Press, 1956) 269 pp., 9 rubles, 40 kopecks.

The Use of Radioactive Isotopes in Nonferrous Metallurgy, Collection of articles, S. A. Dubinsky (ed.) (Central Information Inst., 1956) 115 pp., no price.

Ratnikov, E. F., Atomic Energy in the National Economy (Sverdlovsk Book Press, 1956) 94 pp., 1 ruble, 60 kopecks.

Segalin, V. G., The Use of Radioactive Methods for Control and Automation in the USSR Coal Industry (Coal Tech. Press, 1956) 43 pp., no price.

Serebrennikov, V. V., The Chemistry of Actinides (Actinium, Protoactinium, and Transuranium Elements) (Tomsk Inst. Press, 1956) 101 pp., 6 rubles, 30 kopecks.

Chernavsky, D. and Shabansky, V., Atomic Energy (State Instructional Press, 1956) 72 pp., 1 ruble, 20 kopecks.

Articles in Journals

Abasov, I. T., "The study of erythropoesis in radiation damage by the method of marked atoms," Azerbaijan Med. Jour. 1956, No. 8.

Alimarin, I. P. and Stepanyuk, E. I., "The separation of niobium and tantalum from titanium with selenious acid," Factory Lab., 22, 10 (1956).

Atabek, A. A., "Radioactive iodine in thyroid therapy," Sov. Medicine 1956, No. 8.

Belyavskaya, T. A. and Fadeeva, V. I., "The quantitative separation of beryllium from some elements by the method of ion-exchange chromatography," Vestnik Moskow. Univ. 1956, No. 6.

Beus, A. A. and Zalashkova, N. E., "On the origin of the soda-type beryllium in granite pegmatites," Mineralogy Collection (Lvov Geological Soc.) 1956, No. 10.

Bibergal, A. V. and Korotkova, M. M., "A new type of gamma indicator," Biophysics 1, 6 (1956).

Bobkova, V. I. et al., "The determination of the blood-flow velocity using radioactive sodium," Soviet Med. 1956, No. 8.

Borgardt, A., "The nonlinear meson field of a nucleon at rest," Proc. Acad. Sci. USSR 109, 6 (1956).

Borodin, L. S., "On the occurrence of beryllium in the Khibinsk mountain range and on beryllium in nephelinic syenites," Proc. Acad. Sci. USSR 1956, No. 4, p. 109.

Brodsky, A. I., "The calculation of the kinetic isotope effect from experimental data," Ukrain. Chem. J. 22, 4 (1956).

Vaynberg, M.Sh. "On terminology in the field of gamma technology," Standardization 1956, No. 4.

Glazov, A. N., "The use of radioactive isotopes in engineering-research practice," Hydrotech. and Improvement 1956, No. 9.

Golovin, B. M. and Dzhelepov, V. P., "The study of the elastic scattering of 590-Mev neutrons by neutrons," J. Exptl.-Theoret. Phys. (USSR) 31, 2 (1956).

Zavolosnova, V. S., "The treatment of erythema with radioactive phosphorus," Therapeutic Archive 28, 6 (1956).

Zaitseva L. L., "V. A. Borodovsky and his work on radioactivity," Questions on the History of Science and Technology 1956, No. 2.

Zaporozhets, V. M., "Radioactive oil prospecting," Science and Life 1956, No. 9.

Ilyukhine, N. V., "The use of nuclear fuel in English power engineering," Power Machine Building 1956, No. 9.

Kazarinov, Yu. M. and Simonov, Yu. N., "Elastic neutron-proton scattering at 580 Mev," J. Exptl.-Theoret. Phys. (USSR) 31, 2 (1956).

Kaliteevsky, N. I. and Chaika, M. P., "The spectroscopic determination of Cu^{63} and Cu^{65} nuclear moments," Optica i Spektroskopiya 1, 5 (1956).

Klyucharev, A. P. et al., "The study of the reaction of He^3 with deuterons," Proc. Acad. Sci. USSR 109, 4 (1956).

Korobochko, Yu. S. and Mineev, V. I., "On the construction of injectors for electron accelerators," Experimental Apparatus and Techniques 1956, No. 1.

Lakatosh, B. K., "The use of radioactive isotopes for wood-pulp control," Wood-Working Industry 1956, No. 6.

Levkovsky, V. N., "The relative cross sections of (n,p)-reactions with nuclei of several stable isotopes," (Letter to the editor), J. Exptl.-Theoret. Phys. (USSR) 31, 2 (1956).

Lifshits, I. M., "On temperature bursts in a medium subjected to nuclear radiation," Proc. Acad. Sci. USSR 109, 6 (1956).

Margulis, O. M. and Karaulov, A. G., "The use of 'labelled atoms' for the determination of the influence of refractory materials in the contamination of steel by nonmetallic impurities," Refractory Materials 1956, No. 6.

Marei, A. N., "Some questions on the protection of water reservoirs from radioactive contamination," Hyg. and Sanit. (USSR) 1956, No. 9.

Medvedev, B. I., "On V. F.Smirnov's Article 'On some possible applications of radioactive isotopes in the coal industry'," Coal (USSR) 1956, No. 10.

Nefedov, V. D. and others, "The enrichment of radioactive-mercury isotopes," J. Phys. Chem. (USSR) 30, 8 (1956).

Petrov, E. A. and Ovcharenko, N. L., "A protective device with a radioactive isotope," Ind. Power (USSR) 1956, No. 9.

Ronzhin, N., "Radioactive radiation indicators," Radio 1956, No. 10.

Rudenko, N. P., "The separation of the radioactive indium isotope In^{113}," J. Inorg. Chem. 1, 7 (1956).

Svenson, A. N. and Sigorsky, V. P., "A directed radioactive indicator of relay action," Automation and Remote Control (USSR) 17, 9 (1956).*

Sidorov, V. M., "π^0-meson production in (p-p) collisions at an energy of 660 Mev," J. Exptl.-Theoret. Phys. (USSR) 31, 2 (1956).

Sitenko, A. G., "The production of γ-quanta in the collision of fast charged π-mesons with nuclei," Proc. Acad. Sci. USSR 109, 6 (1956).

Starik, I. E. and Alekseenko, N. I., "A radiographic method for the study of the state of radioactive elements in dilute solutions," J. Inorg. Chem. 1, 7 (1956).

Trebukhovsky, Yu. V. et al., "An electron multiplier with a window of 44 x 44 mm^2," Experimental Apparatus and Techniques 1956, No. 1.

Tyurikov, G. S. and Fedotov, N. A., "A laboratory method for the analysis of a radioactive gas with soft radiation ($C^{14}O_2$ H_1^3)," Factory Lab. (USSR) 22, 10 (1956).

Shakhbazyan, V. A., "On the question of the energy losses of fast charged particles in an absorbing medium," Bull.Acad. Sci. Armenian SSR, Div. Phys.-Math., Natural and Tech. Sci. 9, 5 (1956).

Shamanskaya, N. S., "The determination of the branching ratio for the decay of Po^{210}," J. Exptl.-Theoret. Phys. (USSR) 31, 2 (1956).

* Original Russian pagination. See C. B. Translation.

ERRATA

In the paper by V. E. Gerasimovsky, "Minerals of Uranium," in the Soviet Journal of Atomic Energy, No. 4, 1956, pp. 573-586, the following misprints in the original Russian were not corrected in the English translation.

Page no.	Line	Reads	Should read
577	12 from bottom	$Ca(UO_2)_2(PO_4)_2 \cdot 12H_2O$	$Cu(UO_2)_2(AsO_4, PO_4)_2 \cdot 11H_2O$
	10 from bottom	$Ba(UO_2)_2(PO_4)_2 \cdot 12H_2O$	$Ba(UO_2)_2(PO_4)_2 \cdot 8H_2O$
	6 from bottom	$(U, Ca_2, TR)_2(PO_4)_4 \cdot 6H_2O$	$(U, Ca_2RE)_2(PO_4)_4 \cdot 6H_2O$
579	Col. 2, line 6 from bottom	$Cu(UO_2)(AsO_4)_2 \cdot 12H_2O$	$Cu(UO_2)_2(AsO_4)_2 \cdot 12H_2O$
	4 from bottom	$K_2(UO_2)(VO_4) \cdot 3H_2O$	$K_2(UO_2)_2(VO_4)_2 \cdot 3H_2O$
580	Col. 8, line 2 from bottom	5.8-39.7	5.8-39.2 (in ash composition)
	1 from bottom	54.2	54.2 (in ash composition)